Università degli Studi di Messina

Dipartimento di Scienze chimiche, biologiche, farmaceutiche e ambientali

"Doctor of Philosophy in "Chemical Science"

"Use of Advanced Mass Spectrometry Technologies for the Analysis of High Complex Samples"

Ph.D. Thesis of:

Marco Piparo

Supervisor:

Prof. Luigi Mondello

Coordinator:

Prof. Sebastiano Campagna

Dottorato di Ricerca in "Scienze Chimiche" XXX ciclo

TABLE OF CONTENTS

Chapter 2. Comprehensive two-dimensional gas chromatography fundamentals and theoretical/practical considerations

Chapter 3. Research in the field of comprehensive two-dimensional gas chromatography coupled to various forms of mass spectrometry

Chapter 4. Fast gas chromatography

Scope of the research work

My research work, during the Ph.D. course, has been focused mainly on the use different mass spectrometry techniques for the analysis of complex sample. Much of the experimentation has been performed in the field of gas chromatography, even though liquid chromatography has also been exploited. The techniques used have been: single quadrupole mass spectrometry tandem with comprehensive gas chromatography (GC×GC-MS), single quadrupole mass spectrometry tandem with fast comprehensive gas chromatography, and quadrupole time of flight tandem with ion mobility (IM-Q-ToF). The use of such powerful analytical instrumentation, enabled the attainment of detailed information of sample, and in particular related to food safety. Comprehensive 2D GC is a relatively new technique, developed in 1991 and can be considered, without a doubt, at the same level of the OTC, in terms of the revolutionary impact that it has had on the GC field.

With regards to loop-type cryogenic modulation, I have been involved in food-sample applications (mussels, claim and fish) and in the optimization and development studies. In the latter case the use of micro bore columns in both dimensions is emphasized.

Regarding the ion mobility Q-ToF I have involved in the separation of isomers in different type of milk and in the calculation of collision cross section value improve lipid identification.

Chapter 1

Mass spectrometry: Fundamental and Instrumentation

1.0 Introduction

For over 100 years, mass spectrometry has played a crucial role in a variety of scientific disciplines. With a small beginning in the late nineteenth century as a tool to detect cathode rays, mass spectrometry currently has assumed a major role in identification of proteins in biological experiments, with the aim of unravelling their functional role and detecting biomarkers of a specific disease. Mass spectrometry has become an integral part of proteomics and the drug development process. Several diverse fields, such as physics, chemistry, medicinal chemistry, pharmaceutical science, nuclear science, food science, petroleum industry, forensic science, and environmental science, have benefited from this highly sensitive and specific instrumental technique.

Mass spectrometry's characteristics have raised it to an outstanding position among analytical methods: unequalled sensitivity, detection limits, speed and diversity of its applications. In analytical chemistry, the most recent applications are mostly oriented towards biochemical problems, such as proteome, metabolome, high throughput in drug discovery and metabolism, and so on. Other analytical applications are routinely applied in pollution control, food control, forensic science, natural products or process monitoring.

Regardless of the analytical purpose, mass spectrometry aims to provide structural information of a compound for an unambiguous identification. The fundamental requisite for a successful mass spectrometric experiment is the generation of stable ions of the molecules of interest capable to "survive" along their path inside the mass spectrometer and, thus, to become detectable. In this respect, the molecule has to be firstly transferred from its existing physical state (either liquid or solid) to the gas phase into the vacuum of an ion source block, and afterwards it has to acquire one or several charges to be

separated and detected into a mass analyser

From the 1950s to present, mass spectrometry has evolved tremendously in terms of developing of new and/or improving existing methods of ion sampling, generation and transfer into mass analyzers, as well as data recording and generation of mass spectra [1]. In particular, in the decade between 1995 and 2005 this progress has led to the advent of entirely new instruments. New atmospheric pressure sources were developed [2-5], existing analysers were perfected and new hybrid instruments were realized by new combinations of analysers.

There is no one-and-only approach to the wide field of mass spectrometry. Is necessary to learn about the ways of sample introduction, generation of ions, their mass analysis and their detection as well as about registration and presentation of mass spectra and each of these parts play a key role in the importance of successful application of mass spectrometry (Figure 1.1)

1.1. Brief history and basic principles of mass spectrometry

In 1897, Joseph John Thomson, a physicist, demonstrated the existence of the electron and measured its mass-to-charge (*m/z*) [6]. He later applied similar methods to the analysis of positive ions with positive ray parabolas [7]. In 1919, Aston, a student of Thomson, refined such an instrumentation by improving the use of electric and magnetic fields to focus ions on a photographic plate used as detector (focusing speed) [8]. Aston himself called that device mass spectrograph. After, Dempster constructed an instrument with a deflecting magnetic field angled at 180°. In order to detect different masses, it could have a variable magnetic field, and after focus them onto an electric point detector [9]. Later, the term mass spectrometer was coined for those type of instruments using a scanning magnetic field [10]. Aston and

Dempster, along with the aforementioned Thomson, can therefore be considered as the pioneers of mass spectrometry.

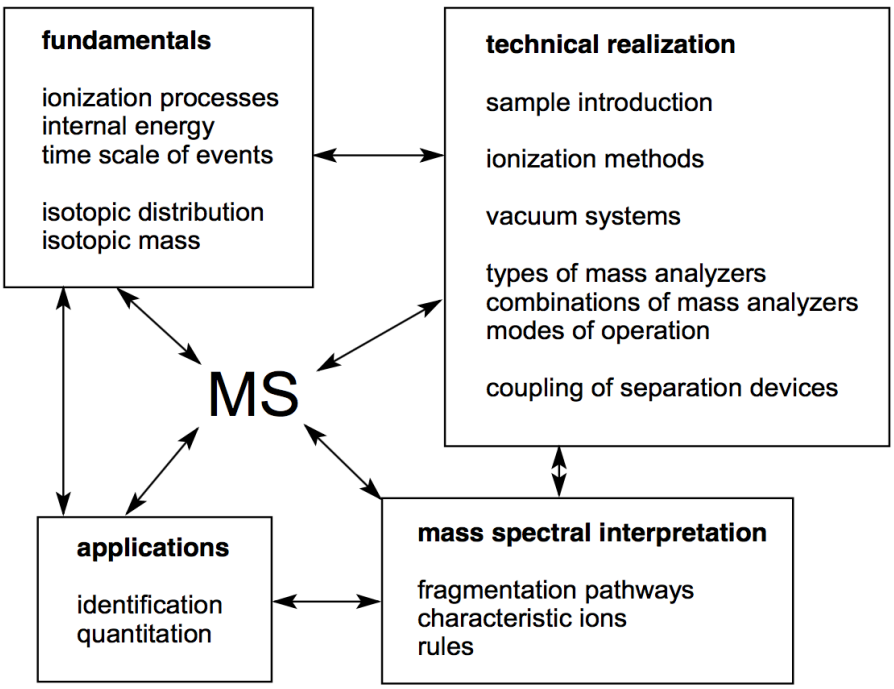

Figure 1.1. The main domains of mass spectrometry

Three basic steps are involved in mass spectrometry analysis (Figure 1.2):

1. The first step is ionization that converts analyte molecules or atoms into gas-phase ionic species. This step requires the removal or addition of an electron or proton(s). The excess energy transferred during an ionization event may break the molecule into characteristic fragments.

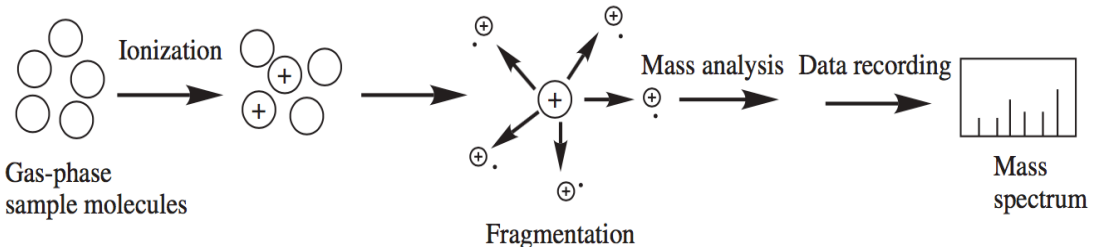

Figure 1.2. Basic concept of mass spectrometry analysis.

2. The next step is the separation and mass analysis of the molecular ions and their charged fragments on the basis of their *m/z* (mass-to-charge) ratios. Ion separation is effected by electric and/or magnetic fields. This former definition of mass spectrometry dates back to 1968 [11]

3. Finally, the ion current due to these mass-separated ions is measured, amplified, and displayed in the form of a mass spectrum.

The first two steps are carried out under high vacuum, which allows ions to move freely in space without colliding or interacting with other species. Collisions may lead to fragmentation of the molecular ions and may also produce a different species through ion–molecule reactions. These processes will reduce sensitivity, increase ambiguity in the measurement, and decrease resolution. In addition, the atmospheric background will introduce interference.

The analyte may be ionized thermally, by electric fields or by impacting energetic electrons, ions or photons. The energy deposited on the analyte during ionization processes can be varied, and this leads to classification of the various ionization techniques on the basis of their relative “softness” or “hardness” features. Another consideration is that ions can be mass separated

in field-free regions (*e.g.,* in time-of-flight analyzers). In such a case, the separation of ions within a given *m/z* range would be entirely governed by their masses, which will determine the time they spend into the drift region (a detailed discussion of the main mass analyzers will be presented in the next sections).

1.2. Mass spectrometers

A simplistic view of the essential components of a mass spectrometer is given in Figure 1.3. These components are:

1) *An inlet system*: transfers a sample into the ion source. An essential requirement is to maintain the integrity of the sample molecules during their transfer from atmospheric pressure to the ion-source vacuum.

2) *An ion source:* converts the neutral sample molecules into gas-phase ions. Several ionization techniques have been developed for this purpose.

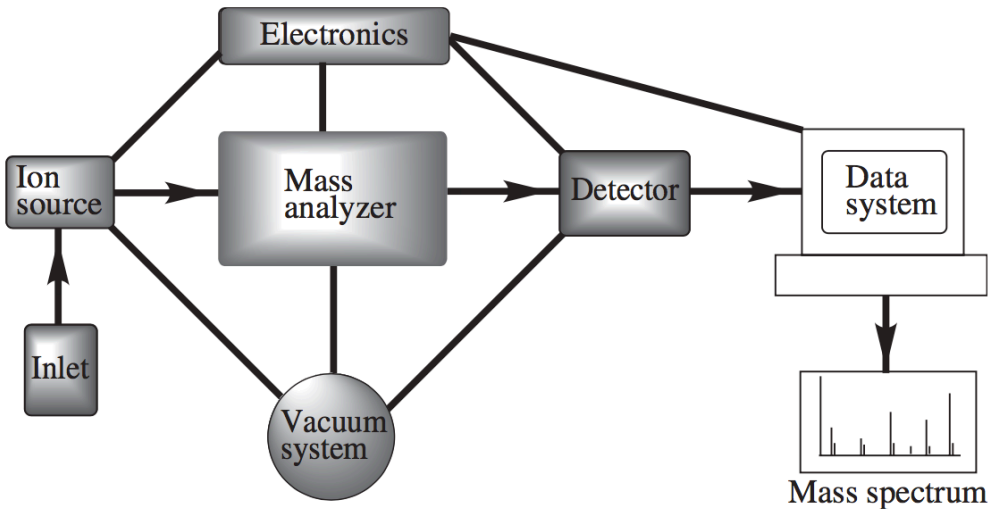

Figure 1.3. Basic components of a mass spectrometer.

3) *A mass analyser:* separates and mass-analyzes the ionic species. Magnetic and/or electric fields are used in mass analyzers to control the motion of ions. A magnetic sector, quadrupole, time-of-flight, quadrupole ion trap, quadrupole linear ion trap, orbitrap, and Fourier transform ion cyclotron resonance instrument are the most common forms of mass analyzers currently in use.

4) *A detector:* measures and amplifies the ion current of mass-resolved ions.

5) *A data system:* records, processes, stores, and displays data in a form that human eye can easily recognize (computer screen or printer output).

6) *A vacuum system*: maintains a very low pressure in the mass spectrometer. The ion source region is usually maintained at a pressure of 10^{-4} to 10^{-8} torr; somewhat lower pressure is required in the mass analyzer region (around 10^{-8} torr). Most instruments use a differential pumping system to maintain an optimal vacuum.

7) *Electronics:* controls the operation of various units.

Since its introduction, electron ionization (EI) became wide-spread used in organic mass spectrometry; however, with particular restrictions to gas phase low-mass thermally stable molecules [12,13]. Consequently, the strong need to extent the applicability of mass spectrometry to also large non-volatile molecules has triggered the development of the so-called “soft” ionization methods, among which chemical ionization (CI) was first discovered in 1966 [18]. Newly developed fast atom bombardment (FAB) (1981 [14]), electrospray ionisation (ESI) (1989 [15]), and matrix-assisted laser desorption/ionisation (MALDI) (1985 [16]) marked a breakthrough in the dramatic expansion of the range of applications in the field of the life science.

Concurrent, and parallel, to the development of ionization methods, several innovations in mass analyzers technology marked the historical development of mass spectrometers, and their ongoing improvement is being made at an enormous rate. A large number of mass spectrometers have been developed since Thomson's experiments in 1897 [6]. From the beginning to present, almost any physical principles ranging from time-of-flight to cyclotron have been exploited to construct mass analyzing devices.

Time-of-flight (TOF) were the first mass analyzers to be described in 1947 [17]. It took almost a half-decade for quadrupoles and sector instruments to be invented, *i.e.,* in 1953 and 1952, respectively [18,19]. Concurrently to the introduction of quadrupoles, Paul and Steinwedel also described the first ion trap (IT) in 1960 [20]. Finally, hence more recent (1974), was developed the Fourier transform ion cyclotron resonance (FT-ICR) mass analyzer, whose ICR principles were, however, first described in 1949 [21]. However, it took almost 20 years for FT-ICR mass analyzers to be finalized

1.2.1 Mass spectrum

A mass spectrum is the two-dimensional representation of signal intensity (ordinate) versus *m/z* (abscissa). The intensity of a peak, as signals are usually called, directly reflects the abundance of ionic species of that respective *m/z* ratio that have been created from the analyte within the ion source.

Often, but not always, the peak at highest *m/z*, which is also called as base peak, corresponds to the entire ionized molecule, the so-called molecular ion, $M^{+\bullet}$, and is arbitrarily assigned the relative abundance of 100%. The abundances of all the other peaks, *i.e*., the fragment ions, are given as percentages of the base peak. The relative intensity for expressing ion

abundances helps to make mass spectra more easily comparable.

The mass-to-charge ratio, i.e., the physical property that is measured in mass spectrometry, is a dimensionless term in which the mass of the ion, expressed in atomic mass units (u) corresponding to 1/12 of the mass of the most abundant ^{12}C isotope, and synonymous of dalton (Da), is divided by the number of carried charges.

A mass spectrum can be represented as a bar graph, usually referred as centroid view (figure 1.4b), which derives from the data reduction of the initially acquired profile data (figure 1.4a) by the mass spectrometer.

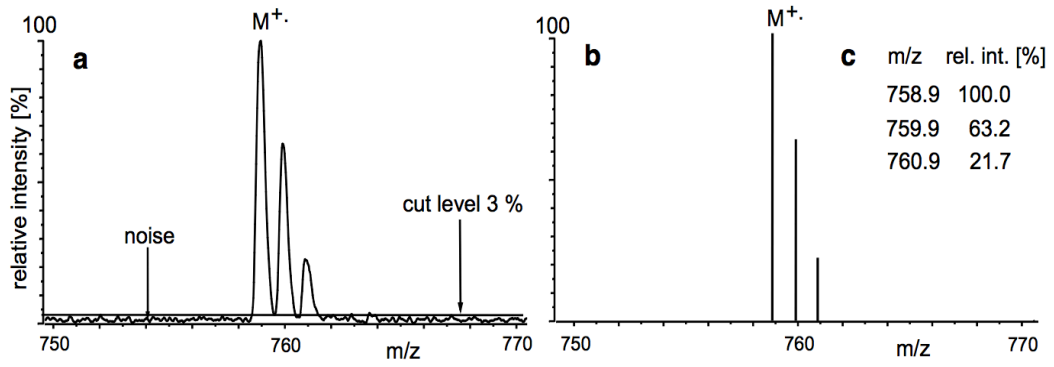

Figure 1.4. Tetrapentacontane, $C_{54}H_{110}$: representations of the molecular ion signal as (b) centroid, (a) profile spectrum. and (c) tabular listing.

When a mass spectrometer is employed as the detector of (gas or liquid) chromatographic systems, its output must provide a series of mass spectra each one ideally corresponding to an eluted compound. According to a recent IUPAC definition, the total ion current refers to the summation of the entire separated ion currents carried by the different ions contributing to a mass spectrum [22]. The total ion chromatogram (TIC) represents a plot of the total

ion current vs. retention time obtained from a chromatography experiment with mass detection. Differently, the term extracted ion chromatogram (EIC) refers to a plot of the intensity of the signal observed at a chosen (or a set) *m/z* as a function of retention time [22]. Finally, the base peak chromatogram (BPC) is a chromatogram obtained by plotting the signals of the base peak ions as a function of retention time.

1.3 Mass resolution and mass accuracy

1.3.1 Resolution and resolving power

The resolution and mass accuracy of a mass spectrometer are the primary features to be considered for determining whether an instrument suits the demanded tasks. But why is mass resolution important? The answer is: an adequate mass spectral separation enables accurate mass measurements (and thereby the elemental composition determination), leading to an unambiguous identification, or highly reliable quantification through the exclusion of a large proportion of possible isobaric interferences. A poor resolving power will obviously result in the generation of false positive or false negative signal responses.

The term mass resolution, *R*, or simply resolution, usually refers to the ability of a mass spectrometer of separating two narrow mass spectral peaks. The ability of an instrument to distinguish between ions differing by a small increment in their *m/z* value ($\Delta m/z$) is called as *resolving power*:

$$R = \frac{m}{\Delta m} = \frac{m/z}{\Delta m/z}$$

The terms resolution and resolving power are basically interchangeable [23]. It is, however, necessary to define the Δm term.

Unite mass resolution means that only integer masses can be separated, that is, you can distinguish, e.g., mass 1000 from 1001.

Resolution on magnetic sector instruments is normally given according to the 10% valley definition, which defines Δm by the mass difference between two resolved peaks with a 10% valley between them. The 10% valley definition is equivalent to that where Δm is defined by the peak width at 5% peak height (figure 1.5).

The most commonly used method to measure the resolution of quadrupoles, FT-ICR, orbitrap and TOF follows the full width at half maximum (FWHM) definition, which uses the width of a peak at 50% of its height as a measure for Δm (figure 1.5).

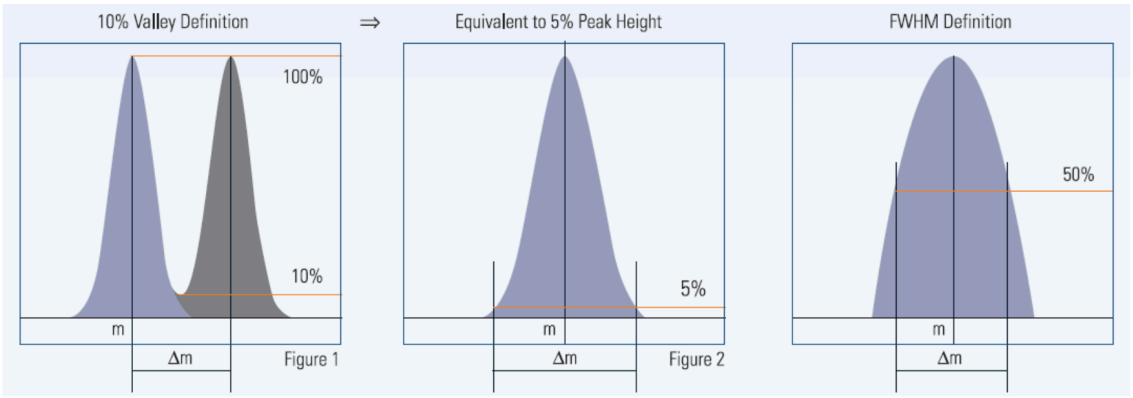

Figure 1.5. Examples of different definitions of resolution.

Instruments capable of low resolution (LR) operates at a R= 500– 2000. High resolution (HR) refers to a R> 5000. However, there is no exact definition of these terms. Furthermore, one should be aware that increased settings of resolving power are usually obtained at the cost of transmission of the analyzer, thereby reducing the absolute signal intensity.

1.3.2 Mass accuracy

In mass spectrometry, resolution and accurate mass measurements are closely related to each other, because mass accuracy tends to improve as peak resolution is improved. However, a high-resolution measurement does not necessarily implies measuring the accurate mass, as the former aims to separate adjacent signals, while accurate mass measurements can deliver molecular formula determination [24,25]. The newly developed orbitrap and the new generation of orthogonal acceleration time-of-flight analyzers contributed to an increased demand for accurate mass data.

There are different ways to define and thus to calculate the mass of an atom, molecule or ion. Basically, an element is specified by the number of protons in its nucleus, i.e., the atomic number, which determines its place within the periodic table of the elements. Atoms with nuclei of the same atomic number but differing in the number of neutrons, i.e., by the mass number, are termed isotopes [23]. Those elements, which do exist in the form of only one single naturally occurring stable isotope, are termed monoisotopic elements. The distribution of the isotopic composition in a mass spectrum is named the isotopic pattern.

For stoichiometric calculations, chemists use the average mass that is the result of the weighted average of the atomic masses of the different isotopes of each element in the molecule. In mass spectrometry, the nominal mass is generally used; the latter being calculated using the mass of the predominant isotope of each element rounded to the nearest integer value. However, the exact masses of isotopes are not exact whole numbers. They differ weakly from the nominal mass by a determined value, so-called mass defect, which is unique for each isotope. The monoisotopic mass is then calculated by using

the exact mass of the most abundant isotope for each constituent element. It is very close to but not equal to the nominal mass of the isotope. As a consequence, almost no combination of elements in a molecular formula has the same calculated exact mass as any other one. The only exception is the carbon isotope ^{12}C, whose mass has been assigned precisely 12 u.

As an example, the molecular ions of nitrogen, $N_2^{+\bullet}$, carbon monoxide, $CO^{+\bullet}$, and ethene, $C_2H_4^{+\bullet}$, have the same nominal mass of 28 u, *i.e.*, they are so-called isobaric ions. The isotopic masses of the most abundant isotopes of hydrogen, carbon, nitrogen, and oxygen are 1.007825 u, 12.000000 u, 14.003074 u, and 15.994915 u, respectively. Thus, the calculated exact masses are 28.00559 u for $N_2^{+\bullet}$, 27.99437 u for $CO^{+\bullet}$, and 28.03075 u for $C_2H_4^{+\bullet}$. This means they differ by several 10^{-3} u, and none of these isobaric ions measure precisely 28.00000 u.

The type of mass measured by mass spectrometry depends largely on the resolution and accuracy of the analyzer.

1.3.2.1 Exact mass and role of the electron mass

The exact mass of a positive ion formed by the removal of one or more electrons from a molecule is equal to its monoisotopic mass minus the mass of the electron, m_e [23]. The question is whether the mass of the electron *m*e (5.48×10^{-4} u) has really to be taken into account. It strictly depends on the level of mass accuracy which is required. In fact, in FT-ICR, orbitrap, and orthogonal acceleration ToF (oaToF) instruments, which deliver mass accuracies in the order of $<10^{-3}$u, one should definitely include the electron mass in exact mass calculations [26], as otherwise it could generate a

considerable mass error.

1.3.2.2 Mass accuracy and determination of molecular formulas

The mass accuracy indicates the deviation of the instrument's response between the measured accurate mass and calculated exact mass. It can be expressed as absolute mass accuracy, $\Delta m/z$:

$$\Delta m/z = \frac{m}{z}_{exp} - \frac{m}{z}_{cal}$$

or, alternatively, as relative mass accuracy, δ *m/m*, *i.e.,* the absolute mass accuracy divided by the exact mass, and expressed as parts per million (ppm):

$$\delta\, {}^{m}/_{m} = (\delta m/z)/(m/z) * 10^{6}$$

Accurate mass measurements allow to determine the elemental composition of an analyte, and thereby to confirm the identification of target compounds or to support the identification of unknowns. Assuming infinite mass accuracy, we should be able to assign the molecular formula of any ion simply through its exact mass. In reality, deviations between the accurate and exact mass of an ion always exist to some extent and, thus, we normally deal with errors in the order of one to several ppm depending on the type of instrument and the mode of its operation. Whatever the type of instruments or operation mode may be used, the assignment of molecular formulas must follow two general rules: i) it must always be in accordance with the experimentally observed; ii) the formula has to obey the nitrogen rule.

1.3.2.3 High-mass molecules – influence of resolution on isotopic pattern and mass accuracy

Terms such as large molecules, or high mass, generally refer to masses in the range of 10^3–10^4 u or above. By increasing *m/z*, the centre of the isotopic pattern is shifted to values higher than the monoisotopic mass. The center, *i.e.,* the average mass, tends to be close to the peak of the most abundant mass. The monoisotopic mass is of course still related to a real signal, but it may be of such a low intensity that it is difficult to recognize [27]. It is certainly desirable to have at least sufficient resolution to resolve isotopic patterns of high-mass molecules, in order to be able to measure its monoisotopic mass. However, not every mass analyzer is capable of doing so. Mass analyzers such as quadrupole, time-of-flight or quadrupole-ion trap often generate some changes in spectral appearance thus affecting the actual measured mass [28].

For example, figure 1.6 illustrates the isotopic pattern of bovine insulin $[C_{254}H_{378}N_{65}O_{75}S_6]^+$ calculated at R= 1000, 4000, and 10,000. At R = 1000, the isotopic peaks are not resolved and smoothly covered by an envelope. At R = 4000, the isotopic peaks become almost sufficiently resolved. Finally, at R = 10,000, the isotopic pattern is well resolved and interferences between isotopic peaks are avoided.

With regard to mass accuracy and determination of molecular formulas, it has been demonstrated that unequivocal formula assignment only works in a range up to about *m/z* 500 [29]

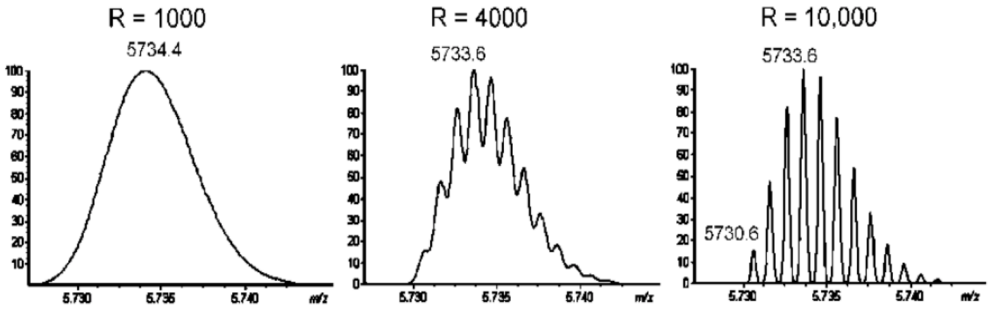

Figure 1.6. Bovine insulin: isotopic pattern calculated for $[M+H]^+$ at different resolutions.

In fact, a high level of mass accuracy measurement is unattainable if the peak shape is abnormal, due to instrumental reasons or unresolved isotopic envelopes, that is the case of large molecules. It has been reported that accuracy is limited to ± 0.1 Da for masses below 10 kDa [30], and with instruments capable of achieving ±0.5−5 ppm mass accuracy, that is necessary to distinguish peptide elemental compositions, it is possible to match homologous proteins having > 70% sequence identity [31]. Others have reported that, even at a high mass accuracy of 1 ppm, and with the particular case of peptides, the elemental composition can only be unambiguously identified up to about 800 u [32].

1.4 Instrumentation

"A modern mass spectrometer is constructed from elements which approach the state-of-the-art in solid-state electronics, vacuum systems, magnet design,

precision machining, and computerized data acquisition and processing" [33]. This is and has ever been a fully valid statement about mass spectrometers. The basic type of mass spectrometer consists of three major parts: the ion source, the mass analyzer, and the detector. All mass spectrometers require low pressures (vacuum) conditions for operation. This is necessary to allow ions to survive along their path inside the mass spectrometer, and to reach the detector without undergoing collisions with other gaseous molecules. Indeed, collisions would produce a deviation of the ion trajectory and, in the worst case, its loss through the hitting of the mass analyzer surfaces. Besides, ion–molecule collisions could produce unwanted secondary reactions and hence increases the complexity of the spectrum. Introducing a sample into a mass spectrometer requires its transfer from atmospheric pressure into a region of high vacuum. An efficient pumping system uses mechanical pumps, which allow a vacuum of about 10^{-3} Torr to be obtained, in conjunction with turbo molecular pumps that allows a vacuum as high as 10^{-10} Torr to be reached.

Furthermore, mass spectrometry can be coupled with separation methods such as gas chromatography (GC) and liquid chromatography (LC). "Hyphenation", i.e., as GC-MS or LC-MS, delivers high selectivity and low detection limits for the analysis of trace compounds, or the possibility to resolve complex samples. In such a case, the mass spectrometer would act as the chromatographic detector, and its output must somehow represent the chromatogram that would have been obtained with other chromatographic detectors, *e.g.,* flame ionization (FID), thermal conductivity (TCD) and ultraviolet detectors (UV).

Summarizing, a mass spectrometer should always perform the following processes: 1) produce ions from the sample in the ionization source; 2)

separate these ions according to their mass-to-charge ratio in the mass analyser; 3) eventually, fragment the selected ions and analyze the fragments in a second analyser; 4) detect the ions emerging from the last analyzer, measure their abundance, and convert the ions into electrical signals; 5) process the signals coming from the detector through a computer.

1.4.1 Ion sources

In the ion source, the sample is ionized in the gas phase prior to analysis in the mass spectrometer. The choice of the ion source depends on the application, the internal energy transferred during the ionization process and the physic-chemical properties of the analyte that can be ionized. Some ionization techniques, so-called "hard", are very energetic and cause extensive fragmentation of the analyte with even loss of its intact ion. Electron ionization belongs to such a group of sources. On the contrary, so-called "soft" ion sources, *e.g.,* chemical ionization, do allow for generating intact ions of the molecular species. However, it is worthy to say that both EI and CI sources are only suitable for gas phase ionization, and thus their use is limited to sufficiently volatile and thermally stable compounds. In fact, when dealing with large non-volatile fragile (bio) molecules, that is the case of proteins, nucleic acids, polymers, it is necessary to introduce them into the vacuum of the mass analyzer after a process of nebulization of the containing solution (*i.e.,* in ESI, APCI and APPI) or, alternatively, to bring them from the solid-state to the gas phase directly into the ion source housing, usually by means of a matrix (either solid or liquid) which promote both desorption and ionizations of the intact analytes. That is the case of MALDI and FAB.

The number of available ion sources is quite large, even some of them are no longer commonly used today, but are of historical interest. Among them,

electron ionization deserves an extensive treatment, given that its invention dates back to the infancy of mass spectrometry in the early 20th century [34].

1.4.1.1 Electron ionization (EI) ion sources

EI was introduced in 1921 by Dempster, who used it to measure lithium and magnesium isotopes [35]. Figure 1.7 illustrates a schematic representation of the electron ionization source. It consists of a chamber, so-called ionization chamber, which is region of the ion source block where analyte molecules are directly introduced and ionized. A resistively heated metal filament, typically made of rhenium or tungsten, creates the electron beam. The high-energy electrons produced are accelerated towards an anode and collide with the gaseous molecules to affect their ionization.

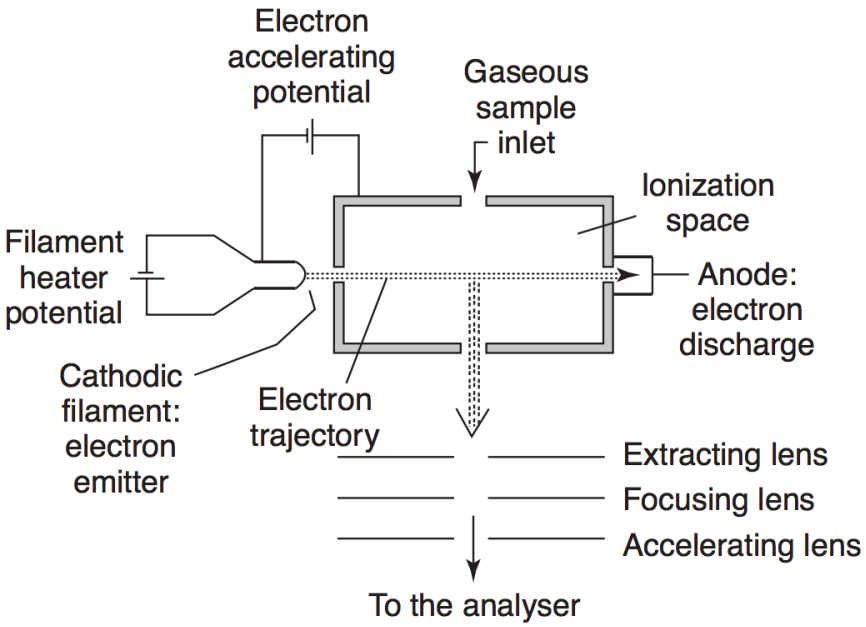

Figure 1.7. Schematic representation of an electron ionization source.

Each electron has a given wavelength. If one of the frequencies has an energy corresponding to a transition in the molecule, an energy transfer that leads to various electronic excitations can occur. When there is enough energy, an electron can be expelled. The electrons do not “impact” molecules. For this reason, the former term electron impact has been correctly re-named as electron ionization. At the end of such an interaction, typically positive radical molecular ions are formed. For positive ions the electron energy is in most cases set to 70 eV. However, between only 10 and 20 eV energy is transferred to the molecules during the ionization process. The obvious consequence is that the excess energy leads to extensive fragmentation, which can be advantageous as it provides structural information for the elucidation of unknown analytes. Moreover, since the EI-mass spectra are relatively reproducible, a compound fingerprint scan be recorded, and that has triggered the construction of mass spectral databases for a quick and reliable compound identification.

Fragmentation can be more or less limited by lowering the electron energy. For example, using 12–15 eV electrons, instead of 70 eV, extended fragmentations are reduced. On the other hand, unfortunately, there is the considerable drawback of a general loss of intensity due to the decrease in ionization efficiency.

Nevertheless, during the first years of mass spectrometry, low- energy EI spectra were the only way to achieve mass spectra with a minimized fragmentation. It was only in the 1960s that chemical ionization was introduced as a valid technique in mass spectrometry for its “softness” features [36]

Chemical ionization (C.I.) is a technique that produces ions with little excess

energy. Thus this technique presents the advantage of yielding a spectrum with less fragmentation in which the molecular species is preserved. Consequently, C.I. can be considered as complementary to electron ionization. The ionization process is based on a chemical reaction between the analyte and an "ion reagent", formed by subjecting to EI reagent gas molecules introduced in the source in large excess. This excess, which determines pressure in the source higher than those used in the EI, ensures that an electron entering the source block will preferentially ionize the reagent gas molecules, and that the resulting ions will mostly collide with other gas molecules. Subsequent ion-molecule interactions, by means of complex reactions involving proton transfer, hydride abstractions, adduct formations, charge transfers, and so on, will produce positive and negative ions of the substance, the latter particularly useful to analyze highly electronegative compounds.

1.4.1.2 Sample introduction

A sample introduction system has the function of transferring the analyte from their physical state and atmospheric conditions into low-pressure ion source. The type of sample inlet depends, strictly, on the type of sample to be analysed.

The reference inlet system instead, introduces the mass calibrant to perform the calibration of the system for accurate mass measurements.

A chromatography system can be coupled to a mass spectrometer, thus operating as a sample introduction system. This coupling also provides a second dimension to the chromatographic analysis, in terms of information. Coupling on-line a chromatograph with a mass spectrometer implies that the mobile phase, liquid or gas, has to be selectively removed while preserving the analyte as much as possible [37]. The first coupling between gas

chromatography and mass spectrometry was realized at the end of the 50s [38]. Over the last decades, many efforts have been performed towards the development of proper interfaces capable to perform such a demanding task and to ensure the best throughput. Among them, electrospray ionization, atmospheric pressure chemical ionization and photoionization, each of them following different operations, marked the breakthrough in the feasible coupling between LC and MS.

1.4.1.3 Databases of EI mass spectra

In order to analyze a complex mixture, a separation technique is coupled with the mass spectrometer, provided that the separated compounds must be introduced one after the other into the spectrometer. The most obvious advantage consists of obtaining a spectrum that can be used to identify the separated compounds.

Within the context of GC-MS, low- and medium-polarity analytes are usually well suited for EI, while highly polar or even ionic compounds, *e.g.,* diols or polyalcohol, amino acids, organic salts, should be properly derivatized [39,40]. In any case, EI mass spectra are excellently reproducible when measured under standard conditions (70 eV, ion source at 150–250°C), in both cases of measurements performed on the same or different types or brand of instruments. This fact has triggered the construction of mass spectral databases, commonly named as libraries. The most comprehensive EI mass spectral databases are those provided by the National Institute of Standards and Technology (NIST), and the Wiley/NBS [41]. Furthermore, the 2017 version of the NIST/EPA/NIH mass spectral database is equipped with a compilation of *Linear* Retention Index (LRI) values determined on non-polar and polar columns.

1.4.2 Mass analyzers

A mass analyzer is a device that enables to separate the gas phase species produced according to their mass.

There are several types of mass analyzers used in mass spectrometric research that use different physical principles. They can be divided into two broad classes on the basis of many properties. Scanning analyzers allow only the ions of a given mass-to-charge ratio to go through at a given time. They are either magnetic sector or quadrupole instruments. On the contrary, mass analyzers such as time-of-flight, ion trap, ion cyclotron resonance or orbitrap, allow the simultaneous transmission of all ions across a given mass range. Analyzers can be also grouped on the basis of other properties, for example ion beam *vs.* ion trapping types, or continuous beam *vs.* pulse based.

Another trend in mass analyzer development is to combine different analyzers in sequence in order to allow multiple experiments to be performed. For example, triple-quadrupoles and more recently hybrid instruments such as quadrupole-TOF allow the generation of fragments over several decomposition experiments (MS^n).

The main characteristics for measuring the performance of a mass analyzer are: 1) the mass range limit; 2) the analysis speed; 3) the transmission; 4) the mass accuracy and finally 5) the resolution.

Table 1.1 contains an overview of the analyzers available in mass spectrometry. In the context of the present thesis, two types of mass analyzers have been used, namely single quadrupole (qMS) and ion mobility Q-ToF (IM-Q-ToF)

1.4.2.1 Quadrupole mass spectrometers

Quadrupole instruments are probably the most widely used type of mass spectrometer (Figure 1.8). The principle of the quadrupole mass analyzer was first by described by Paul and Steinwegen in 1953 [18]. A quadrupole consists of four precisely matched parallel metal rods. The mass separation is accomplished by the stable vibratory motion of ions in a high-frequency oscillating electric field that is created by applying direct-current (DC) and radio frequency (RF) potentials to these electrodes [42,43,44]. Opposite rods are connected electrically in pairs. The two pairs will, at any given time, have potentials of the same magnitude, but of opposite sign. Ions entering the space between the rods oscillate in the directions *x* and *y*, whose amplitude depends on the frequency of the potential applied and the masses of the ions. A positive ion will be attracted towards a negative rod. If the potential changes sign, the ion will change direction avoiding to discharge itself on the rod.

At given values of the DC and RF potentials, only ions within a certain narrow *m/z* range will have stable trajectories and be allowed to reach the detector. The motion of an ion traveling through the quadrupole is described by an equation established in 1866 by the physicist Mathieu, so-called Mathieu equation [45]. The DC potential applied to the electrodes of the X-Z plane is positive, while that applied to the electrodes of the Y-Z plane is negative. To understand the influence of potential on the trajectory at which a charged particle undergoes, it is convenient to examine the X-Z and Y-Z planes separately.

Table 1.1. Common mass analyzers available in mass spectrometry.

Type	Acronym	Principle
Time-of-flight	TOF	Time dispersion of a pulsed ion beam; separation by time-of-flight
Magnetic sector	B	Deflection of a continuous ion beam; separation by momentum in magnetic field due to Lorentz force
Linear quadrupole	Q	Continuous ion beam in linear radio frequency quadrupole field; separation due to stability of trajectories
Linear quadrupole ion trap	LIT	Continuous ion beam and trapped ions; storage and eventually separation in linear radio frequency quadrupole field due to stability of trajectories
Quadrupole ion trap	QIT	Trapped ions; separation in three-dimensional radio frequency quadrupole field due to stability of trajectories
Ion cyclotron resonance	ICR	Trapped ions; separation by cyclotron frequency (Lorentz force) in magnetic field

Let's start from X-Z plane (Figure 1.9). At positive (DC) potentials, ions will be rejected and focused toward the central axis of the electrodes.

When the potential is switched to negative value, the beam of positive ions will be accelerated towards the electrodes. If the potential at the electrodes changes rapidly, heavy ions will preferably be affected by the positive DC component, which means that they will be forced to move towards the middle between the electrodes. Conversely, in the presence of lighter ions, the negative, tough brief, potential can be sufficiently intense to attract and lead them to collide with the electrode. In such a X-Z plane configuration, one pair of rods will act as a "high pass mass filter". In the Y-Z plane, the situation is similar except from the fact that the DC potential is negative.

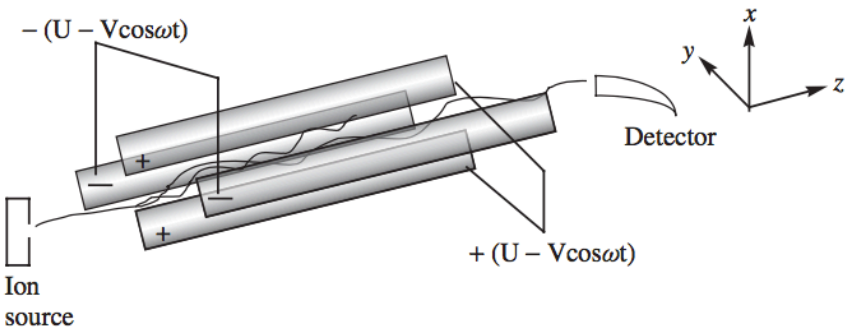

Figure 1.8. Schematic of the quadrupole analyzer.

The obvious consequence is that high-mass ions will preferably experience an attractive force and will hit one of the electrodes. On the contrary, tough low-mass ions also experience an attractive force most of the time, they are light enough to respond to the positive potential, and thus will be pushed back towards the middle between the electrodes. In this way, the rods act as a "low pass mass filter".

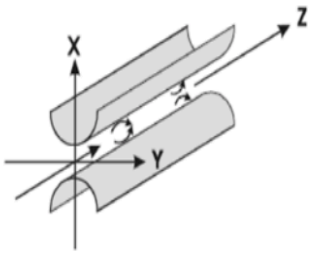

Figure 1.9. Schematic representation of the motion of the ions inside the quadrupole analyzer.

The quadrupole is a real mass-to-charge ratio analyzer. It does not depend on

the kinetic energy of the ions leaving the source. The only requirements are: i) the time for ions to go through the analyzer is short compared with the time necessary to switch from one mass to the other, and ii) the interscan delay, i.e., the time between one scan and the next, has to be small. Quadrupole analyzers generally are operated at unit resolution, thus restricting their use to low resolution applications. The mass range depends on the settings of the DC and RF voltages. Typical m/z ranges are 25 to 2000 u with unit mass resolution. Commonly to scanning analyzers, the quadrupole detects one ion at any given time, so most of the ions produced are not detected, thus decreasing the sensitivity. The sensitivity can be vastly improved when scanning a narrow m/z range, or operating in single ion monitoring (SIM) mode, namely choosing only on or few ions to be detected. In such an operation mode, the quadrupole mass spectrometer has a duty cycle of 100%.

The quadrupole mass analyzer has a relatively good dynamic range, which means that the quantification capabilities are generally very good. Thus, quadrupoles are preferably chosen alternatively to magnetic sectors which, tough more stable, are definitely costlier.

Because of the scanning property of quadrupole mass analyzers, they are well suited for continuous ion sources such as EI and ESI, but are not suitable for pulsed ionization methods. They are very often used in combination with GC and LC, and single (q) or triple quadrupole (QqQ) mass spectrometers are nowadays very common benchtop instruments for routine measurements.

1.4.2.2 Time-of-flight spectrometers

The concept of time-of-flight (TOF) analysers was described by Stephens in 1946 [46]. Wiley and McLaren published in 1955 the design of a linear TOF

mass spectrometer which later became the first commercial instrument [47]. The principle of TOF is quite simple: ions of different *m/z* are dispersed in time during their flight along a field-free drift path of known length. All ions start at the same time or at least within a sufficiently short time interval and the lighter ones will arrive earlier at the detector than the heavier ones.

The first-generation TOF instruments were designed for coupling with gas chromatography; however, linear quadrupole analyzers soon surpassed it. Only in the end of 1980s there was a renewed interest in TOF analyzer thanks to the new-pulsed ionization methods and the development of matrix-assisted laser desorption/ionization sources (MALDI) [48]. TOF analyzers were adapted for use with other ionization methods and are now even strong competitors to the well-established magnetic sector instruments in many applications. [49,50,51].

Figure 1.10 shows the scheme of a linear TOF instrument. Ions are expelled from the source in "packages" by a transient application of the required potentials on the source focusing lenses. These ions are then accelerated towards the flight tube by a difference of potential applied between an electrode and the extraction grid. When this ions leaving the acceleration region, they will have the same charge and, ideally, the same kinetic energy, and will enter into a field-free region where will be separated according to their velocities, and reach the detector positioned at the other extremity of the flight tube. Provided that all the ions start their journey at the same time, or at least within a suitable short time interval, the lighter ones will arrive earlier at the detector than the heavier ones.

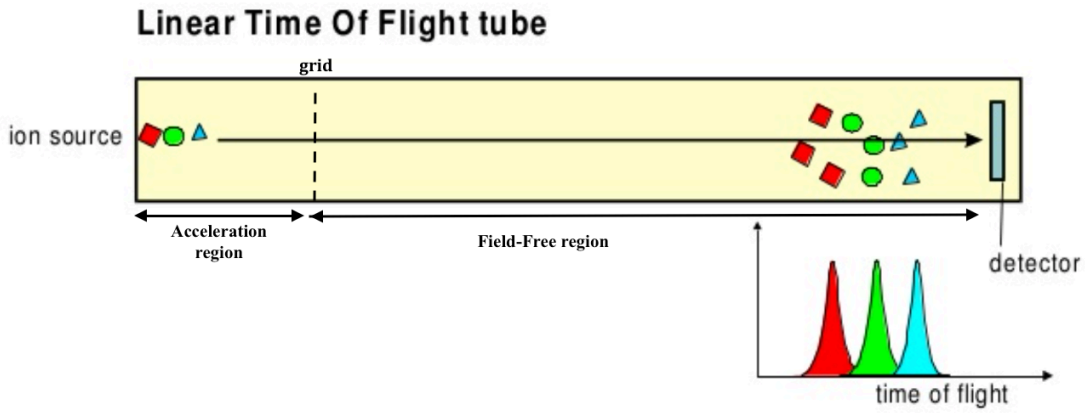

Figure 1.10. Schematic representation of a linear TOF mass spectrometer.

Such an instrumental setup where the ions are traveling on a straight line from the point of their generation towards the detector is called "linear" TOF. The time difference between the starting signal of the pulse and the time at which an ion hits the detector is the time of flight (TOF) and can be expressed as:

$$t_{tof} = \frac{L}{v} = L\sqrt{\frac{m}{2qU_a}} \propto \sqrt{m/z}$$

where L is the length of the field-free region, v is the ion velocity after acceleration, m is the mass of the ion, q the charge of the ion, U_a the accelerating electric potential difference, and z the charge state. This equation shows that, higher is the mass of an ion slower it will reach the detector, and vice versa.

In principle, the upper mass range of a TOF analyzer has no limit, which makes it especially suitable for analyzing large molecules, *e.g.*, up to 300 kDa [52].

Another advantage of these instruments is their high transmission efficiency which leads to very high sensitivity compared to quadrupole and sector analyzers. That is because all the mass range is simultaneously analyzed

contrary to the scanning analyzers where ions are transmitted successively along a time scale.

Generally, the TOF analyzer is very fast, and a spectrum over a broad mass range can be obtained in the microseconds time interval. As the mass resolution is proportional to the flight time and the flight path, one solution to increase the resolution of these analysers is to lengthen the flight tube. However, too long a flight tube decreases the performance of TOF analysers because of the loss of ions by scattering after collisions with gas molecules or by angular dispersion of the ion beam. It is also possible to increase the flight time by lowering the acceleration voltage. But lowering this voltage reduces the sensitivity. Therefore, the only way to have both high resolution and high sensitivity is to use a long flight tube with a length of 1 to 2 m for a higher resolution and an acceleration voltage of at least 20 kV to keep the sensitivity high.

The most important drawback of the first TOF analysers was their poor mass resolution. Mass resolution is affected by factors that create a distribution in flight times among ions with the same m/z ratio. These factors are: i) different time distribution; ii) different in space distribution and iii) different kinetic energy distribution. These drawbacks are substantially improved with the development of two techniques: delayed pulsed extraction and the reflectron.

1.4.2.2.1 Reflectron

As aforementioned a way to improve mass resolution is to use an electrostatic reflector also called a reflectron. The reflectron was proposed for the first time by Mamyrin [53]. It creates a retarding field that acts as an ion mirror by deflecting the ions and sending them back through the flight tube. The term reflectron time-of-flight (RTOF) analyser is used to differentiate it from the

linear time-of-flight (LTOF) analyser. The simplest type of reflectron, which is called a single-stage reflectron, consists usually of a series equally spaced grid electrodes or more preferably ring electrodes connected through a resistive network of equal-value resistors.

As shown in Figure 1.11 the reflectron is situated behind the field-free region opposed to the ion source while detector is positioned on the source side of the ion mirror to capture the arrival of ions after they are reflected. The reflectron corrects the kinetic energy dispersion of the ions leaving the source with the same *m/z* ratio. Consequently, ions with more kinetic energy and hence with more velocity will penetrate the reflectron more deeply than ions with lower kinetic energy. Consequently, the faster ions will spend more time in the reflectron and will reach the detector at the same time than slower ions with the same *m/z*. Although the reflectron increases the flight path, though without increasing the dimensions of the mass spectrometer, the beneficial increase in mass resolution comes at the expense of sensitivity and mass range limitation. The choice of operating TOF instruments in "linear" or "reflectron" mode heavily depends on the species to be detected. For example, when operating in linear mode, the aim is usually to detect larger species, which will not be stable enough to survive along the strong electric field of the reflectron. Therefore, the given resolving power is much lower, as the width of the isotopic envelope do not allow for its decent resolution. The opposite is the case of ReTOF, because especially in the presence of metastable fragmentations (*i.e.,* in tandem MS), only fragments still having kinetic energies close to that of the precursor can be successfully and sensitively detected.

1.4.2.2.2 Orthogonal acceleration.

The major breakthrough in the technological development of TOF analyzers arose from the design of the orthogonal acceleration TOF analyzer (oaTOF). In an oaTOF analyzers, pulses of ions are extracted orthogonally from a continuous ion beam. Specifically, ions fill the first stage of the ion accelerator in the space between the extraction plate and a grid. A pulsed electric field is then applied at a frequency of several kilohertz, which force ions to assume a direction orthogonal to their original trajectory, and then begin to fly towards the analyzer. The most significant advantages of oaTOF analyzers are: *i)* high mass resolving power, and *ii*) mass accuracies even up to or below 1 ppm. Therefore, it is not surprising that oaTOF instruments are currently widespread used in combination with GC and fast GC.

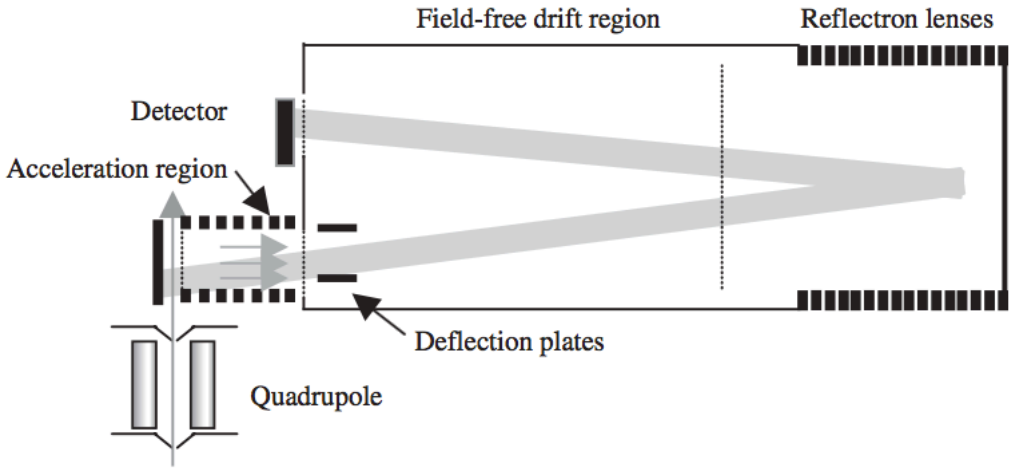

Figure 1.11. The working principle of a single-stage reflectron.

1.4.2.3 Ion mobility spectrometers

Ion mobility spectrometry (IMS) arose in the 1970s as a modern analytical

technique for the separation and subsequent detection of volatile and semi-volatile organic compounds based on the separation of their gaseous ions in a low or high electric field at ambient pressure. The first coupling of ion mobility to MS is attributed to McDaniel who, between the 1950s and 1960s, developed drift cells coupled to a magnetic sector mass analyzer, with the objective of studying ion mobility and ion-molecule reactions [54] IMS enables the discrimination of ions by size, shape, charge as well as mass, thus providing additional information to the chromatographic separation of molecules and mass spectrometric separation of ions. Four methods of ion mobility separation can be combined with MS, namely drift-time ion mobility spectrometry (DTIMS), aspiration ion mobility spectrometry (AIMS), differential-mobility spectrometry (DMS) also called field-asymmetric waveform ion mobility spectrometry (FAIMS) and traveling- wave ion mobility spectrometry (TWIMS).

Ions exposed to an electric field experience a force and are accelerated along the field lines. Upon addition of a buffer gas, the motion of the ions becomes more complicated as collisions with the gas scatter the ions in random directions as it diffuses. However, if an ion cloud is given enough time to reach equilibrium and the electric field is uniform throughout, the ion cloud will travel with constant velocity parallel to the field lines and simultaneously grow in size due to diffusion. This constant equilibrium velocity is the result of forward acceleration by the field and decelerating friction by collisions. Following Mason and McDaniel [55], for weak electric fields of magnitude E, the drift velocity v is directly proportional to E with the proportionality constant K called ion mobility

$$v = KE \qquad (\mathbf{1.1})$$

Since v is inversely proportional to the buffer gas number density N, the mobility K is also inversely proportional to N. Here N (in units of molecules per volume) is used as the relevant quantity to express pressure because N is, in contrast to pressure p, decoupled from the temperature T. Because K depends on N it is practical to convert K into the pressure-independent quantity $K_o \propto NK$, where K_o is termed the reduced mobility

$$K_0 = \frac{p}{p_0} = \frac{T_0}{T}K \quad (\mathbf{1.2})$$

with the constants p_o = 760 Torr and T_o = 273.15 K.

A field is considered weak if the average ion energy acquired from the field is small compared to the thermal energy of the buffer gas molecules. This ion field energy is proportional to v^2 or $(KE)^2$. However, for a given ion with given Ko $\propto NK$ it is the ratio E/N which determines whether a field is weak or strong, and collisional heating due to the field is given by equation

$$T_{\text{eff}} - T = (M/3k_b)\,(NK)^2(E/N)^2 \quad (\mathbf{1.3})$$

Here T_{eff} is the effective temperature, M the mass of the buffer gas particle, and k_B the Boltzmann constant.

Following Equation (1.1), a measurement of K involves measuring the drift time t of a pulse of ions traveling in a weak field E over a given drift length L. The spread, Δx, of a cloud of identical ions due to diffusion, the random part of motion, is given by

$$x = \sqrt{\frac{4k_bTL}{\pi Ee}} = \sqrt{\frac{4k_bTL^2}{\pi Ve}} \quad (\mathbf{1.4})$$

where *e* is the ion charge and *V* the voltage across the drift region.

Because the resulting acceleration of the ion by *E* is proportional to *e*, the mobility is also proportional to *e*. In addition, because the deceleration of the ion by friction is proportional to the buffer gas number density *N* and because large ions experience more friction than small ions, the mobility is inversely proportional to both *N* and the collision cross section σ of the ion. Using momentum transfer theory, a statistical approach to balance ion energy and momentum gained in the electric field and lost in buffer gas collisions, a quantitative relationship between *K* and the quantities *e*, *N*, and σ can be derived,

$$K = \frac{3e}{16N}\sqrt{\frac{2\pi}{k_bT}}\frac{1}{\sigma} \quad (\mathbf{1.5})$$

where μ = *Mm / (M* + *m*) is the reduced mass of buffer gas (with mass *M*) and ion (with mass *m*).

1.4.2.3.1 Collision cross section

Ion mobility separations are based on differences in ion structures (or cross sections) and charge states. The latter is established by the excess charge on each species. Ion cross sections represents the effective area for the interaction between an individual ion and the neutral gas through which it is travelling [56]. Two ions of equal mass and charge, but different three-dimensional conformation, will travel through an IMS device at velocity dependent on their mobilities, providing different drift times. Specifically, the ion with a more

compact conformation will undergo fewer collisions with the neutral gas than do more open. Therefore, compact species with small collision cross sections (CCS, Ω) will have higher mobilities than do more open forms of the ion.

The mobility can be used to obtain a CCS for a specific ion according to the Mason-Schamp equation [57] where K_0 is the reduced mobility (measured mobility at standard temperature and pressure), z is the charge state of the ion, e is the elementary charge, N is the number density of the drift gas,

$$\Omega = \frac{3ze}{16N}\left(\frac{2\pi}{\mu k_b T}\right)^{1/2}\frac{1}{K_0} \quad (\mathbf{1.6})$$

μ is the reduced mass of the ion-neutral drift gas pair, k_B is the Boltzmann constant and T is the gas temperature. The proportional relationship between Ω and K_0 is true for value equal or under the "low-field limit", where the ratio between electric field strength and buffer gas density is small than 2×10^{-17} V cm^2 [58]. Despite the IMS devices previous discussed will all separate ions according to differences in their mobility through a buffer gas, only the time-based mobility devices (DT-IMS, TW-IMS) can be used to determine information about cross- sectional area.

1.4.2.3.2 Resolution

The resolution of an IMS device depends in practice not only on the spread of ions Δt due to diffusion in the drift region relative to the drift time t, but also on the drift tube-independent spread of the ion cloud, Δt_o, brought about by the initial width of the ion pulse entering the drift region and the spread of ions after the drift region (e.g., in the ion funnel). Following Equation (1.4), the resolution $t/\Delta t$ is affected only by the two parameters: temperature T and drift voltage V.

$$\frac{t}{\Delta t} = \frac{L}{\Delta x} = \sqrt{\frac{\pi V e}{4 k_b T}} \quad (\mathbf{1.7})$$

Reducing T decreases diffusion and thus Δt. Increasing the voltage reduces both t and Δt, with the ratio $t/\Delta t$ being proportional to $\sqrt{V/T}$. However, whereas increasing L is a reasonable approach to improve resolution, increasing E requires simultaneous increase in N in order to keep E/N constant and to stay in the low-field regime desirable for ion mobility experiments. For high-resolution devices the pulse width Δt_o may be an additional limitation to resolution. Once Δt reaches a small value and the resolution is determined by Δt_o, further optimization of the parameters E, N, and T does not further improve the resolution. Hence the design of an ion mobility instrument requires a careful balance of ion energy, technical feasibility, and all the quantities determining the resolution. High voltage supplies, insulators, and discharge problems set limits to V; discharge and pumping requirements may set limits to N; space requirements set limits to L; choice of materials, insulation, discharge due to water condensation, and thermal equilibration set limits to T; and speed of switches, ion space charge, and signal intensity set limits to Δt_o.

Therefore, an instrument with given fixed parameters L, Δt_o, and T and with maximum allowable pressure N may operate with maximum resolution at a field value E_{max} smaller than the instrument limit and smaller than allowed due to E/N limitations. Hence whereas the resolution is optimum for $E = E_{max}$, it drops both for $E < E_{max}$ due to smaller $t/\Delta t \propto \sqrt{\frac{v}{t}}$ values [Equation (1.7)] and for $E > E_{max}$ due to smaller $t/\Delta t_o \propto t \propto 1/E$ values [Equation (1.1)].

$$t = \frac{L}{v} = \frac{L}{KE} \quad (\mathbf{1.8})$$

1.4.3 Tandem mass spectrometry

The goals of any mass spectrometry analysis are to obtain more structural information on the analyte of interest, sometimes unattainable either (*i*) because the ionization technique used produces relatively few structurally diagnostic fragments (as for soft ionization), or (*ii*) because its fragmentation is suppressed by the presence of other compounds in the mixture introduced in the ion source, or (*iii*) because it is obscured by other ions generated from the matrix in the course of ionization. For such reason, the strong need of new techniques able to bypass these problems, and provide much valuable information about the molecular structure, led to development of tandem mass spectrometry. The term tandem mass spectrometry, or simply tandem MS, refers to any general methods where a given ion is subjected to a second mass spectrometric analysis, either in conjunction with a dissociation process or in a chemical reaction (59). Tandem MS is also defined as mass spectrometry/mass spectrometry (MS/MS). Several modern mass spectrometers consist of two or more mass analyzers to perform the so-called *tandem-in-space* MS/MS, where different mass analyzers are involved "in different spaces". This MS/MS technology is based on the isolation of a specific precursor ion (*m/z*), and then undergone to dissociation and production of fragment or product ions. However, due to rapidly decreasing transmission and increased instrumental complexity and size, only MS/MS experiments are allowed, while MS^3 experiments and beyond are rarely

performed in tandem-in-space instruments. Systems such as QqQ, Q-ToF, ToF/ToF belong to such a tandem MS technique. In all these combinations, the first and the final analyzers operate the ion isolation and scan, whereas the second analyzer is a collision cell that allows ion fragmentation.

There are four mains MS/MS scan modes usually used: product ion scan, precursor ion scan, neutral loss scan, and selected reaction monitoring. In the product ion mode, the first analyzer selects a precursor ion of interest, which is fragmented into the collision cell, thus generating the product ions analyzed by the second analyzer. In the precursor ion scanning, the second analyzer is held static at the *m/z* of a specific product ion only after collision, whereas the first mass analyzer is scanned across the desired *m/z* range. This experiment results in a spectrum of precursor ions that produce that particular product ion during collision induced dissociation (CID) fragmentation. During the neutral loss scanning process, both the first and the second analyzer work in concert with a constant mass offset of "x". When a precursor ion is transmitted through the first mass analyzer, this ion is recorded if it produces a product ion corresponding to the loss of a neutral fragment of ''x'' from the precursor ion after collision cell. In the selected reaction monitoring scan mode, the first analyzer is set on the specific precursor mass, the collision energy is optimized to produce a diagnostic fragment of that precursor ion, and the second analyzer focuses on the specific mass of that fragment. Only ions with this exact transition will be detected. This process is also known as multiple reaction monitoring (MRM) in the case of first or second or both mass analyzers are set to monitor for multiple reactions. This technique is broadly used for quantitative analysis of individual molecular species.

Along the tandem-in-space, the tandem-in-time is the other possible MS/MS method processing, which employs a single mass analyzer where ions are

trapped, isolated, and subsequently fragmented “in the same space”. This is only possible in trapping devices, such FT-ICR and IT-ToF. The time spent by the ions in the trap defines the number of MS^n measurements that can be performed. In fact, such a trapping device-based mass analyzers are well suited for multiple stage MS experiments.

References

[1] W.A. Harris, P.T.A. Reilly, W.B. Whitten, Anal. Chem. 79 (2007) 2354.

[2] D.B. Robb, T.R. Covey, A.P. Bruins, Anal. Chem. 72 (2000), 3653

[3] V.V. Laiko, M.A. Baldwin, A.L. Burlingame, Anal. Chem., 72 (2000), 652.

[4] Z. Takats, J.M. Wiseman, B. Gologan, R.G. Cooks, Science, 5695 (2004) 471–3.

[5] R.B. Cody, J.A. Larame, H.D. Durst, (2005) Anal. Chem., 77, 2297–302.

[6] J.J. Thomson, Philos. Mag. 44 (1897) 293.

[7] J.J. Thomson, Philos. Mag. 13 (1907) 561.

[8] F.W. Aston, Philos. Mag. 38 (1919) 709.

[9] A.J. Dempster, Phys. Rev. 11 (1918) 316.

[10] A.O. Nier, Int. J. Mass Spectrom. Ion Proc. 1990, 100, 1-13.

[11] K.H. Einführung, H. Kienitz (Ed.), Massenspektrometrie, Weinheim, Verlag Chemie (1968).

[12] W. Bleakney, Phys. Rev. 34 (1929) 157.

[13] A.O. Nier, Rev. Sci. Instrum, 18 (1947) 415.

[14] M. Barber, R.S. Bordoli, R.D. Sedgwick, A.N. Tayler, J. Chem. Soc., Chem. Commun. 7 (1981) 325.

[15] J. B. Fenn, M. Mann, C.K. Meng, S.F. Wong, C.M. Whitehouse, Science 246 (1989) 64.

[16] M. Karas, D. Bachmann, F. Hillenkamp, Anal. Chem. 57 (1985) 2935.

[17] W. E. Stephens, Phys. Rev. 69 (1946) 691.

[18] W. Paul, H. Steinwedel, Z. Naturforsch. A, 8 (1953) 448.

[19] E.G. Johnson, A.O. Nier, Phys. Rev. 91 (1953) 12.

[20] W. Paul, H.S. Steinwedel, (1960) US Patent, 2939952.

[21] H. Sommer, H.A. Thomas, J.A. Hipple, Phys. Rev. 76 (1949) 1877.

[22] K.K. Murray, R.K. Boyd, M.N. Eberlin, G.J. Langley, L. Li, Y. Naito, Pure Appl. Chem. 85 (2013) 1515.

[23] J.F.J. Todd, Int. J. Mass Spectrom. Ion Proc. 142 (1995) 211.

[24] M.P. Balogh, Spectrosc. 19 (2004) 34.

[25] A.W.T. Bristow, Mass Spectrom. Rev. 25 (2006) 99.

[26] I. Ferrer, E.M. Thurman, Rapid Commun. Mass Spectrom. 21 (2007) 2538.

[27] J. Yergey, D. Heller, G. Hansen, R.J. Cotter, C. Fenselau, Anal. Chem. 55 (1983) 353.

[28] R.C. Werlen, Rapid Commun. Mass Spectrom. 8 (1994) 976.

[29] S. Kim, R.P. Rodgers, A.G. Marshall, Int. J. Mass Spectrom. 251 (2006) 260.

[30] R.A. Zubarev, P.A. Demirev, P. Håkansson, B. Sundqvist, Anal. Chem. 67 (1995) 3793.

[31] K.R. Clauser, P. Baker, A. Burlingame, Anal. Chem. 71 (1999) 2871.

[32] R.A. Zubarev, P. Håkansson, B. Sundqvist, Anal. Chem. 68 (1996) 4060.

[33] W.V. Ligon, Jr. Science 205 (1979) 151.

[34] F.H. Field, J.L. Franklin, Electron Impact Phenomena and the Properties of 3Gaseous Ions; New York, Academic Press (1957).

[35] A. J. Dempster. Phys. Rev. 18 (1921) 415.

[36] M.S.B. Munson, F.H. Field, J. Am. Chem. Soc., 88 (1966) 2681.

[37] J. Abian, J.Mass Spectrom. 34 (1999) 157.

[38] A.S. Gohlke, F.W. McLafferty J. Amer. Soc. Mass Spectrom. 4 (1993) 367.

[39] J.S. Svendsen, L.K. Sydnes, J.E. Whist, Org. Mass Spectrom. 22 (1987) 421.

[40] P. Scribe, J. Guezennec, J. Dagaut, C. Pepe, A. Saliot, Anal. Chem. 60 (1988) 928.

[41] F.W. McLafferty, D.B. Stauffer, A.B. Twiss-Brooks, S.Y. Loh, J. Am. Soc. Mass Spectrom. 2 (1991) 432.

[42] P. H. Dawson, Quadrupole mass analyzers: performance, design, and some recent applications, Mass Spectrom. Rev. 5, (1986), 1–37.

[43] J. E. Campana, Elementary theory of quadrupole mass spectrometry, Int. J. Mass Spectrom. Ion Proc. 33, (1980), 101–117.

[44] P. E. Miller, M. Bonner Denton, The quadrupole mass filter: basic operating concepts, J. Chem. Educ. 63, (1986), 617–622.

[45] D.W. McLachlan. Theory and Applications of Mathieu Functions. Oxford, Clarendon Press (1947).

[46] Stephens, W. Phys. Rev., 69, (1946), 691.

[47] Wiley, W.C. and McLaren, J.B. Rev. Sci. Instrum., 16, (1955), 1150.

[48] M. Guilhaus, Adv. Mass Spectrom. 13 (1995) 213.

[49] Weickhardt, C.; Moritz, F.; Grotemeyer,. Mass Spectrom. Rev. 15, (1997), 139-162.

[50] Cotter, R.J. Time-of-Flight Mass Spectrometry: Instrumentation and Applications in Biological Research; ACS: Washington, DC, 1997.

[51] Enke, C.G. The Unique Capabilities of Time-of-Flight Mass Analyzers. Adv. Mass Spectrom. 1998, 14, 197-219.

[52] M. Moniatte, F.G. van der Goot, J.T. Buckley, F. Pattus, A. van Dorsselaer, FEBS Lett., 384 (1996) 269.

[53] Mamyrin, B.A., Karataev, V.I., Schmikk, D.V. and Zagulin, V.A. Sov. Phys. JETP, 37, (1973), 4.

[54] McDaniel E.W., Martin D.W., Barnes W.S., Rev. Sci. Instrum. 33, 1962, 2-7.

[55] Mason, E. A.; McDaniel, E. W., Transport properties of ions in gases; Wiley: New York, 1988.

[56] Mason E.A., McDaniel E.W., WILEY VCH Verlag GmbH& Co. KGaA, Weinheim, Federal Republic of Germany 1988.

[57] Mason E.A., Schamp H.W. Jr., Ann. Phys. 4, (1958), 233-270.

[58] Creaser C.S., Griffiths J.R., Bramwell C.J., Noreen S., Hill C.A, Thomas C.L. P., Analyst, 129, (2004), 984-994.

[59] Busch K.L., Glish G.L., McLuckey S.A., Wiley VCH 1988.

Chapter 2

Comprehensive two-dimensional gas chromatography: fundamentals and theoretical/practical considerations

2.0. Introduction

The real world is characterized by enormously heterogeneous matrices in terms of complexity and chemical composition. Some substances, such as natural oils and fats (e.g. butter, olive oil, etc.) are relatively simple, while others, such as coffee aroma or crude oil, are very complex.

The most challenging step of the modern separation science is to provide analytical methods suitable for a whole range of diversified purposes; some analysts, for example, focused their attention to rapid and efficient separations, while others require high-resolution power and/or highly selective and sensitive detection systems.

The term “chromatography" was first employed by the Russian scientist Mikhail Tswett in 1903 [1]. Tswett made a separation on a vegetable extract using a column packed with carbonate calcium and observed the formation of a series of coloured bands. The term "chromatography" comes from Greek words “χρώμα” (color) and “γραφειν” graphein” writing”, connected to that visible separation.

Unfortunately, the scientific community did not immediately accept that brilliant and revolutionary idea, and its dissemination occurred only in the 1930s.

Today, the definition of chromatography, officially recognized by IUPAC, is that of a physical separation method in which the components to be separated are distributed between two phases, one of these is stationary (stationary phase) while the other (mobile phase) moves in one specific direction [2].

An efficient chromatographic process is observed when different forces characterize the physical interactions of analytes and when the transfer properties of system between phases are favourable. An ideal separation process made when all the components of a mixture are located in different zones, so that they occupy distinct bands along the stationary phase. Band

broadening is the process of increase in width of the chromatographic band and it's closely related to the separating capacity of the chromatographic system: a big band broadening has a negative effect on peak capacity. The latter can be defined as the maximum number of peaks that can be separated, with a specific resolution, in one analysis. Chromatographic techniques are usually classified on the basis of the physical state of the phases involved in the separation process. For example, in liquid-liquid chromatography (LLC or simply LC) the two phases are liquid. When instead the mobile phase is a gas and the stationary phase is a solid or liquid, the separation techniques are defined respectively as gas-solid chromatography (GSC) and gas-liquid chromatography (GLC). Gas-liquid chromatography is often called as gas chromatography (GC) and it is the most used technique.

Gas chromatography (GC), with open-tubular capillaries (OTC), is a powerful separation technique that is particularly suitable for the analysis of volatile and semi-volatile compounds. Since the introduction of open-tubular capillaries gas chromatography by Golay [3], many examples have showed the potential of this approach for an exact identification and quantification of complex matrices. The excellent resolution obtained by one-dimensional (1D) GC makes this technique the favourite one in many applications. Improvements of detectors have shown that many food, petrochemical and environmental sample are much complex than we assumed in the past, for this reason is required a further separation dimension, through which these analytes can be differentiated. For example, if in the first dimension the compounds are separated in according to their different volatiles propriety in the second dimension is required a different mechanism (e.g. different polarities) so as to separate possible co-elution(s). Proper use of the information provided by the several separation procedures will yield accurate information on the composition of the analysed sample. If each separation mechanism applied for

the resolution of a mixture is called as separation “dimension”, then we call it multidimensional approach.

2.1 Theory of gas chromatography

The schematic representation of a gas chromatographic system is shown in Figure 2.1. The heart of the system is the column, in which the crucial physicochemical process of the separation occurs. The column contains the stationary phase, while the mobile phase (the carrier gas) is flowing through this column from a pressurized gas cylinder (source of the mobile phase). A pressure and/or flow-regulating unit controls the rate of mobile-phase delivery. An exclusive separation mode for the analytical GC is elution chromatography, in which the sample, a mixture of chemical compounds, is introduced at once, as a sharp band into the mobile-phase stream.

The introduction of the sample is performed through a unit called injector. The whole sample is transferred from that part to the chromatographic column, where continuous redistributions between the mobile phase and the stationary phase occur.

Due to their different affinities for the stationary phase the individual components, eventually, form their own concentration bands, which reach the column’s end at different times. A detector is situated at the column’s end to identify and/or quantify the single components eluting from the column. The detector, together with auxiliary electronic and recording devices, generates the chromatogram of which an example is shown in Figure 2.2 A chromatogram is, basically, a plot of the sample concentration (y axis) versus time (x axis). It represents the individual component bands separated by the chromatographic column.

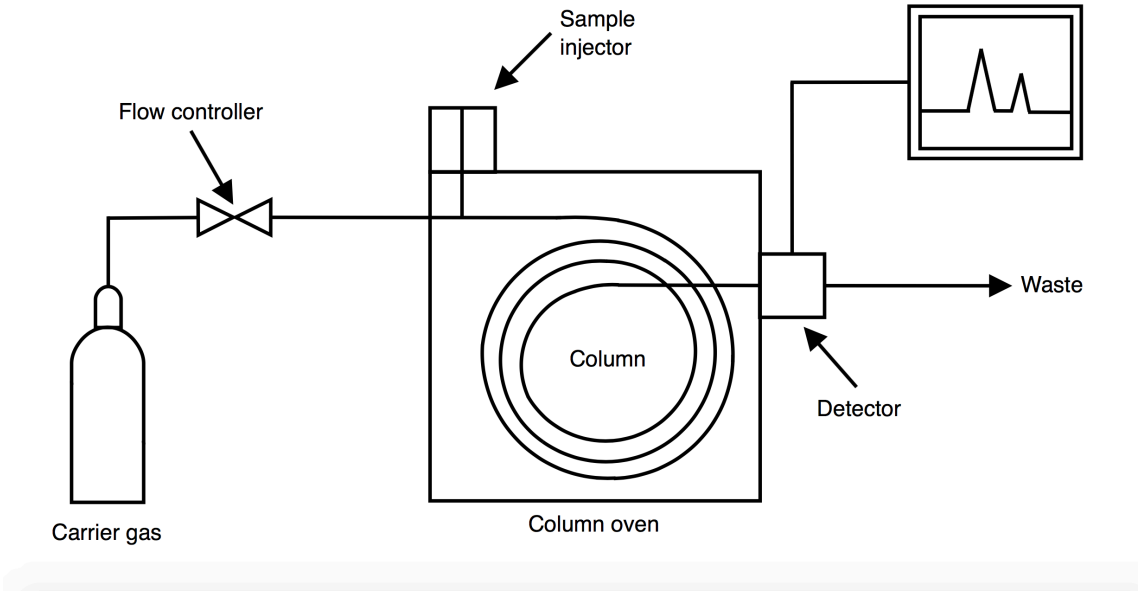

Figure 2.1. The main components of a gas chromatograph.

The position of a peak on the time scale of the total chromatogram brings some qualitative information, sine each chromatographic peak represents at least one chemical substance. The areas under the peaks are, however, related to the amounts of individual substances separated in time and space.

A typical gas chromatograph has three independently controlled thermal zones:

i. the injector zone that ensures rapid volatilization of the introduced sample;
ii. the column temperature that is controlled to optimize the separation process;
iii. the detector zone that must be at temperatures where the individual sample components are measured in the vapour phase.

As shown in Figure 2.2, different sample components appear at the column's end at different times.

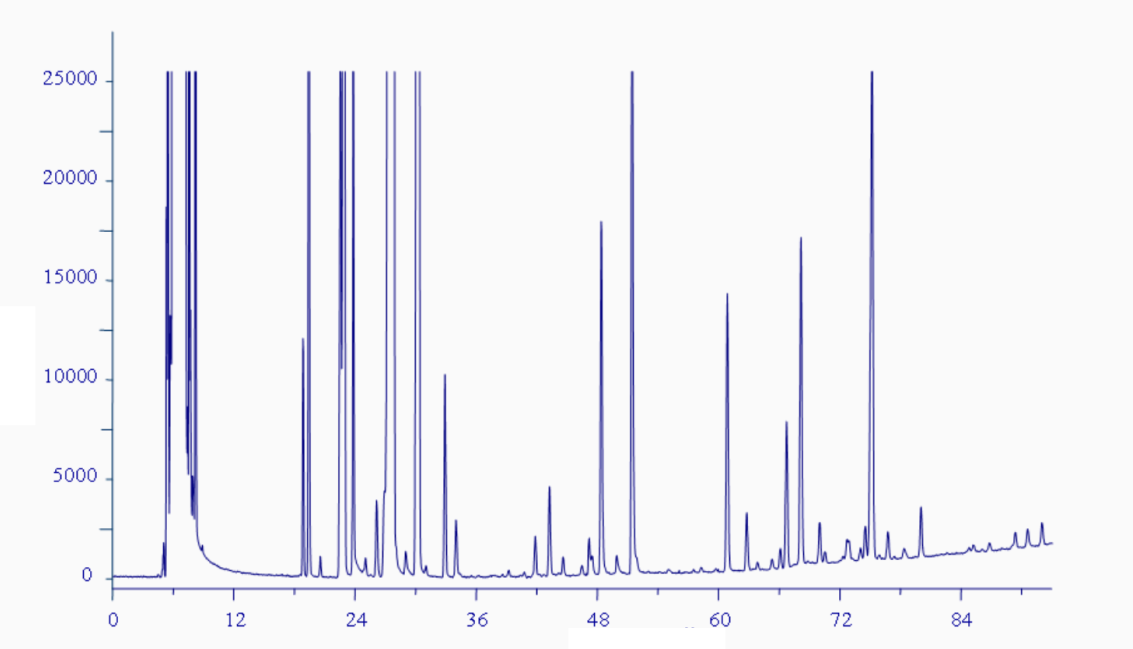

Figure 2.2. GC chromatogram example. (personal data)

The retention time t_r is the time elapsed between injection and the maximum of a chromatographic peak. It is defined as

$$t_r = t_0 1 + k \quad (\mathbf{2.1})$$

where t_0 is the retention time of a component that has no interaction with the stationary phase, and k is the capacity factor. The capacity factor is further defined as:

$$k = \mathrm{K}\,\frac{\mathrm{V_s}}{\mathrm{V_m}} \quad (\mathbf{2.2})$$

where k is the solute's distribution coefficient (concerning to a distribution between the stationary and the mobile phases), V_s is the volume of the stationary phase, and V_m is the volume of the mobile phase in a chromatographic column.

The distribution coefficient $K=C_s/C_m$ (where C_s is the solute concentration in the stationary phase and C_m is the solute concentration in the mobile phase) is a thermodynamic quantity that depends on temperature. The molecular interactions between the phases and the solutes under separation are strongly temperature-dependent. If, for example, a solid adsorbent (column material) is brought into contact with a permanent (inorganic) gas and a defined concentration of organic (solute) molecules in the gas phase at a certain temperature, some solute molecules become adsorbed on the solid, and others remain in the permanent gas. When the system temperature increases, less solute molecules are adsorbed, and more of them join the permanent gas; the distribution (adsorption) coefficient, as defined above, changes correspondingly. Likewise, if the stationary phase happens to be a liquid, the solute's solubility in it decreases with increasing temperature, according to Henry's law, resulting in a decrease of the distribution (partition) coefficient. According to equations (2.1) and (2.2), the retention time in GC depends on several variables: (a) the chemical nature of the column phase and its temperature, as reflected by the distribution coefficient; (b) the ratio of the phase volumes in the column V_S/V_M; and (c) the value of t_0. These variables are used to maximize the component separation and the speed of analysis. Unlike some other chromatographic processes, the physical interactions between the mobile phase and solute molecules in GC are, for all practical purposes, negligible. Thus, the carrier gas serves only as means of molecular (solute) transport from the beginning to the end of a chromatographic column. The component separation is then primarily due to the interaction of solute molecules with those of the stationary phase. Since a variety of column materials are available, various molecular interactions can be used to enhance the component separation. Moreover, these interactions are temperature-dependent. For the mixture component with no affinity for the stationary

phase, the retention time t_0 serves merely as the marker of gas linear velocity μ (in cm/s) and is actually defined as:

$$t_0 = L/u \quad (\mathbf{2.3})$$

where L is the column length. The gas velocity is, in turn, related to the volumetric flow rate F since:

$$\mu = F/s \quad (\mathbf{2.4})$$

where s is the column cross-sectional area. The gas-flow rate is mainly regulated by the inlet pressure value; higher inlet pressure results in greater gas-flow rate (and linear velocity), and consequently, shorter t0.
Correspondingly, fast GC separations are performed at high gas-inlet pressures. The so-called retention volume VR is a product of the retention time and volumetric gas-flow rate:

$$\mathrm{V_R} = \mathrm{t_r F} \quad (2.5)$$

Since the retention times are somewhat indicative of the solute's nature, a means of their comparison must be available. Within a given chemical laboratory, the relative retention times (the values relative to an arbitrarily chosen chromatographic peak) are frequently used:

$$\alpha_{2,1} = \frac{\mathrm{t_{R2}}}{\mathrm{t_{R1}}} = \frac{\mathrm{V_{R2}}}{\mathrm{V_{R1}}} = \frac{\mathrm{K_2}}{\mathrm{K_1}} \quad (2.6)$$

This equation is also a straightforward consequence of Eqs. (2.1) and (2.2). Because the relative retention represents the ratio of distribution coefficients

for two different solutes, it is frequently utilized (for the solutes of selected chemical structures) as a means to judge selectivity of the solute–column interactions.

For interlaboratory comparisons, the retention index is the best method for documenting the GC properties of any compound. The retention index system compares retention of a given solute (on a logarithmic scale) with the retention characteristics of standard solutes solution that usually are a homologous series of compounds:

$$I = 100_z + 100\,\frac{\log t_{R(x)} - \log t_{R(z)}}{\log t_{R(z+1)} - \log t_{R(z)}} \qquad (2.7)$$

The term z represents the number of carbon atoms within a homologous series, while x relates to the unknown. For example, a series of n-alkanes can be used in this direction; each member of a homologous series (differing in a single methylene group) is assigned an incremental value of 100 (e.g., 100 for methane, 200 for ethane, and 300 for propane, etc.) and if a given solute happens to elute from the column exactly half-way between ethane and propane, its retention index value is 250. Retention indices are relatively independent of the many variables of a chromatographic process.

In the program temperature mode, the n-paraffin elutes linearly. Each peak adds a steady increase to the retention time of its predecessor. The relationship between retention time and carbon atoms number is:

$$t_r T = a' x\, c_n + b' \quad (2.8)$$

where a' e b' are constant of proportionality

In case of program temperature analysis, the retention index is expressed as follows:

$$I^T = 100 \left[z + (t^T R\, i - t^T R / t^T R\, (z+1) - t^T R\, z) \right] \quad (2.9)$$

The index calculated in this mode are called “linear retention index” (LRI). For each compound and a specific stationary phase, the index values obtained in isothermal and in program temperature are different. Furthmore, in temperature program the IT could also changes in relation to specific temperature program and initial temperature of the oven.

The success of GC as a separation method is primarily dependent on maximizing the differences in retention times of the individual mixture components. An additional variable of such a separation process is the width of the corresponding chromatographic peak. Whereas the retention times are primarily dependent on the thermodynamic properties of the separation column, the peak width is a function of the efficiency of the solute mass transport from one phase to the other one and of the kinetics of sorption and desorption processes. Figure 2.3 is important to understanding the relative importance of both types of processes. In Figure 2.3a a situation where two sample components are eluted too closely together is showed, so the resolution of their respective solute zones is incomplete; Figure 2.3b represents a situation where the two components are resolved from each other through choosing a (chemically) different stationary phase that retains the second component more strongly than the first one; finally, Figure 2.3c shows the same component retention but much narrower chromatographic peaks, thus represents the most “efficient” handling of the two components. This efficiency, represented by narrow chromatographic zones, can actually be

achieved in GC practice by a proper design in physical dimensions of a chromatographic column.

The width of a chromatographic peak is determined by various column processes such as diffusion of solute molecules, their dispersion in flow streamlines of the carrier gas, and the speeds by which these molecules are transferred from one phase to another. An arbitrary, but the most widely used, criterion of the column efficiency is the number of theoretical plates, N. Figure 2.4 demonstrates its determination from a chromatographic peak.

This number is simply calculated from the measured retention distance t_R (in length units) and the peak width at the peak half-height $W_{1/2}$:

$$N = 5.54\left(\frac{t_r}{w_{1/2}}\right)^2 \quad (2.10)$$

The length of a chromatographic column L is viewed as divided into imaginary volume units (plates) in which a complete equilibrium of the solute between the two phases is attained. Obviously, for a given value of tR, narrower peaks provide greater numbers of theoretical plates than broader peaks.

Equation 2.8 is used to determine the number of theoretical plates, relates to a perfectly symmetrical peak (Gaussian distribution). While good GC practice results in peaks that are nearly Gaussian, departures from peak symmetry occasionally occur. In Figure 2.5, (a) is usually caused by a slow desorption process and undesirable interactions of the solute molecules with the column material, and (b) is associated with the phenomenon of column overloading (if the amount of solute is too large, exceeding saturation of the stationary phase, a fraction of the solute molecules is eluted with a shorter retention time

than the average).

When feasible, GC should be carried out at the solute concentrations that give a linear distribution between the two phases.

The length element of a chromatographic column occupied by a theoretical plate is the plate height *(H):*

$$H = {}^{L}/_{N} \quad (\mathbf{2.11})$$

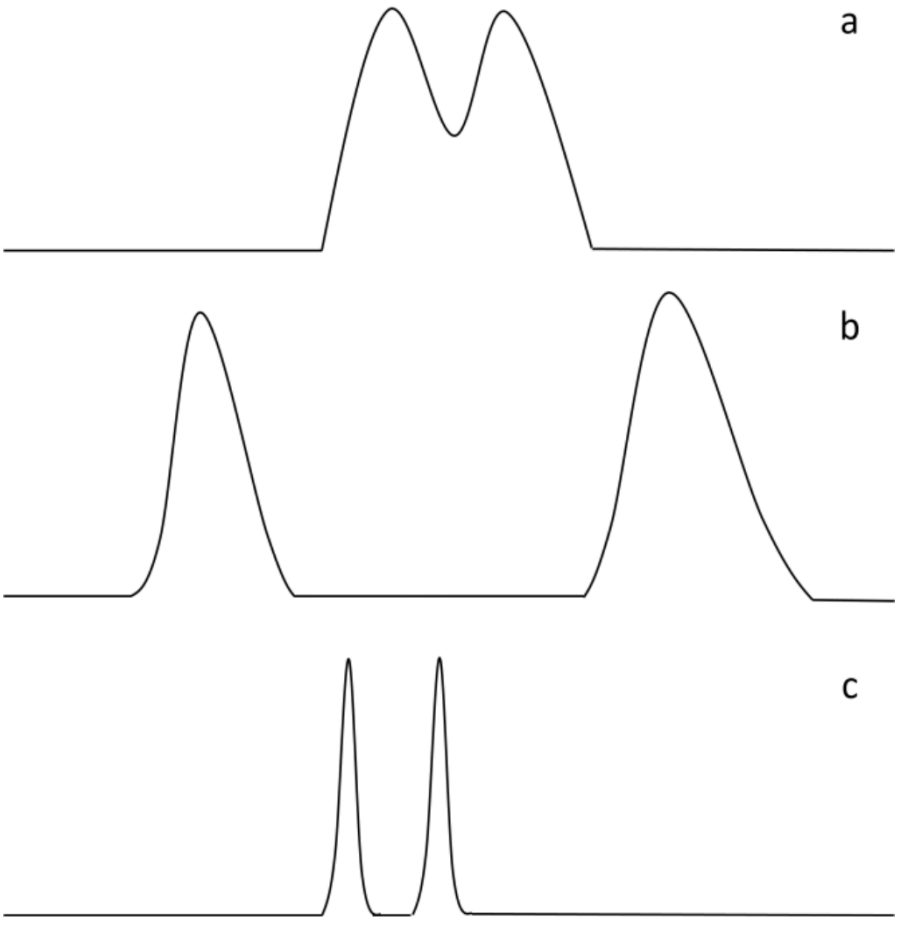

Figure 2.3. Component resolution based on the selectivity and efficiency of the separation process: (a) two not resolved components, (b) resolution based on the column selectivity, and (c) resolution based on the column kinetic efficiency.

The column efficiency N can be dependent on a number of variables. Most importantly, the plate height is shown to be a function of the linear gas velocity μ according to the van Deemter equation:

$$H = A + \frac{B}{u} + Cu \quad (\mathbf{2.12})$$

where the constant A describes the chromatographic band dispersion caused by the gas-flow irregularities in the column. The B-term represents the peak dispersion due to the diffusion processes occurring longitudinally inside the column, and the C-term is due to a flow-dependent lack of the instantaneous equilibrium of solute molecules between the gas and the stationary phase.

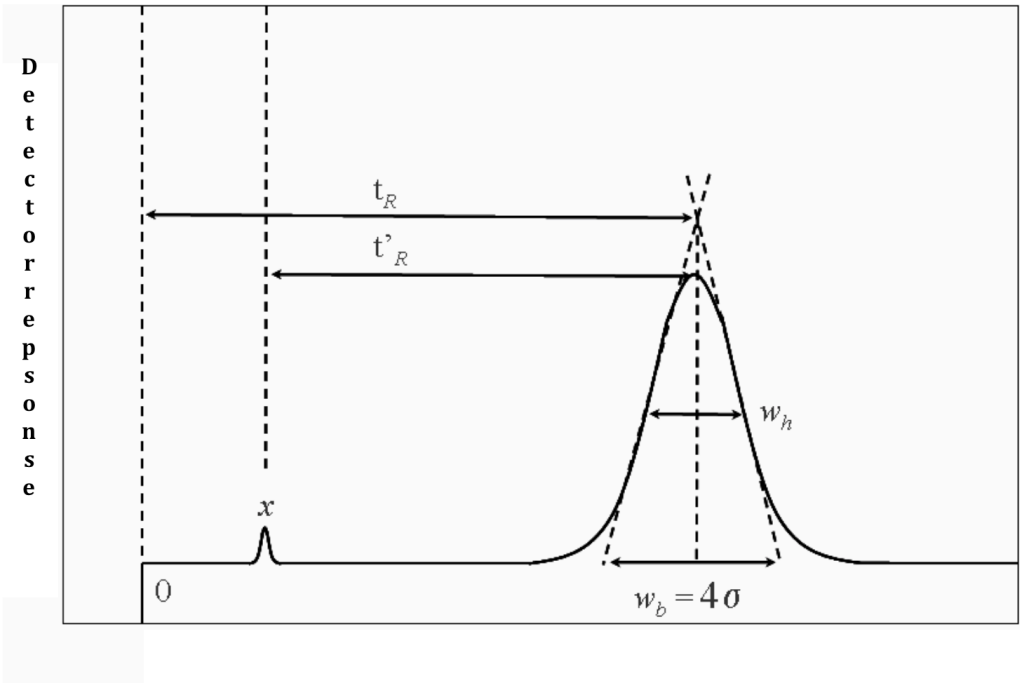

Figure 2.4. Determination of the number of theoretical plates of a chromatographic column.

The mass transfer between the two phases occurs due to a radial diffusion of the solute molecules. Equation (10) is represented graphically by a hyperbolic plot, the van Deemter curve, in Figure 2.6.

The curve shows the existence of an optimum velocity at which a given column exhibits its highest number of theoretical plates. Shapes of the van Deemter curves are further dependent on a number of variables: solute diffusion rates in both phases, column dimensions and various geometrical constants, the phase ratio, and retention times. Highly effective GC separations often depend on thorough understanding and optimization of such variables [4]

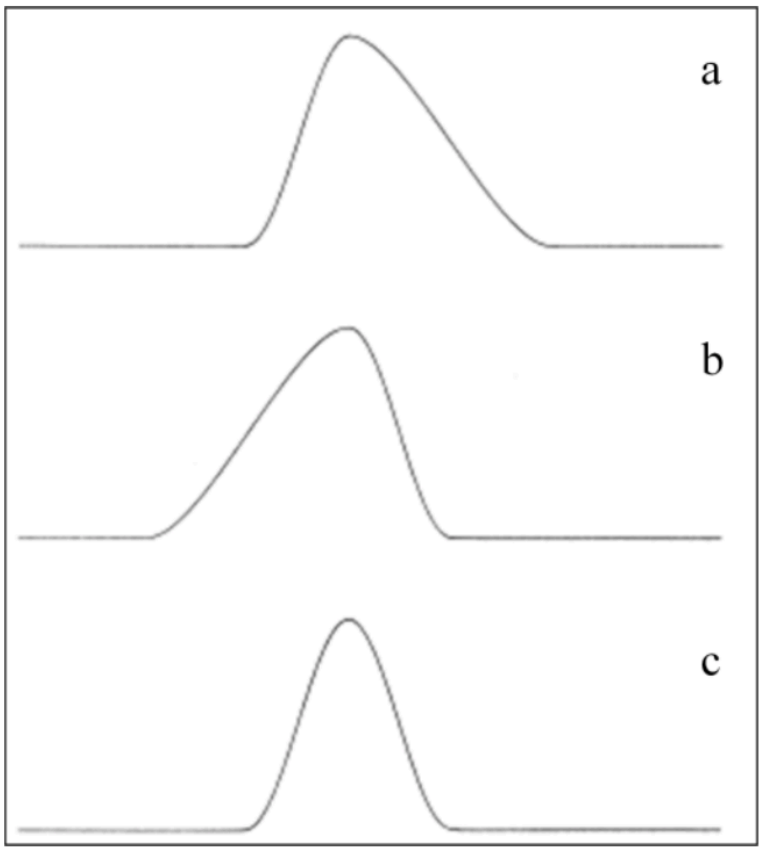

Figure 2.5. Departures from peak symmetry: (a) slow desorption process and (b) column overloading. (c) Gaussian distribution. (personal data)

Since open tubular or capillary columns were introduced in GC, the absence of any packing material inside the column modified the van Deemter equation because their rate equation does not have the *A*-term. This conclusion was pointed out by Golay [5] who also proposed a new term to deal with the diffusion process in the gas phase of open tubular columns.

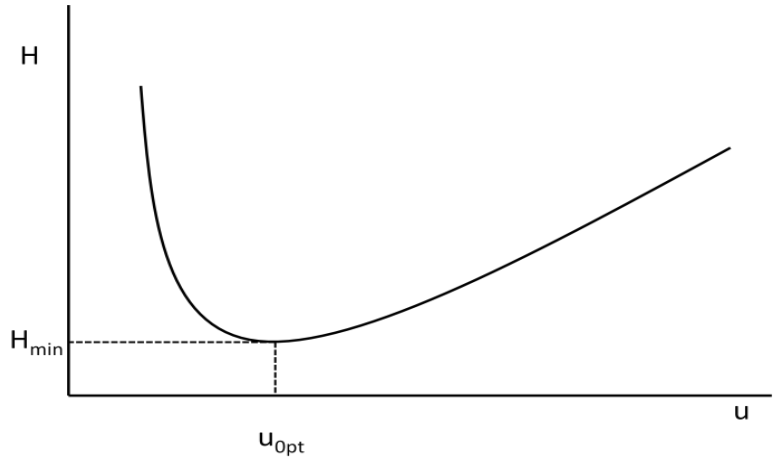

Figure 2.6. Relationship of the plate height and linear gas velocity (van Deemter curve).

His equation had two C-terms, one for the mass transfer in the stationary phase, C_s (similar to van Deemter), and one for mass transfer in the mobile phase, C_m. Thus the Golay equation is:

$$H = \frac{B}{u} + (C_s + C_m)u \quad \mathbf{(2.13)}$$

The *B*-term of equation 2.13 represents the well-known molecular diffusion. The equation governing molecular diffusion is:

$$B = 2D_G \quad (\mathbf{2.14})$$

where DG is the diffusion coefficient for the solute in the carrier gas.

In the Golay equation (eq. 2.13), this term is divided by the linear velocity, so a large velocity or flow rate will also minimize the contribution of the B-term to the overall peak broadening. That is, a high velocity will decrease the time a solute spends in the column and thus decrease the time available for molecular diffusion. The C-terms in the Golay equation relate to mass transfer of the solute, either in the stationary phase or in the mobile phase (6se). Ideally, fast solute sorption and desorption will keep the solute molecules close together and keep the band broadening to a minimum.

The C_S-term in the Golay equation is:

$$C_s = \frac{2kd_f^2}{3 + (1 + k)^2 D_s} \quad (2.15)$$

where d_f is the average film thickness of the liquid stationary phase and D_s is the diffusion coefficient of the solute in the stationary phase. To minimize the contribution of this term, the film thickness should be small and the diffusion coefficient large. Rapid diffusion through thin films allows the solute molecules to stay closer together. Thin film can be achieved by coating small amounts of liquid on the capillary walls, but diffusion coefficients cannot usually control except by selecting low viscosity stationary liquids. Minimization of the C_S- term results when mass transfer into and out of the stationary liquid is as fast as possible. The other part of the C_S-term is the ratio $k/(1 + k)^2$. Large values of 20 result from high solubilities in the stationary phase. This ratio is minimized at large values of k, but very little decrease occurs beyond a k value of about 20. Since large values of retention factor

result in long analysis times, little advantage is gained by k-values larger than 20.

Mass transfer in the mobile phase is shown in the Figure 2.7, which shows the profile of a solute zone as a consequence of non-turbulent flow through a tube. Inadequate mixing in the gas phase can result in band broadening because the solute molecules in the centre of the column move ahead of those at the wall. Small diameter columns minimize this broadening because the mass transfer distances are relatively small.

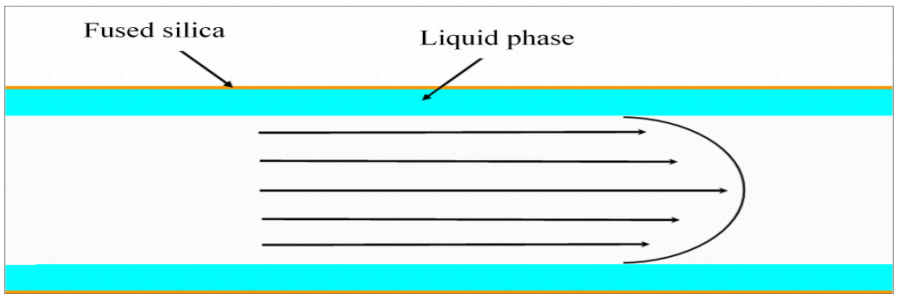

Figure 2.7. Illustration of mass transfer in the mobile phase.

Golay's equation for the C_M term is:

$$C_M = \frac{(1 + 6k + 11k^2){r_c}^2}{24(1 + k)^2 D_G} \quad \mathbf{(2.16)}$$

where r_C is the radius of the column.

The relative importance of the two C-terms in the rate equation depends primarily on the film thickness and the column radius. We can say that for thin films (< 0.2 μm), mass transfer controls the C-term in the mobile phase; for thick films (2-5 μm), it is controlled by mass transfer in the stationary phase; and for the intermediate films (0.2 to 2 μm) both factors need to be considered.

For the larger wide bore columns, the importance of mass transfer in the mobile phase in considerably greater. Finally, another consideration can be made on the C-terms that are multiplied by the linear velocity in equation 2.13: they are minimized at low velocities and so there is much time for the molecules to diffuse in and out of the liquid phase and to diffuse across the column in the mobile gas phase [6]

2.2 Why comprehensive two-dimensional gas chromatography

At present, chromatography is the most commonly applied method for the separation of real-world samples. However, in the last three decades it has become increasingly clear that the baseline separation of all the constituents of a sample is often an arduous challenge when using a single chromatography column. A chromatographic process is governed by two main parameters: i) peak capacity (n_c), and ii) stationary-phase selectivity. The former is related to the column characteristics (*i.e*. length, internal diameter, particle diameter, stationary-phase thickness, intensity of analyte stationary phase interactions, etc.), and to the experimental conditions (*i.e*. mobile phase flow and type, temperature, outlet pressure, etc.). The second parameter is related to the chemical composition of the stationary phase, and hence to the specific type of analyte-stationary phase interactions (*i.e*. dispersion, dipole-dipole, H-bonding, electrostatic, size exclusion, etc.). Selectivity is also dependent on analyte solubility in the mobile phase, whenever this type of interaction occurs. An experienced chromatographer, with an in-depth knowledge of basic theory, will easily get the best out of a column or, in other words, will maximize the number of peaks that can be stacked side by side (with a specific resolution value) in a one-dimensional separation. However, it has been emphasized that such an analytical capability will fall far short of the peak capacity requirements for many applications. In a significant work, Giddings

demonstrated from a theoretical viewpoint that "no more than 37% of the peak capacity can be used to generate peak resolution" and that "many of the peaks observed under these circumstances represent the grouping of two or more close components", and concluded that "s" (the number of single component peaks) can never exceed 18% of n_c [7]. Although such a value does not take stationary phase selectivity into account, it provides an excellent indication of the separation power of a one-dimensional chromatography system. Equation 2.17 is well-known to be the master equation for calculating resolution of two compounds, and it indicates that the resolution (R_S) is affected by three important parameters: efficiency (N, plate number), selectivity (α, separation factor) and retention ($k_1$and k_2, retention factor of the later-eluting compounds):

$$R_s = \frac{\sqrt{N}}{4}\left(\frac{\alpha - 1}{\alpha}\right)\left(\frac{k_2}{k_2 + 1}\right) \quad (\mathbf{2.17})$$

The different degrees of influence of N, α and k on R_S, can be observed in an excellent example shown in figure 2.8, where the separation of two analytes (k_1= 4.8; k_2= 5.0; α = 1.05) on a GC column (N = 20,000), under fixed conditions, is considered. If we drive our attention towards the three variables contained in equation 2.17, and to the effects of their variation on resolution, we can derive the following conclusions:

k) If the column phase ratio is reduced (or a lower temperature applied) leading to an increase in the retention factors, then the benefits gained are very limited in terms of resolution. An increase in k has a substantial effect on R_S only for analytes with low k value (≤ 3).

α) If a more selective stationary phase is employed, by increasing the

separation factor, the resolution will benefit greatly. From equation 2.17 it can be concluded that at lower values, an increase in α will lead to a considerable improvement in resolution, e.g. up to an α value of circa 3. At higher separation factor values, the function tends to level off. Of the three variables, selectivity has the greatest effect on resolution and, thus, it is fundamental to select the most suitable stationary phase for a given separation. However, it is worthy of note that equation 2.17 is valid only for a single pair of analytes and not for a complex mixture of compounds. In the latter case, a change of stationary phase will often lead to a resolution improvement for some analytes, and a poorer result for others. The choice of the most selective stationary phase has the best effects only when a low-complexity sample is subjected to separation.

N) If the column length is extended by four times, leading to an increase in *N* by the same factor, then resolution of the two analytes is only doubled. It follows that an evident improvement in peak resolution can only be achieved by extending the column length considerably. Such a modification is usually not desirable and certainly not a practical solution in view of the greatly increased analysis time.

Thus, it seems that the most effective way of enhancing the separation efficiency (and the selectivity) of a chromatography system, with equivalent detection conditions, is by using a multidimensional chromatographic system. The main driving force behind the interest in multidimensional separations [8-16] was the unrelenting need to resolve more components in complex mixtures from a qualitative and quantitative viewpoint.

2.3 The concept of multidimensionality

A significant variety of combinations of different separation mechanisms can be used to generate multidimensional separations. The basic requirements for achieving a multidimensional separation were discussed by Giddings [7]:

- The components of a mixture should be subjected to two (or more) separation steps in which their displacement is governed by different factors.

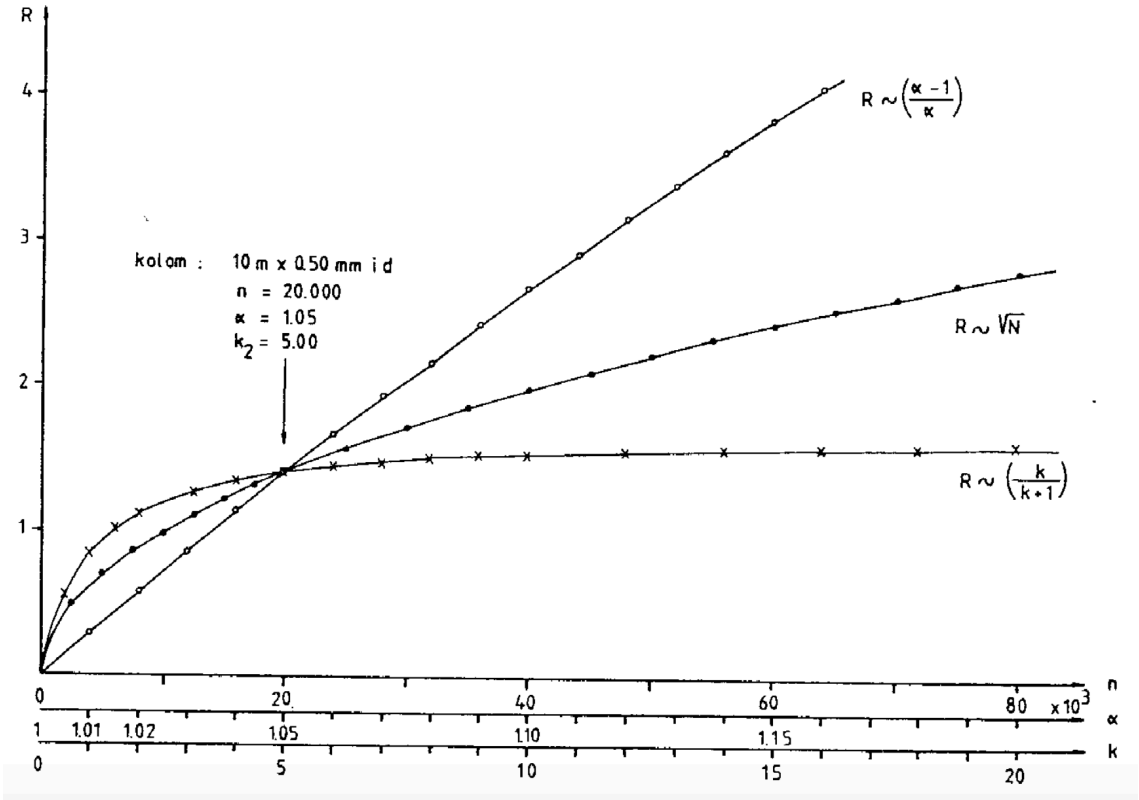

Figure 2.8. Resolution: influence of N, α and k.

- Analytes that have been resolved in the previous step should remain separated until the following separation process is completed.

When two (or more) independent separation mechanisms are used, this will result in an equal number of parameters to define the identity of an analyte [17]. Considering two-dimensional gas chromatography, this approach requires the separate analysis of relatively small fractions of eluate on a first and a second column. If the two dimensions are based on different interaction mechanisms, the separation is said to be "orthogonal" [18]. To illustrate the concept of orthogonality, figure 2.9 represents three degrees of correlation between two separation dimensions. In case of totally orthogonal separations, the peaks are distributed over the entire plane (a). The more the dimensions are correlated, the more the distribution will be centred along the diagonal (b). In the extreme case of total correlation (c), the solutes will have the same retention in the two dimensions. Therefore, the separation dimensions must be correctly selected to produce efficient multidimensional systems. A coherent choice is essential to obtain ordered distributions of compounds and therefore a true increase.

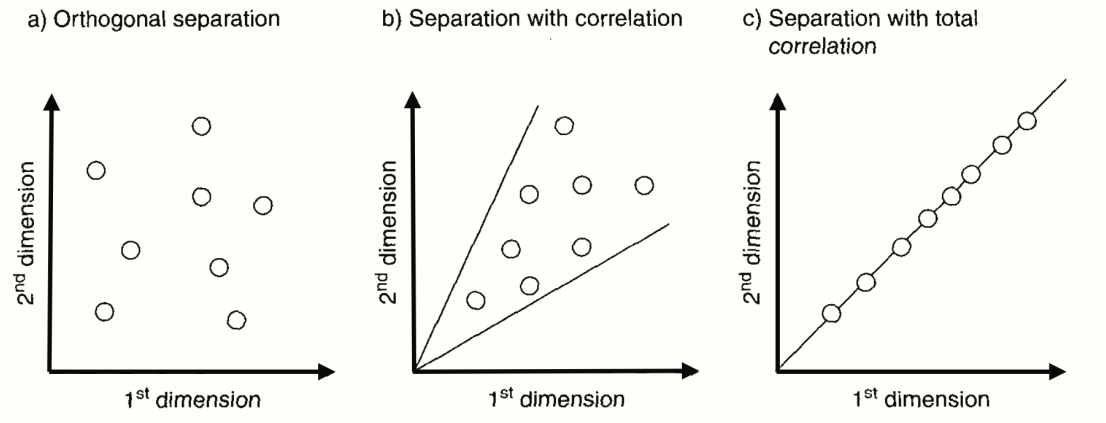

Figure 2.9. Illustration of various degrees of correlation between two separation dimensions.

2.3.1 From MDGC to GC×GC

An on-line multidimensional system is generally characterized by the combination of two columns of different selectivity, with a transfer device located between them. There are two types of multidimensional gas chromatographic approaches, namely: heart- cut GC (MDGC or GC-GC) and comprehensive two-dimensional GC (GC×GC or 2D GC).

In MDGC (figure 2.10 a), two different columns are used, but only a fraction of the material eluting from the first dimension ("heart-cut") is sent into the second dimension for further separation. The number of heart-cuts can be increased only if the time allowed for the separation of the cuts in the second dimension is proportionally reduced (figure 2.10 b). When the number of heart-cuts gets high enough (and the time for their separation short enough), one accomplishes a "comprehensive" separation (figure 2.10 C), in which the entire sample is subjected to separation in both dimensions. Consequently, one can say that GC×GC is essentially an extension of conventional heart-cut GC.

In MDGC, the peak capacity equals the sum of that of the first and second dimensions, the latter multiplied by the number (x) of heart-cuts [$n_{c_1} + (n_{c_2} \times x)$].

The benefits of combining two independent separation processes were recognized very early within the chromatography community. For example, heart-cut multidimensional gas chromatography was first introduced in 1958 by Simmons and Snyder [19], who described a first-dimension boiling-point separation of C_5-C_8 hydrocarbons, and a polarity-based separation in the second dimension, in four distinct analyses. The transfer of chromatographic bands between the two dimensions was achieved by using a valve-based interface.

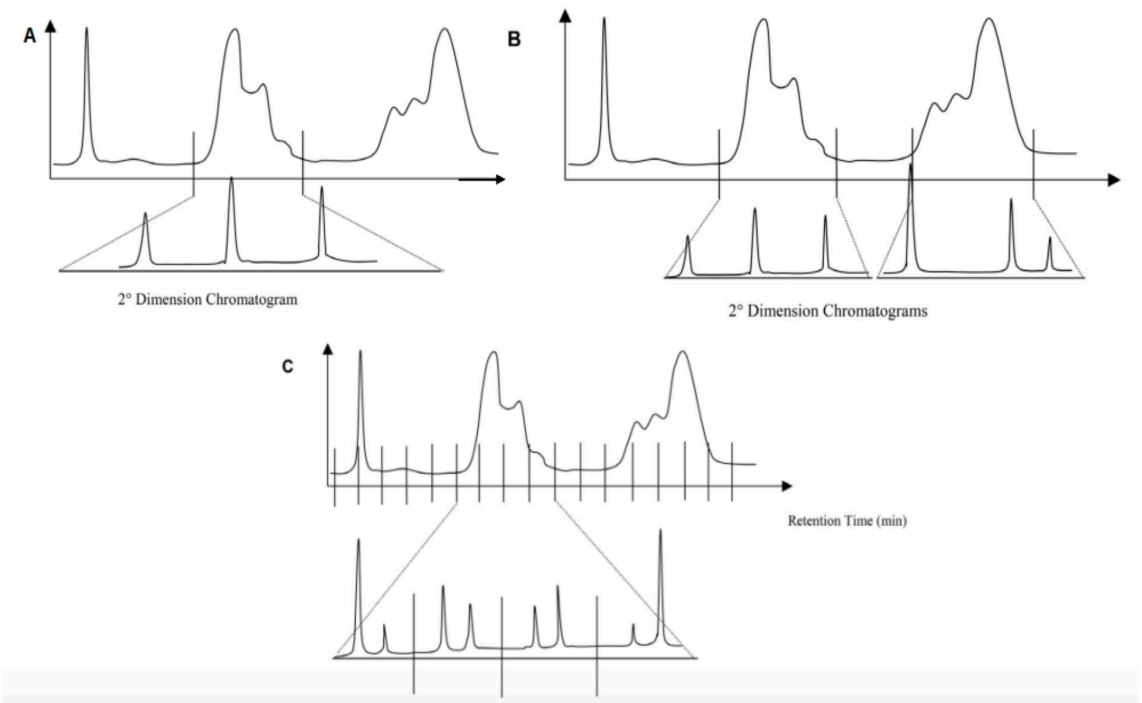

Figure 2.10. The concept of multidimensional GC. (A) single heart-cut GC analysis, where a large portion of the effluent from the primary column is diverted to the second dimension column and separated over an extended period of time. (B) dual heart-cut GC analysis, where two regions are diverted to the second dimension column, but with less time available for each separation. (C) comprehensive two-dimensional GC analysis occurs when the size of the sequential heart-cuts is very short, as are the second dimension chromatograms.

The typical procedure in MDGC is to select the fraction(s) of interest (those containing the target compounds) eluting from the first column and to subject these, one after the other, to the second, independent, separation. MDGC was used quite widely in the final decades of the twentieth century, but it still never became very popular. It probably did not catch on because the instrumental setup, though considered ‘‘fairly simple’’ today, was thought to be too complex for routine use. The main advantages of the MDGC approach are that, in principle, the most powerful ^{2}D column can be selected for each individual target analysis problem. However, MDGC has an important limitation, i.e. that the transfer of one or more fractions to a second column

dramatically increases the total runtime. For example, each ^{2}D analysis will easily add 30 to 45 minutes to the runtime. In summary, the MDGC technique is well suited for the analysis of a limited number of target compounds in highly complex samples, but contrarily it is unsuitable for the general monitoring of entire samples and/or the search for unknowns.

On the other hand, if the entire initial sample requires analysis in two different dimensions, then a different analytical route must be taken, namely a comprehensive chromatographic approach. In an ideal comprehensive chromatography system, the total peak capacity becomes that of the first dimension multiplied by that of the second dimension ($n_c^1 \times n_c^2$).

The first example of comprehensive multidimensional chromatography dates back to over 60 years ago. In 1944, chromatography pioneers described a two-dimensional procedure for the analysis of amino-acids on cellulose as follows [20]: “A considerable number of solvents has been tried. The relative positions of the amino-acids in the developed chromatogram depend upon the solvent used. Hence, by development first in one direction with one solvent followed by development in a direction at right angles with another solvent, amino-acids (e.g., a drop of protein hydrolysate) placed near the corner of a sheet of paper become distributed in a pattern across the sheet to give a 2D chromatogram characteristic of the pair of solvents used”. The combination of solvents was chosen on the basis of R_F values (retardation factor, *i.e.*, movement of band/solvent front), a parameter introduced in that same paper. The amino-acid R_F values for a series of solvent combinations were used to both predict and construct what today we would define as “dot plots”.

With regards to gas-phase chromatographic separations, comprehensive two-dimensional gas chromatography was invented by Phillips in the early 1990s

[8,21], and was developed to meet the increasing need for complex sample analysis and to address limitations regarding peak capacity and restricted specificity of one-dimensional (conventional) GC systems. In the comprehensive chromatographic approach, one can schematically illustrate the usefulness of such a system for the separation of a complex mixture of analytes (figure 2.11). Let's consider a hypothetical sample that contains a large number of analytes that differ in shape, colour, and size. According to Giddings's guidelines [13] the sample can be characterized by a dimensionality of three. In these conditions, there is virtually no chance to separate all the analytes using a conventional single dimension system. In fact, the separation can either be performed according to size, but then colour and shape will remain unseparated, and the same if for colour and shape. A viable approach to achieve the separation of all the constituents of such a sample is to use an orthogonal two-dimensional separation system with a dimensionality that can match the dimensionality of the sample [13]. In practice, in GC×GC, everything starts by injecting a sample, as in 1D GC. However, rather than entering the detector when exiting the GC column, solutes arrive to an interface, called modulator, placed between the two separation dimensions (columns). The modulator ensures high sampling rates and the transfer of the sample from the ^{1}D to the ^{2}D, while respecting Giddings's conservation rules [22]. In other words, the modulator acts as an on-line injector that produces very narrow injection pulses (down to 50 msec peak width) at the head of the second column. The entire ^{1}D chromatogram is thus ''sliced'' following a modulation period (P_M) of a few seconds and re-injected into^{2}D for a fast-GC-type separation (figure 2.12a) [23].

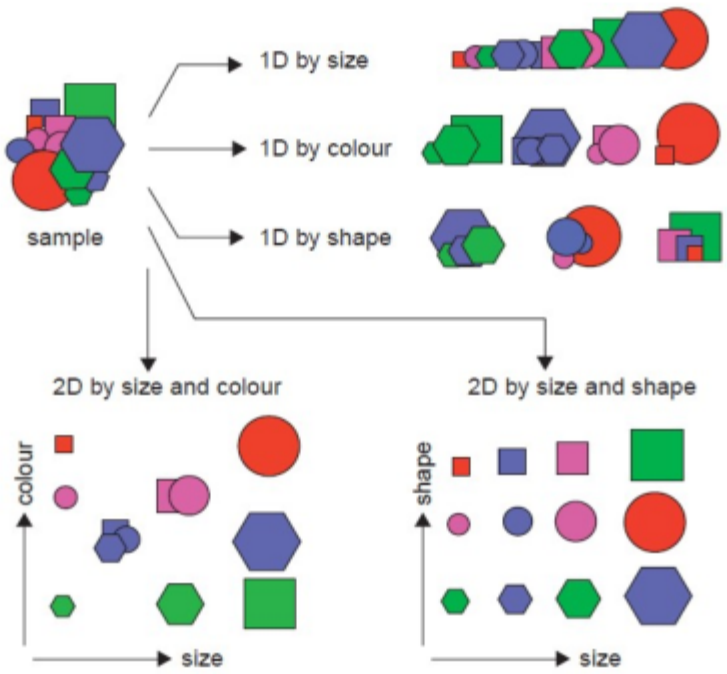

Figure 2.11. Match between separation and sample dimensionality in GC×GC.

Ideally, the separation of analytes in the ^{2}D has to be completed before another pulse is injected in the ^{2}D to avoid overlap of peaks issued from different modulation cycles (an effect called "wraparound"). It is interesting to note, however, that, as far as no co elutions are generated due to the wrapping around of compounds, there is no reason to spend time and effort to avoid wraparound in a separation procedure.

The second column analysis is normally much faster than the first one, and sometimes a secondary GC oven is used to heat independently the ^{2}D column. As a result, the separation time in the ^{2}D is about 100 times more rapid than that in the ^{1}D. For the detector, everything occurs as in classical GC and a trace is monitored continuously. Actually, a series of high-speed secondary chromatograms of a length equal to P_M (3–10 sec) are recorded one after another (figure 2.12b). They can at the end be combined to describe the elution

pattern by means of a two-dimensional plane (figure 2.12c). Specifically, data elaboration and visualization have to be performed through dedicated software (figure 2.13). Peak areas are attained by summing the areas relative to each modulated peak while signal intensity is considered as the height of the highest modulated peaks. Peaks can be visualized in different ways: 1) by the means of colours (colour plot); 2) by contour line (contour plot); 3) by a 3D plot.

As discussed, the potential ability to provide substantially larger peak capacity, which implies the resolution of more peaks of interest from a complex mixture, is not the only advantage of GC×GC over 1D GC [24-27]. In fact, the other advantages of GC×GC are the following: *i)* speed - considering the number of peaks resolved/unit of time; *ii)* selectivity - two stationary phase with different selectivity are used; *iii)* sensitivity – through the effect of analyte band compression exerted by modulation; *iv)* spatial order – through the contour plot formation of chemically-similar compound patterns.

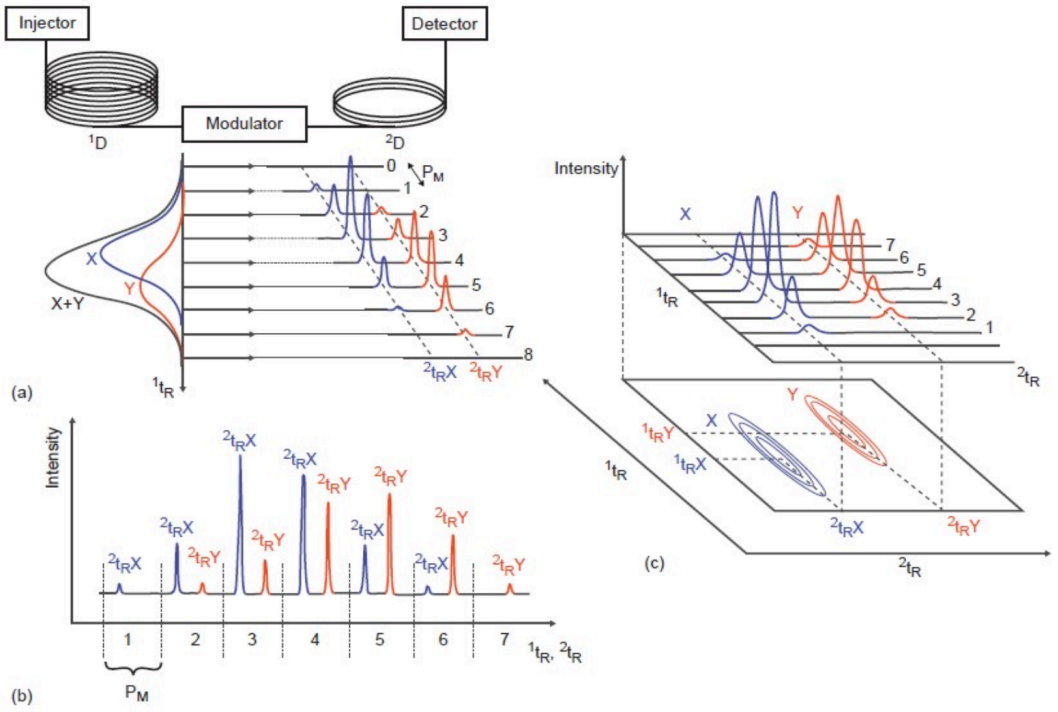

Figure 2.12 a-c. Scheme of the GC × GC setup. (a) The modulator allows rapid sampling of the analytes eluting out from ^{1}D and reinjection in ^{2}D. The modulation process is illustrated for two overlapping compounds (X and Y) coming out from ^{1}D at a defined first-dimension retention time (^1t_R). As the modulation process occurs during a defined PM, narrow bands of sampled analytes are entering into ^{2}D column and appear to have different second-dimension retention times (^2t_RY and ^2t_RX). (b) Raw data signal as recorded by the detector through the entire separation process. (c) Construction of the two-dimensional contour plot from (b).

2.4 GC×GC: basic instrumentation

2.4.1 Columns combination

Although the modulator is considered the key for successful GC×GC separations, the chromatographic column combination plays a significant role. Simply installing the modulator between two columns does not guarantee a good GC×GC separation. Consequently, such a column combination optimization issue, including stationary phase chemistry, column dimensions and film thickness, is required to accomplish efficient GC×GC separations.

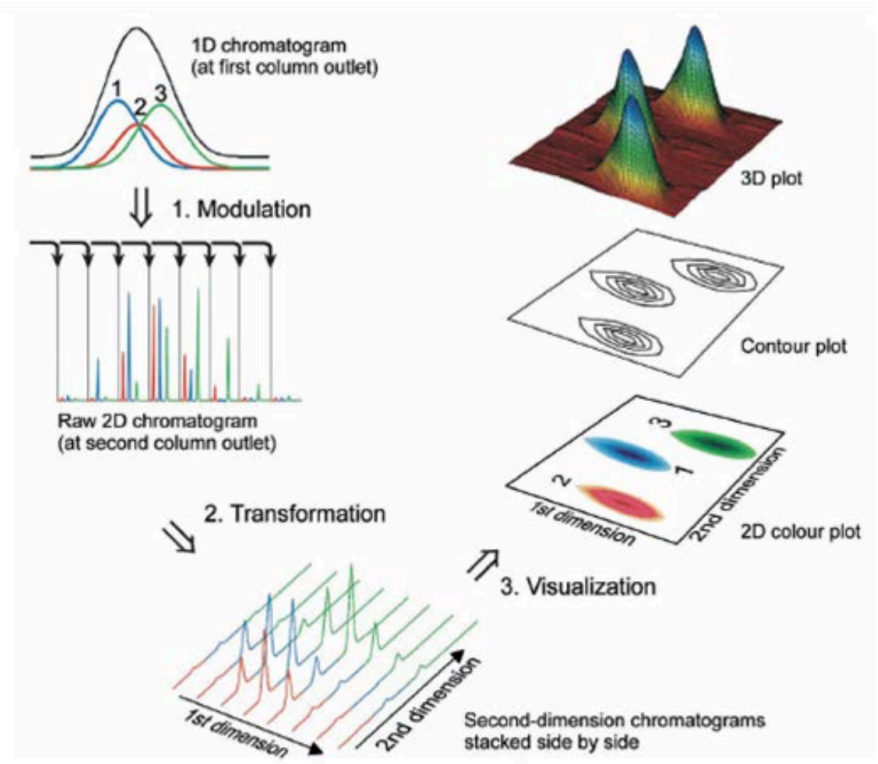

Figure 2.13. Scheme representing the GC×GC data manipulation and visualization process.

Usually, GC×GC systems combine a first column with a non-polar stationary phase, for example, dimethylpolysiloxane, and a second column with a more polar stationary phase, for example, polyethylene glycol, phenylmethylpolysiloxane, or cyclodextrine [27,28]. In this configuration, solutes are generally separated as a function of increasing boiling point in ^{1}D. Meanwhile, separation in ^{2}D is governed by the activity coefficient of the analytes. These are then separated by using two independent, orthogonal, separation mechanisms.

Any existing stationary phases that can be used in GC can also be used in GC×GC. A variety of stationary phases can be selected according to the intended analyte-stationary phase interaction.

Many sample-types are characterized by the presence of homologous series of constituents. The GC×GC analysis of fatty acid methyl esters (FAMEs) is a perfect example to illustrate group-type order [29]. Figure 2.14 shows a complex human plasma fatty acid profile. Homologues compounds are situated in a grid, according to their chemical characteristics. In particular, saturated FAMEs are in the lower part of the 2D chromatogram, while an increase in the number of double bonds (DB) in the fatty acid chain intensifies retention in the second dimension. FAMEs are also separated according to the DB position. Compounds with the DB in the same ω3 position are aligned in parallel diagonal lines, while the higher ω6 positions elute before the lower ones. This highly ordered structure gives a great help for compound identification.

On the other hand, a reversed column set can better satisfy the aims of a specific research. In 2004, Adahchour and co-workers studied and compared a normal and reversed column set for two different complex samples, namely diesel oil and food flavours [30]. For the former sample-type, a completely reversed ordered structure was obtained, with the different classes (alkanes, mono-aromatics, di-aromatics, etc.) grouped tightly together, giving an advantage when group-type determination is required. When food flavour samples were analyzed, the reversed approach improved the peak shape of polar compounds, such as aliphatic acids and alcohols, which also improved the ordered structure of the chromatogram. A recent report from Sidisky and co-workers highlighted the promising thermal properties of ionic liquid stationary phases that were used at temperatures up to 240°C [31].

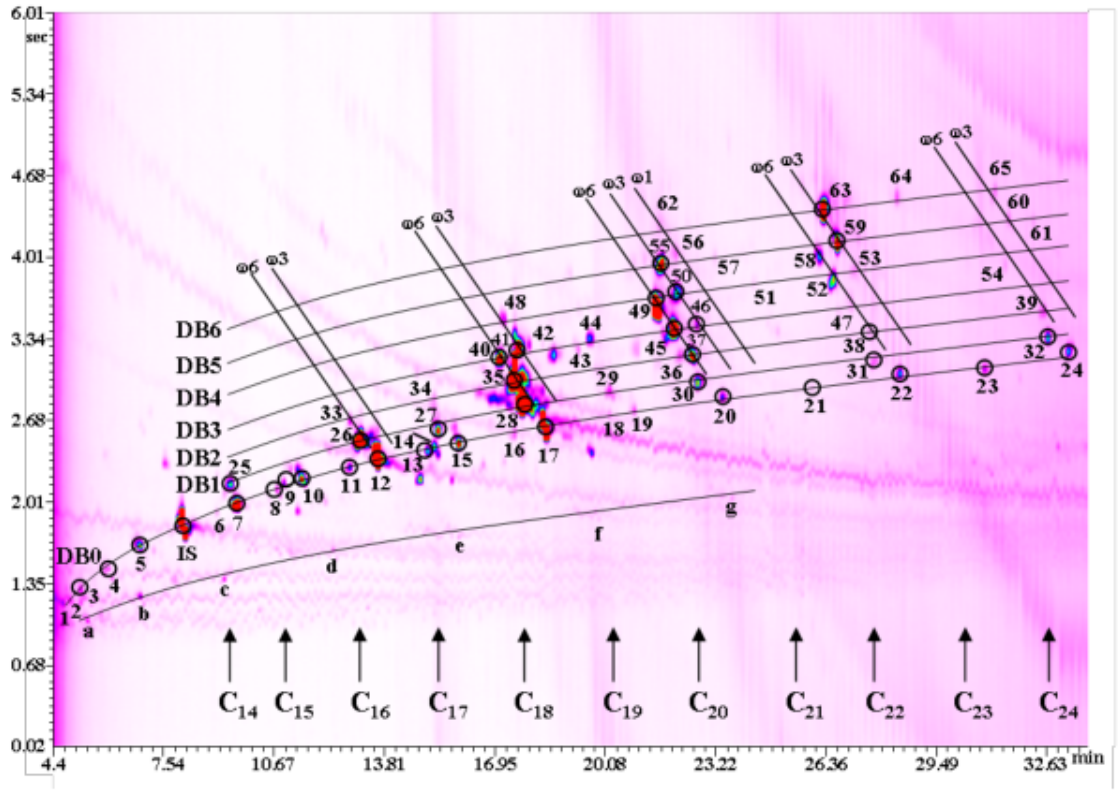

Figure 2.14. GC×GC analysis of human plasma fatty acids.

Also Seeley *et al*. used a high-temperature phosphonium ionic liquid column in a GC×GC application, proving that these phases can be considered as good candidates for the second dimension of a GC×GC setup [32].

Another interesting approach, which can be considered as a good exercise for comparing phase selectivity, is the possibility to use a dual parallel secondary column system by splitting the focused pulse towards two parallel secondary columns instead of a single one. This was first described by Seeley *et al*. [33,34], who used an effluent splitter just after the modulation valve to perform such a splitting. The resulting approach, called *dual-secondary column* GC×GC (GC×2GC), produces a pair of two-dimensional contour or colour plots in a single run.

As for column dimensions, the ^{1}D is commonly 10 to 60 meters long, with an inner diameter in the range of 0.18-0.53 mm and a film thickness of the order of 0.25-1 μm. These columns provide peak widths of 5 to 30 sec [35]. This would be beneficial as it is desirable to have rather large peak widths for ensuring proper sampling by the modulator. On the other hand, the^{2}D is usually shorter, 0.5 to 1.5 meters' length, and has a smaller inner diameter than the ^{1}D column, allowing the ^{2}D analysis being fast. Film thickness is also normally reduced in the 0.1-0.25 mm range, which allows increased separation efficiencies.

2.4.2 Transfer devices

The transfer device, so-called modulator, controls and sets fractions transit between the separation dimensions. Its role consists in sampling, focusing, then releasing first column effluents towards the second column as pulses.

Various technological improvements have been made throughout the development of modulators, and two main families can be distinguished: *thermal* and *pneumatic*, or *flow*, modulators. Another general distinction exists between one- and dual-stage modulators: in the latter, two events in series occur in two different zones of the modulator. Among flow/pneumatic modulators, two more characteristics can be identified, namely those which employ an ''in-line'' column-set, using valve/es (valve-based), and those characterized by a valve located ''out-line'' (Dean's switch assemblies).

Since the transfer device is arguably considered the most important component of any GC×GC system, a deeper insight will be provided in the following sections.

2.4.3 Detectors

The detector is another important GC×GC system component, and must offer rather high sampling rates for a proper peak reconstruction. A brief discussion about the most commonly employed detectors in the GC×GC field will follow.

The most commonly employed detector in GC×GC has been the *flame ionization detector* (FID), which is capable of very high acquisition rates, easily above 100 Hz. The FID is a universal detector, with a response proportional to the compound carbon content, thus suitable for most quantitative applications. With such a detector, group-type 2D chromatograms can be obtained, and tentative peak classification can be achieved. The group type is assigned according to retention time correspondence with even one standard, and then FID quantification can easily be done. Biedermann and Grob exploited GC×GC-FID for the quantification of mineral oil constituents contained in a contaminated sunflower oil [36]. GC×GC-FID has been employed in several fields, such as environmental [37,38], industrial [39], and food [40,41].

More selective detectors are useful in trace analysis, since sensitivity can be greatly enhanced. The electron capture detector (ECD) is characterized by a high sensitivity for organic molecules containing electronegative functional groups (halogens, phosphorous and nitro-groups). The main concern in coupling such a detector, has been related to a rather high internal volume, which can cause band broadening. Recently, Agilent Technology has presented a newly-designed ECD, the micro-ECD (μ-ECD), with a miniaturized internal volume (150 μL). Several applications have been published using GC×GC-ECD to improve detection limits in the trace analysis

of organochlorine (OCs), organophosphorus (OPs), and polychlorinated biphenyl (PCBs) contaminants [42,44].

A discussion apart has to be made on mass spectrometers, the most informative detection systems, considered as an additional third dimension analysis by GC×GC users. The coupling of an MS instrument, to a GC×GC system, has been highly desirable since the birth of comprehensive 2D GC, to add structural information to the great separation power. The first coupling between GC×GC and MS was realized in 1999 by Frysinger and Gaines, who used a quadrupole with a very low acquisition speed (2.43 scan/sec) [45]. The authors intentionally broadened the 2D peaks to a minimum 1-sec baseline width, by using a thick second-dimension stationary phase and by slowing down the heating rate (0.5°C/min); under such conditions, less than 3 data points per peak were obtained. The authors concluded that a time-of-flight mass spectrometer would be the ideal solution to satisfy the requirements of GC×GC narrow peaks.

A year later, van Deursen and co-workers described the first GC×GC-TOF MS application focused on kerosene analysis [46]. The TOF-MS process generates a complete spectrum from every ion pulse from the ion source; up to 500 spectra/sec can be produced, thus a huge quantity of information is collected. However, to optimize a TOF MS method, a compromise among different parameters must be found, namely: *i)* data points per peak, which have to be sufficient for a reliable peak reconstruction; ii) sensitivity, which decreases with an increase of the spectral production rate; iii) data file size, because higher acquisition rates generate large data files, handled with difficulty by normal computers. Consequently, in GC×GC-TOF MS experiments, an acquisition rate of 50 Hz is an accepted compromise. Furthermore, the acquisition of complete spectra and the absence of “peak

skewing" enable the exploitation of spectral deconvolution, a useful tool to unravel peak overlapping. The main software which operate such a function is the LECO ChromaTOF and AMDIS.

Although TOF MS fully satisfies GC×GC acquisition rate requirements, researchers and instrument manufactures have made substantial efforts to improve the existing quadrupoles in order to make their coupling with GC×GC feasible, because of their valuable advantages such as: low cost, robustness, compactness and availability of commercial MS databases.

For instance, Shellie and co-workers attained between 18.5 and 20 scan/sec by using a 4000 amu/sec qMS scan speed and byreducing the mass range, in essential oil applications [47,48]. In 2007, Cordero and co-workers, despite using a qMS with a highscan speed (11,111 amu/sec) in allergens analysis, had to reduce the mass range (40-240 m/z), to achieve 18.52 scan/sec, due to the relatively high inter-scan delay (30 msec) [49]. Mondello and co-workers analysed a commercial perfume by using GC×GC in combination with a rapid-scanning qMS (10,000 amu/sec) [50]. Thanks to the relatively low inter-scan delay (calculated to be 14msec), an acquisition frequency of 20 Hz was achieved by using a"normal" mass range (40-400 m/z).Considering its limitations, the quadrupole mass spectrometer has been considered suitable only for qualitative purposes. Thesingle ion monitoring mode has been often used to meet therequirements for quantitative analysis, since higher acquisitionrates can be attained. Recently, the performance of a novel very-rapid qMS, with a 20,000 amu/sec scan speed and a very low inter-scan delay (5 msec), has been reported [51]. Accurate GC×GC-qMS quantification of perfume allergens was described:an average of more than 15 data points per peak was obtained, through the application of a 50 Hz acquisition rate and a 40-340m/z mass range. The availability of such a very rapid qMS represented

an important step towards the expansion of the applicability of GC×GC-MS in quantitative applications.

2.4.4 Modulators

The analytical benefits of comprehensive two-dimensional gas chromatography have been exploited and emphasized in the past two decades. The unexpected complex nature of many real-world samples amenable to GC analysis has been definitely elucidated only through the enhanced resolving power of GC×GC.

Simple but fundamental devices, i.e., the modulators, enable continuous heart-cutting and re-injection processes (figure 2.15). The direct serial connection of two different columns without a modulator will results in a one-dimensional separation because analytes separated on the first column are not prevented from co-elution at the exit of the second column (figure 2.15 B). Also, their elution order might even be reversed (figure 2.15 C). Following the separation in the first column (figure 2.15 D), the modulator traps and focuses the first band (black, figure 2.15 E), and then injects it into the second column while collecting the following band (grey, figure2.15 F). The grey band is injected into the second column only after the black band had eluted from it. The grey band is then separated on the second column, while the spotted band is collected by the modulator (figure 2.15 G).

The time needed to complete a single cycle of events is called the modulation period. The preservation of the first dimension separation can only be accomplished if every peak eluting from the primary column is sampled at least three times [52], although 2.5 times has also been proposed as the optimal value [53]. Thus, if *e.g.* a 12 seconds wide peak elutes from the primary dimension, the modulation period should be no longer than 4 sec. Górecki *et*

al. illustrated in a review the effect of the length of the modulation period on the preservation of the primary column separation [54].

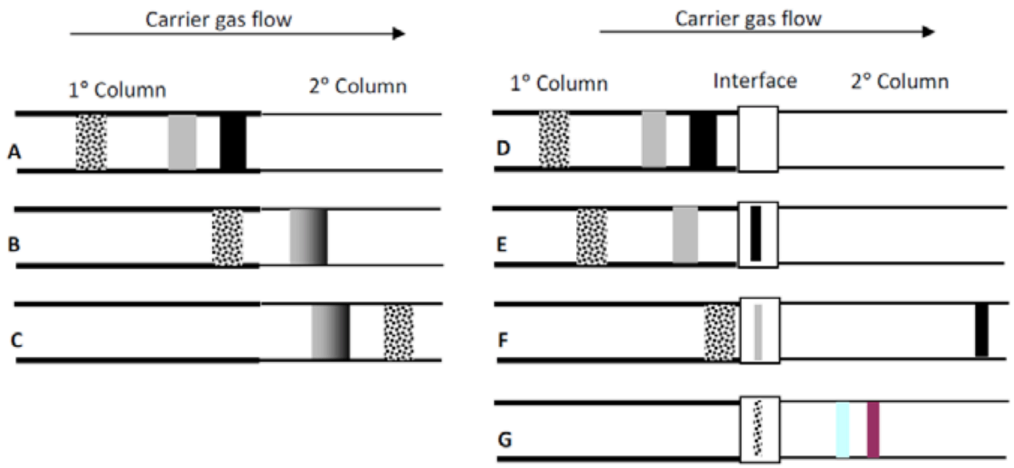

Figure 2.15. The relevance of the modulator in GC×GC. A-C illustrate how bands separated on one column can recombine or change elution order on the second column if they flow uncontrolled from one to the other. D-G illustrate how the interface traps material from the primary column, and then allows discrete bands to pass to the second dimension column while trapping other fractions.

2.4.4.1 Cryogenic interfaces

Following the introduction of the first cryogenic modulators, the use of the thermal sweeper rapidly declined, and it has not been available commercially for several years [55].

The longitudinally-modulated cryogenic system (LMCS) was the first cryogenic system reported [56]. The end part of a 30 m × 0.22 mm ID × 0.25 µm d_f non-polar capillary column was linked to a moving 5-cm cryo-trap, which entrapped/focused effluent fractions by means of an internal CO_2 flow which generated intense cooling. Following the entrapment step, the cold

region was exposed to the GC oven heat through the longitudinal movement of the trap along the column and, thus, the entrapped analyte was launched onto the final 40-cm segment of the column. The use of the LMCS device increased the peak height of $C_{14:0}$ fatty acid methyl ester by ~9 times, while modulated and non-modulated S/N ratios for pentadecane were 56:1 and 7:1, respectively. By using a 7.5 sec modulation time, a comprehensive 2D GC separation of kerosene was performed.

The advantages of the LMCS device, compared to the thermal sweeper, were: *i)* more efficient entrapment/focusing (a general value of +100° C, with respect to the GC temperature, was applied); *ii)* no GC oven temperature limitation, except for that related to the less thermally-stable stationary phase employed; *iii)* less elaborate construction. However, the additional expense related to the consumption of CO_2, and the lack of additional heating for efficient re-mobilization especially with higher MW analytes can represent severe drawbacks.

In 2000, Ledford presented a dual-stage static modulator, which employed two cold and two hot jets, situated at the head of the second column and pulsed in an alternate mode [57]. The first stage of (liquid N_2) cooling, which enabled the concentration of a primary column chromatography band, was attained by the activation of the cold jet upstream [the hot jet (air) downstream was simultaneously activated]. At the end of the first entrapment process, the upstream hot and downstream cold jets were activated, enabling re-mobilization and then second-stage entrapment of the first band. At the end of the second entrapment process, the upstream cold and downstream hot jets were turned on, allowing the first-stage entrapment of another chromatography band and the second-dimension analysis of the previous one. The modulation quality of such a type of modulator was excellent, enabling

the generation of very narrow, second-dimension analyte plugs. Moreover, highly volatile compounds (e.g., propane and butane) were easily entrapped by the low temperatures generated by liquid N_2 (down to -190°C). Contrarily, the need for and the high consumption of liquid N_2 gas were certainly disadvantages. A commercial version of the quad-jet modulator is mounted on GC×GC instruments from LECO Corporation.

Shortly after the introduction of the quad-jet modulator, Ledford et al. proposed a dual-stage interface, equipped with a cold and hot jet, named as loop-type modulator [58]. The latter is commercialized by Zoex Corporation (ZX1). The two stages are created by looping a segment (1-1.5 m) of capillary column (modulator tube) through the pathway of a cold jet of N_2 gas (figure 2.16). Though the modulator loop can be created by using the last part of the first dimension, or the initial segment of the second, such options are not advisable because breakages can occur when a capillary column is coiled tightly. A better choice is to use an uncoated column, or a segment of stationary-phase coated capillary. The cooling gas, which is provided by a heat exchange coil located in a small liquid-N_2 Dewar, flows continuously throughout the GC×GC analysis. The cold jet is directed vertically downward onto the modulator tube, thus generating two cold spots; the cold jet is diverted from the cold spots by activating a hot jet of nitrogen gas, which is activated for a brief period (*e.g.,* 300–600 msec), in a periodic manner (*e.g.*, every 4-6 sec, corresponding to the modulation period). The hot jet is located perpendicularly to the cold one, and rapidly heats the cold spots, remobilizing the entrapped analytes. Recently, Zoex Corporation has commercialized a loop-type modulator with no liquid N_2requirements (ZX2). Specifically, cooling of the N_2 gas is achieved by using a refrigeration unit with a reported minimum temperature of -90°C.

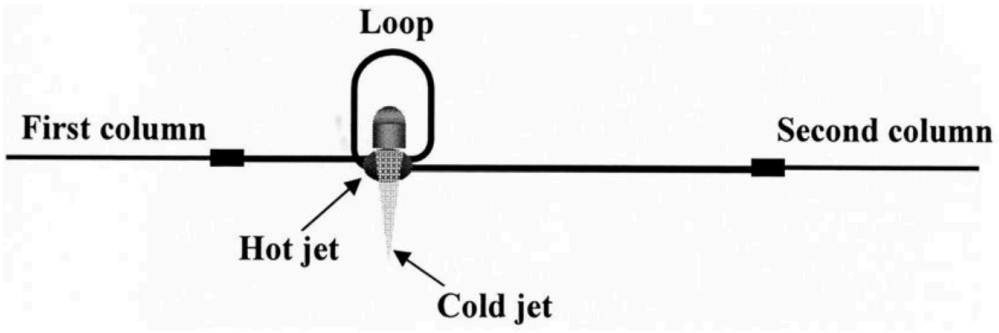

Figure 2.16. Loop-type modulator. The cold N_2 flow is directed downwards, while the hot N_2 jet is located perpendicularly to the cold one.

The concept of stop-flow modulation, published in 2004 by Harynuk and Górecki, added an option to the existing modulation modes [59]. The stop-flow approach was interesting because it enabled decoupling of the first and second-dimension separations, and offered the possibility of optimizing each analytical process separately. For example, long modulation periods could be applied without the risk of insufficient first-dimension sampling. Figure 2.17 shows a schematic of the stop-flow GC×GC modulator. The outlet of the primary column (apolar, 30 m × 0.25 mm ID ×.25 μm d_f) (B), and the inlet of the secondary capillary (polar, 1.5m × 0.25 mm ID × 0.25 μm d_f) (E) were attached to positions 3 and4 (A) of a twin-stage six-port valve, whose 1, 2 and 6 ports were plugged. The valve was located in a chamber heated at 300°C, while a single liquid-N2 jet was employed to focus the chromatography bands exiting port 4 (D). An additional supply of carrier gas to the valve was attained by using a transfer line, made of deactivated fused silica, and with the same flow resistance as that of the primary column. The transfer line was connected on one side to the carrier-gas tubing, via a T-union, and on the other to port 5 of the valve (C). As can be seen from Figure 2.15, when the modulator is in

the ‘‘sample position’’ the primary-column effluent (B) is transferred onto the second dimension (E), and is entrapped by the cold jet (D). When the valve is switched to the “stop position’’ the flow in the first dimension undergoes an interruption (port 2 is plugged), the cold jet is deactivated and the flow in the second dimension is maintained by the auxiliary carrier-gas supply (C).

The performance of such a modulator was evaluated in the analysis of C_5 –C_{13} alkanes; the ^{1}D effluent was subjected to transfer for 2 sec (sample position), and then interrupted for 4 sec (stop position), leading to a 6-sec analysis time in the second dimension. By using such modulation conditions, it means that a hypothetical 8-sec peak would be sampled at least four times, instead of two times by using a ‘‘traditional’’ 6-sec modulation period.

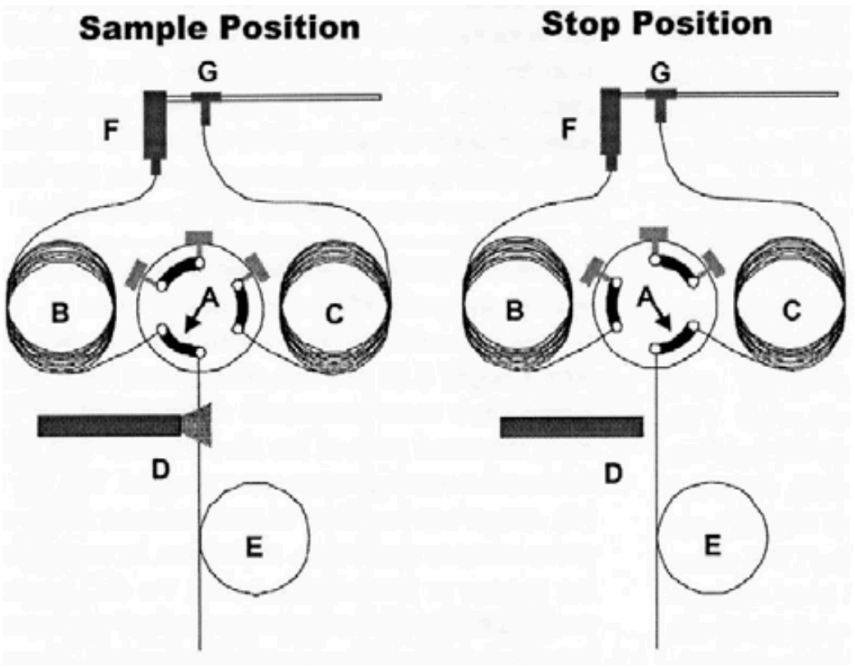

Figure 2.17. Stop-flow valve/cryogenic modulator. **A**: *six-port valve* (1, 2, 6 ports are plugged); **B**: ^{1}D column linked to position 3 of the valve; **C**: transfer line providing the auxiliary carrier-gas supply linked to position 5 of the valve; **D**: cold N_2 jet; **E**: ^{2}D column linked to position 4 of the valve; **F**: injector; **G**: T-union.

However, the drawbacks of such a type of modulating device are the following: i) the rather elaborate instrumental configuration; ii) the limited rotary valve duration; iii) the formation of artefact peaks (derived from the material of the valve); iv) the extended analysis times.

Issues at ii-iii) points were circumvented by eliminating the valve from the column sequence, as reported by Sacks and co-workers (Figure 2.18) [60]. The flow from the primary column was stopped by using an external solenoid valve, which generated sequential pressure pulses at the union point between the first and second dimension. A dual-stage, air-cooled, modulator, located on top of the GC oven, was employed to re-concentrate the first-dimension chromatography bands. The overall disadvantages of the new stop-flow system were certainly reduced. However, it is clear that the instrumentation setup remains still of elaborated construction, and total analysis times remain longer.

2.4.4.2 Valve-based devices

Pneumatic modulation was described for the first time in the same year as the LMCS [61]. In an investigation focused on chemometrics, Bruckner *et al.* employed four ports of a six-port diaphragm valve (located in the GC oven) to achieve a single-stage PM GC×GC analysis (figure 2.19). A 4.9 m × 0.53 mm ID × 3.0 μm d_f apolar column and a 0.85 m × 0.18 mm ID × 0.15 μm d_f polar were used as first and second dimension, respectively. The other two valve ports were connected to an auxiliary pressure source and to a waste line. Excessively high gas flows in the second dimension were avoided by using a split line (0.5 m × 0.18 mm ID fused-silica column).

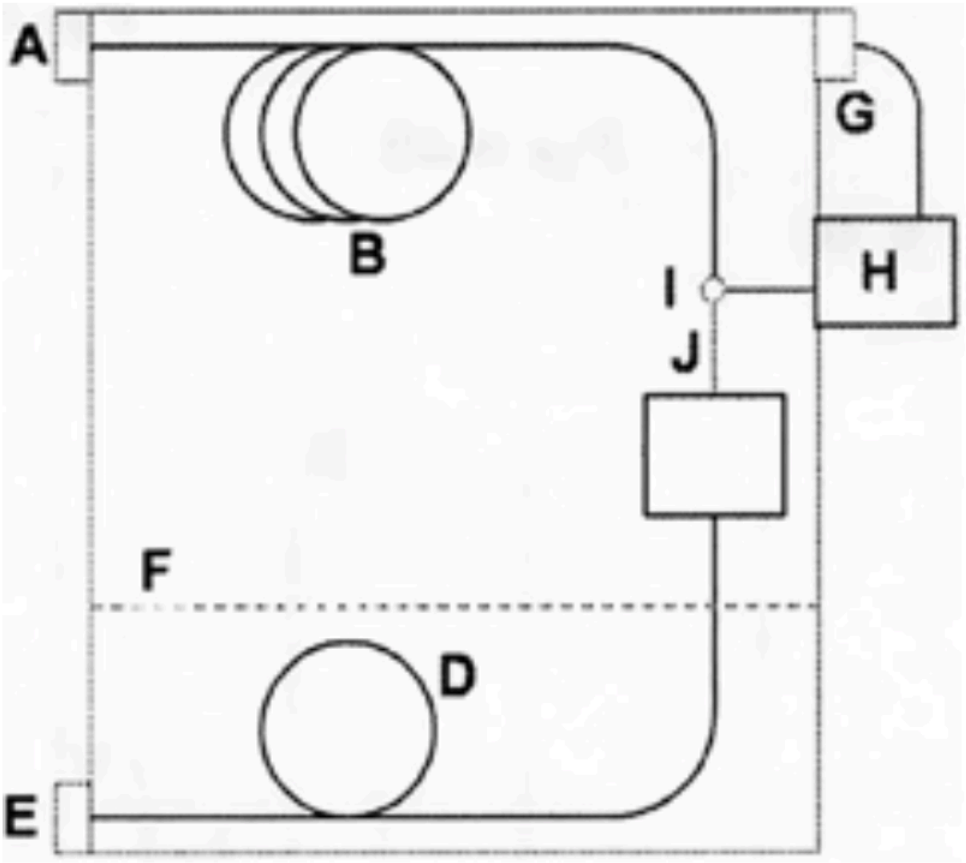

Figure 2.18. A stop-flow GC×GC system with pneumatic switching. Instrumental components include (A) injector, (B) ^{1}D column, (C) modulator, (D) ^{2}D column, (E) detector, (F) optional second oven, (G) cool on-column injector as an auxiliary gas pressure source, (H) a solenoid valve, (I) a three-port junction, and (J) a restricting transfer capillary from the junction to the modulator.

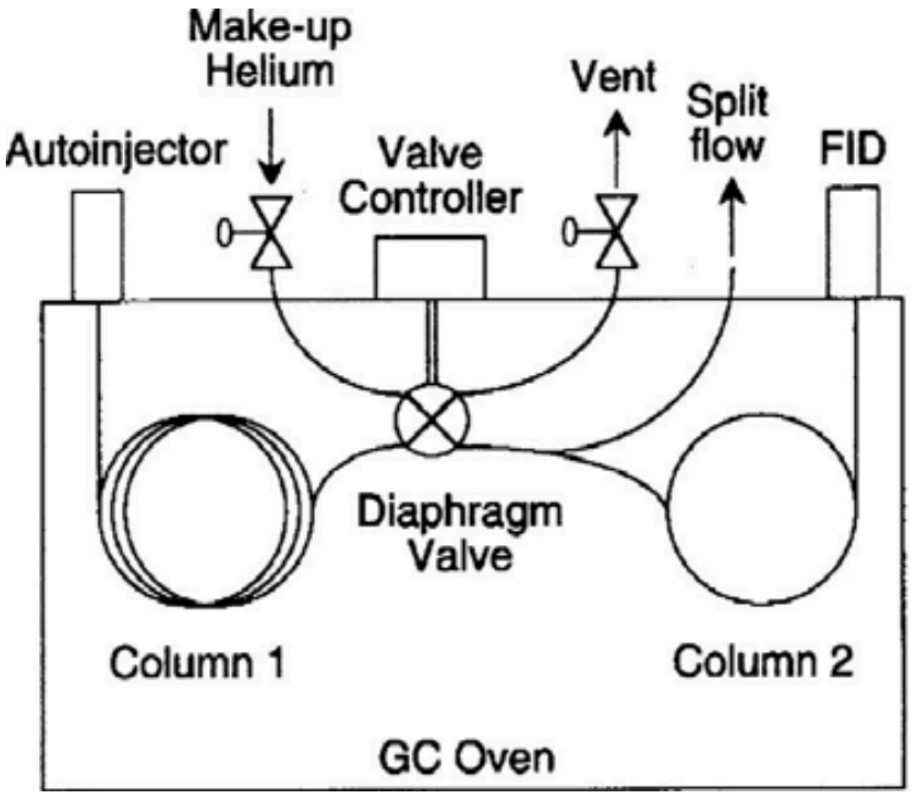

Figure 2.19. The first PM device (in the ‘‘waste’’ mode).

Single-stage PM was carried out with a chromatography band being transferred onto the secondary column for a 50 msec period at the beginning of each modulation process. At the end of the brief injection period, the valve was switched to the other position, and the primary-column effluent was directed to waste (450 msec). The authors used a 0.5-sec modulation period, with 50 msec for the inject mode (0.1 duty-cycle). Apart from the sensitivity issue, a disadvantage of the PM method was the restricted operational temperature of the valve.

In 2000, Seeley and co-workers reported the first dual-stage and high duty-cycle valve PM device, defining the approach as *differential flow modulation* [62], because an independent gas flow was used in each dimension. The PM

device comprised a six-port, two-position, diaphragm valve, equipped with a 20-μL stainless steel sampling loop, connected to a waste line and an additional pressure source, and located between the two columns (figure 2.20). The part of the valve containing non-wetted components was situated outside the oven and was maintained at 125°C by using a heater. Inside the oven, the interface was attached to a 10 m × 0.25 mm ID × 1.4 μm d_f (6% cyanopropylphenyl, 94% dimethylpolysiloxane) primary column and a 5 m × 0.25 mm ID × 0.25 μm d_f polyethylene glycol capillary or a 5 m × 0.25 mm ID × 0.50 μm d_f polyethylene glycol trifluoropropylmethyl polysiloxane capillary. The authors used the valve in the accumulation and injection states for 80% and 20% of the modulation period, respectively.

During the injection state, while the previously accumulated chromatography plug was launched onto the second dimension exploiting a high gas flow (15 mL/min), the primary-column effluent (0.75 mL/min) was directed to waste. Obviously, sensitivity losses were reduced with respect to the modulator developed by Synovec's group [61,63,64simon].

The disadvantage related to the high secondary-column flows was partially resolved in a series of later PM-GC×GC studies by splitting the primary flow between two secondary analytical capillaries (GC×2GC).

In 2003, Synovec's group employed a high-speed, six-port diaphragm valve, equipped with a low-capacity accumulation loop, in a series of flow-modulation studies, exploiting a low duty cycle dual-stage PM [65].

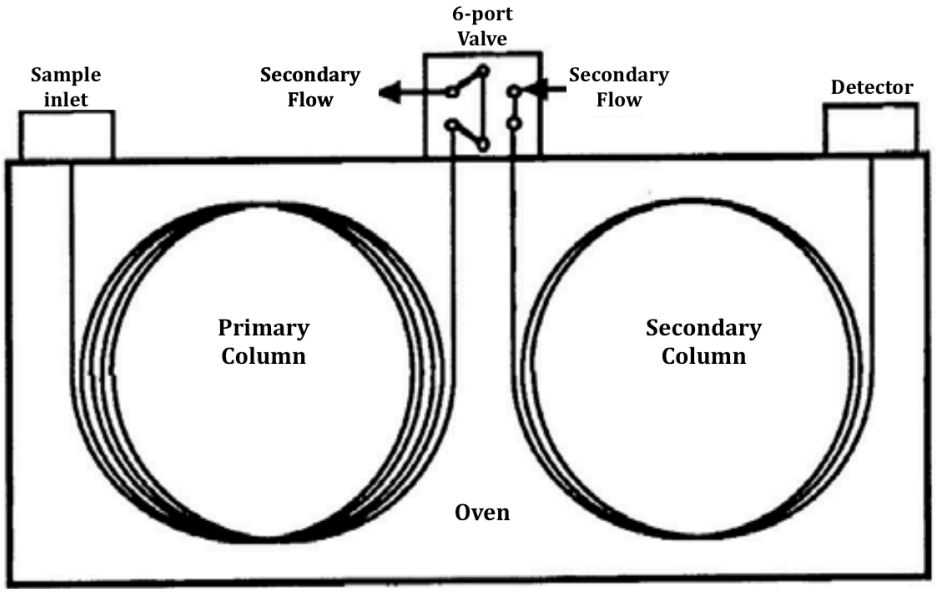

Figure 2.20. The first PM GC×GC device equipped with a sampling loop.

The wetted portions of the valve (equipped with a 5-μL loop) was mounted inside the oven, while the temperature-sensitive O-ring part was located outside. Furthermore, it was the first reported combination of PM-GC×GC with a time-of-flight mass spectrometer. Apart from the disadvantages (limited duty-cycle and loop volume), the most important advantage of the modulator was the extended analysis temperature range (up to 270° C).

A general final comment can be made on the current-day employment of in-line valve systems: the only device still employed on a rather regular basis (in publishing terms) is the low duty-cycle PM developed by Synovec's group in 2003 [65]. Conversely, Seeley has directed his attention to out-line valve systems.

In 2006, Seeley *et al.* introduced an interesting dual-stage flow modulator [66], which was a simplified version of the system previously described by

Bueno and Seeley [67]. The PM device (Figure 2.21) was constructed by using three deactivated fused- silica columns, two micro-volume T-unions and a two-way solenoid valve (located outside the GC oven), connected to an auxiliary pressure source.

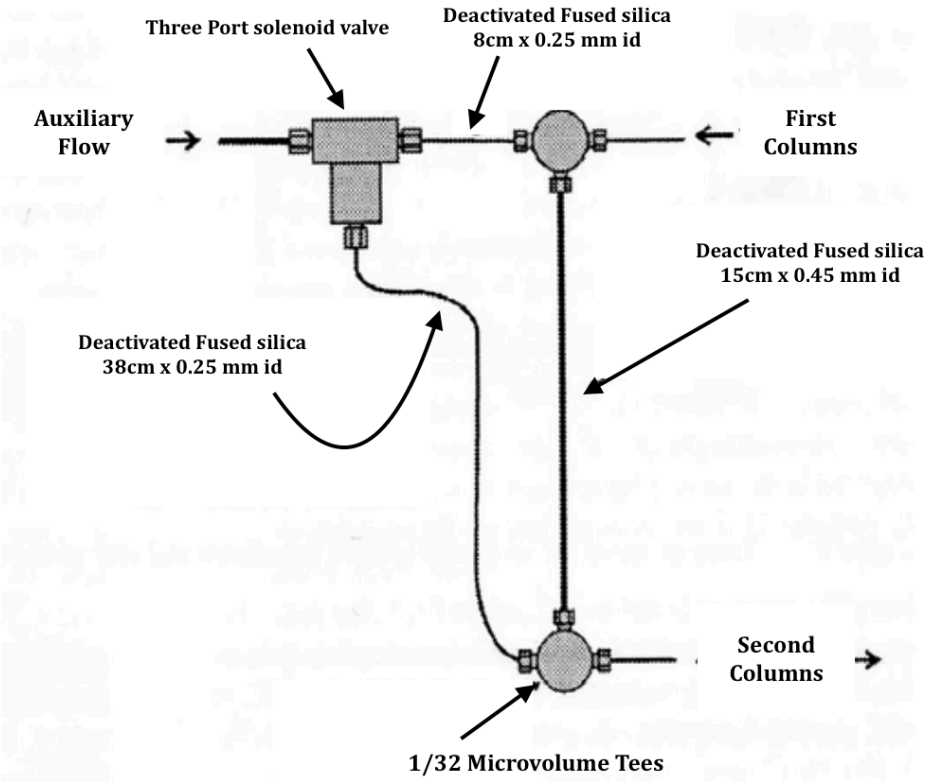

Figure 2.21. The ‘‘out-line’’ single-loop, dual-stage FM device introduced by Seeley [66].

The output ports of the solenoid valve were connected to the unions by using two fused-silica segments. One of the T-unions was linked to the primary-column outlet, while the other directed the flow to the second dimension. A fused-silica segment, bridged between the two unions, acted as sample loop

(volume = ~24 μL). A non-polar 15 m × 0.25 mm ID × 0.50 μm d_f capillary was used as first dimension (flow: 1.0 mL/min), while two polar 5 m × 0.25 mm ID columns were employed as second dimension, one with a 0.25 μm polyethylene glycol film, and the other with a 0.50 μm poly(methyltrifluoropropylsiloxane) film. When the modulator was in the ‘‘fill’’ state, the auxiliary flow (20 mL/min) was directed to the ^{2}D, and the primary-column effluent (~ 17μL/sec) flowed freely within the loop; the accumulation period (1.4 sec) was lower than the time necessary for the effluent to reach the bottom union (~1.5 sec). When the solenoid valve was switched for a brief period (0.1 sec), the auxiliary flow flushed the content of the loop onto the head of the second dimension. The pressure pulse, during the injection stage, temporarily stopped the ^{1}D flow. The 21 mL/min flow exiting the modulator was split between the two columns, corresponding to a linear velocity value of ~240 cm/sec at the beginning of the experiment (40° C).

The dual-stage PM system proposed by Seeley *et al.* was characterized by: *i)* stability at high GC temperatures; *ii)* simple construction; *iii)* duty-cycle = 1. The disadvantages were related mainly to the complexity of method optimization, the rather high second-dimension gas linear velocity, and the low modulation period. However, the novel modulator was very promising and was exploited successfully in PM-GC×GC applications [68,69].

A series of PM-GC×GC works were based on the original research of Seeley *et al.* [66]. Amirav’s group used a rather large storage column (50 cm × 0.53 mm ID) and brass T-unions for realizing the modulator connections in applications with flame- ionization and triple-quadrupole MS detection [70,71]. Harvey *et al.* proposed a symmetric flow-path modulator, *i.e.* the use of transfer lines and storage loop of the same ID (0.25 mm) [72]. The authors affirmed that such a configuration was used to limit flow perturbation issues.

Agilent Technologies introduced a pneumatic modulator based on Seeley's design, constructed using capillary- flow technology [73]. A planar metal structure contained an internal collection chamber, and was connected (in a permanent manner) via two metal branches to a three-way solenoid valve, which received a controlled gas supply from an auxiliary electronic pressure-control module. The interface was a simpler version of the device proposed by Seeley *et al.* [66] (the PM principles were essentially the same), with simplicity being the main advantage.

In 2010, Tranchida *et al.* proposed a flexible loop-type PM device [74], with the characteristics and the advantages of the two previously described interfaces [66,73], plus the possibility to optimize flows, using a waste branch bridging the interface and a needle valve. Figure 2.22 shows the seven-port PM device. The interface comprises a metallic disc (2.5 cm diameter, 7 mm thickness), and internal rectangular channels (250 μm width/75 μm depth), connecting ports 1-2-3 and 4-5-6/7. A two-way electrovalve is located outside the GC oven and is connected to an advanced pressure control (APC) unit. Two metallic branches connect the valve to the interface in positions 2 and 5. The primary and secondary columns are linked to positions 1 and 6, respectively. A 40μL stainless-steel loop (20 cm × 0.71 mm OD × 0.51 mm ID) bridges positions 3 and 4. The size of the loop is chosen considering the modulation period, first-column flow and second-column dimensions. It is noteworthy that the flow exiting the loop is divided between the channels linked to ports 6 and 7. Flow splitting depends on needle-valve regulation and remains unaltered during the analysis because the valve-restriction parts are located within the GC oven.

A twin-oven PM enantio-GC×polar-GC-FID method (employing a 40-μL loop) was used for the analysis of essential oils. The optimized PM method

was characterized by a primary column linear velocity and flow (50°C) of ~40.5 cm/sec (constant linear velocity conditions) and 8.7 μL/sec (0.52 mL/min), respectively. The authors affirmed that a micro-bore 1D was employed because: *i)* low flows generate optimum separation conditions and enable longer accumulation periods; *ii)* efficiency increases with an ID reduction. With respect to the second dimension, a 0.25 mm ID analytical column was used because high flows were generated. Also, the reasons for using a waste line were: *i)* the loop pressure release was much more rapid during flushing; *ii)* to emulate a high split-ratio injection; *iii)* to generate acceptable ^{2}D linear velocities [a value of ~180 cm/sec (~5.5 mL/min) was calculated, with about 95% of the effluent directed to waste]. The loop flow was estimated to be 111 mL/min, while a 0.2-sec injection period was exploited for efficient flushing. The authors concluded that further research was necessary to optimize the PM process, in particular the limitation of sensitivity losses. They emphasized that additional work was also required to define the best column dimensions and to reduce the complexity of the optimization step.

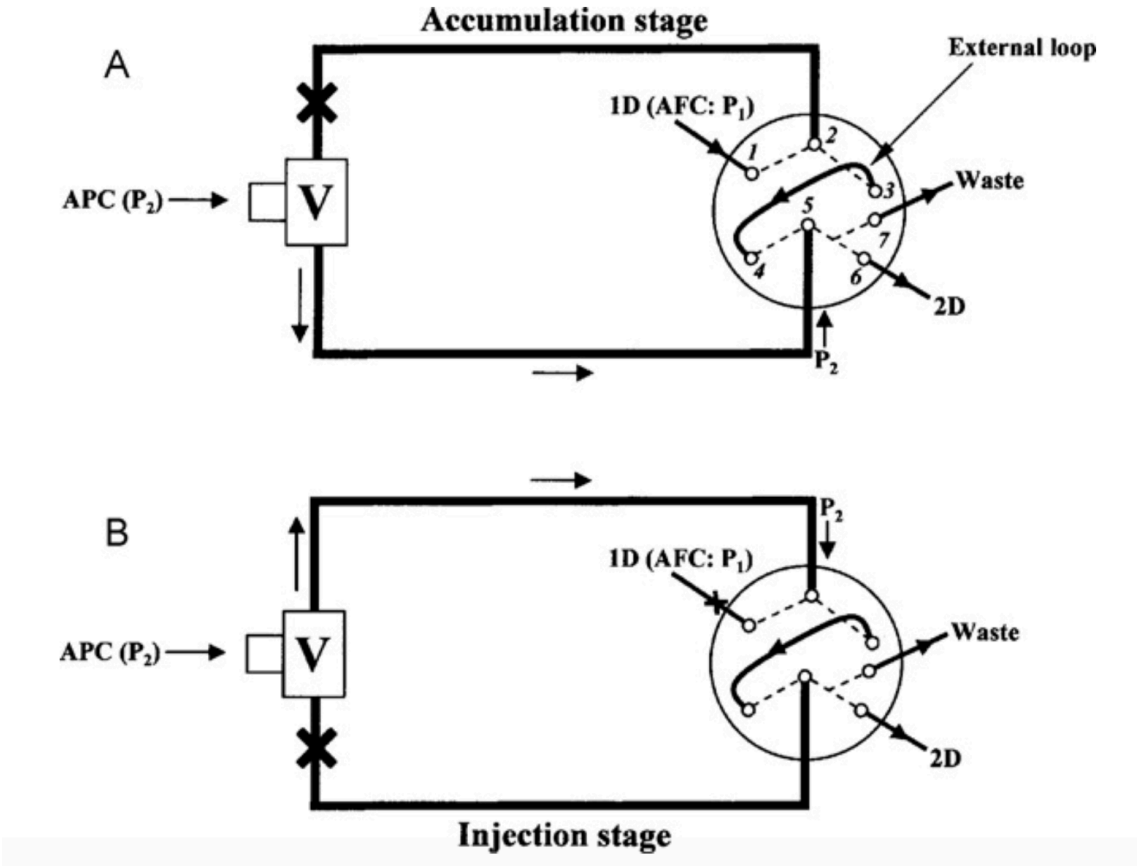

Figure 2.22. *Seven-port PM device (proposed by Tranchida et al. [74]) in the accumulation (A) and injection (B) modes. Abbreviations: V: two-way solenoid valve; AFC: Advanced flow controller.*

References

[1] M. Tswett, Ber. Dtsch. Botan. Ges. 24 (1906) 316.

[2] C.F. Poole. The Essence of Chromatography, Elsevier, Amsterdam, 2003.

[3] M.J.E. Golay, Gas Chromatography, Academic Press, New York, 1958.

[4] M. Novotny, Gas Chromatography in: Encyclopedia of Physical Science and Technology (Third Edition), R. A. Meyers (Editor), Academic Press, San Diego, 2001, pp. 455-472

[5] M. J. E. Golay, in: Gas Chromatography, V. J. Coates, H. J. Noebels, I. S. Fagerson (Editors), Academic Press, New York, USA, 1958

[6] H. M. McNair and J. M. Miller, Basic Gas Chromatography, Wiley & Sons, New York, (1998).

[7] J.C. Giddings, J. High Resolut. Chromatogr. 10 (1987) 319.

[8] Z. Liu, J.B. Phillips, J. Chromatogr. Sci. 29 (1991) 227.

[9] F. Ern, R.W. Frei, J. Chromatogr. A 149 (1978) 561.

[10] M. Zakaria, M.-F. Gonnord, Guiochon G., J. Chromatogr. A 271 (1983) 127.

[11] J.C. Giddings, Anal. Chem. 56 (1984) 1258A.

[12] M.M. Bushey, J.W. Jorgenson, Anal. Chem. 62 (1990) 161.

[13] J.C. Giddings, J. Chromatogr. A 703 (1995) 3.

14] L.M. Blumberg, J. Chromatogr. A 985 (2003) 29.

[15] J. Beens, H.-G. Janssen, M Adahchour, U.A.Th. Brinkman, J. Chromatogr. A 1086 (2005) 141.

[16] L.M. Blumberg, J. Sep. Sci. 31 (2008) 3358.

[17] L. Mondello, A.C. Lewis, K.D. Bartle (Eds.), Multidimensional chromatography, Chichester, John Wiley & Sons, 2002.

[18] C.J. Venkatramani, J. Xu and J.B. Phillips, Anal. Chem. 68 (1996) 1486.

[19] M.C. Simmons, L.R. Snyder, Anal. Chem. 30 (1958) 32.

[20] R. Consden, A.H. Gordon, A.J.P. Martin, Biochem. J. 38 (1944) 224.

[21] J.B. Phillips, Z. Liu, Chromatographic Technique and Apparatus; USA Patent 5, 135, 549, 1992.

[22] P.J. Schoenmakers, P.J. Marriott, J. Beens, LC-GC Eur. 16 (2003) 335.

[23] F. Focant, E. Reiner, K. MacPherson, T. Kolic, A. Sjödin, D.G. Patterson, S. Reese Jr., F. Dorman, J. Cochran, Talanta 63 (2004) 1231.

[24] M. Adahchour, J. Beens, U.A.Th. Brinkman, J. Chromatogr. A 1186 (2008) 67.

[25] P.Q. Tranchida, G. Purcaro, L. Conte, P. Dugo, G. Dugo, L. Mondello, Anal. Chem. 81 (2009) 8529.

[26] J. Beens, J. Blomberg, P.J. Schoenmakers, J. High Resolut. Chromatogr. 23 (2000) 182.

[27] P. Korytár, P. Haglund, J. de Boer, U.A.Th. Brinkman, Trends Anal.Chem. 25 (2006) 373.

[28] J. Dallüge, J. Beens, U.A.Th. Brinkman, J. Chromatogr. A, 1000 (2003) 69.

[29] P.Q. Tranchida, R. Costa, P. Donato, D. Sciarrone, C. Ragonese, P. Dugo, G. Dugo, L. Mondello, J. Sep. Sci. 31 (2008) 3347.

[30] M. Adahchour, J. Beens, R.J.J. Vreuls, A.M. Batenburg, U.A.Th. Brinkman, J. Chromatogr. A 1054 (2004) 47.

[31] L.M. Sidisky, C.A. Baney, J.L. Desorcie, K.K. Stenerson, Organohalog. Compd. 70 (2008) 2183.

[32] J.V. Seeley, S.K. Seeley, E.K. Libby, Z.S. Breitbach, Anal. Bioanal. Chem. 390 (2008) 323.

[33] J.V. Seeley, F.J. Kramp and K.S. Sharpe, J. Sep. Sci. 24 (2001) 444.

[34] J.V. Seeley, F.J. Kramp, K.S. Sharpe and S.K. Seeley, J. Sep. Sci. 25 (2002) 53.

[35] J.V. Seeley, J. Chromatogr. A 962 (2002) 21.

[36] M. Biedermann, K. Grob, J. Sep. Sci. 32 (2009) 3726.

[37] G.S. Frysinger, R.B. Gaines, L. Xu, C.M. Reddy, Environ. Sci. Technol., 37 (2003) 1653.

[38] G.F. Slater, H.K.White, T.I.Eglinton, C.M. Reddy, Environ. Sci. Technol. 39 (2005) 2552.

[39] C. Vendeuvre, F. Bertoncini, L. Duval, J.L. Duplan, D. Thiébaut, M.-C. Hennion, J. Chromatogr. A 1056 (2004) 155.

[40] P.Q. Tranchida, A. Giannino, M. Mondello, D. Sciarrone, P. Dugo, G. Dugo, L. Mondello, J. Sep. Sci. 31 (2008) 1797.

[41] B. Vlaeminck, J. Harynuk, V. Fievez, P.J. Marriott, Eur. J. Lipid Sci. Technol. 109 (2007) 757.

[42] K. Conka, B. Drobna, A. Kocan, J. Petrik, J. Chromatogr. A 1084 (2005) 33.

[43] J. Aybar-Munoz, E. Fernandez-Gonzalez, L.E. Garcia-Ayuso, A. Gonzalez-Casado, L. Cuadros-Rodriguez, Chromatographia 61 (2005) 505.

[44] B. Gomara, L. Ramos, M.J. Gonzalez, J. Chromatogr. B 766 (2002) 279.

[45] G.S. Frysinger, R.B. Gaines, J. High Resolut. Chromatogr. 22 (1999) 251.

[46] M. van Deursen, J. Beens, J. Reijenga, P. Lipman, C. Cramers, J. Blomberg, J. High Resol. Chromatogr. 23 (2000) 507.

[47] R. Shellie, P.J. Marriott, C.W. Huie, J. Sep. Sci. 26 (2003) 1185.

[48] R. Shellie, P.J. Marriott, Analyst 128 (2003) 879.

[49] C. Cordero, C. Bicchi, D. Joulain, P. Rubiolo, J. Chromatogr. A 1150 (2007) 37.

[50] L. Mondello, A. Casilli, P.Q. Tranchida, G. Dugo, P. Dugo, J.Chromatogr. A 1067 (2005) 235.

[51] G. Purcaro, P.Q. Tranchida, P. Dugo, E. La Camera, G. Bisignano, L.Conte, L. Mondello, J. Sep. Sci. 33 (2010) 2334.

[52] R.E. Murphy, M.R. Schure, J.P. Foley, Anal. Chem. 70 (1998) 1585.

[53] L.M. Blumberg, J. Chromatogr. A 985 (2003) 29.

[54] T. Górecki, J. Harynuk, O.J. Paníc, J. Sep. Sci. 27 (2004) 359.

[55] J.B. Phillips, R.B. Gaines, J. Blomberg, F.W.M. van der Wielen, J.-M. Dimandja, V. Green, J. Granger, D. Patterson, L. Racovalis, H.-J. De Geus, J. de Boer, P. Haglund, J. Lipsky, V. Sinha, E.B. Ledford Jr., J. High Resolut. Chromatogr. 22 (1999) 3.

[56] R.M. Kinghorn, P.J. Marriott, J. High Resolut. Chromatogr. 21 (1998) 32.

[57] E.B. Ledford Jr., 23rd International Symposium on Capillary Chromatography, 5–10 June 2000, Riva del Garda, Italy.

[58] E.B. Ledford, C. Billesbach, J. Termaat, Pittcon 2002, 17–22 March 2002, New Orleans, LA, USA.

[59] J. Harynuk, T. Górecki, J. Sep. Sci. 27 (2004) 431.

[60] T. Veriotti, R. Sacks, Anal. Chem. 73 (2008) 3045.

[61] C.A. Bruckner, B.J. Prazen, R.E. Synovec, Anal. Chem. 70 (1998) 2796.

[62] J.V. Seeley, F. Kramp, C.J. Hicks, Anal. Chem. 72 (2000) 4346.

[63] C.G. Fraga, B.J. Prazen, R.E. Synovec, J. High Resolut. Chromatogr. 23 (2000) 215.

[64] C.G Fraga, C.A. Bruckner, R.E. Synovec, Anal. Chem. 73 (2001) 675.

[65] A.E. Sinha, K.J. Johnson, B.J. Prazen, S.V. Lucas, C.G. Fraga, R.E. Synovec, J. Chromatogr. A 983 (2003) 195.

[66] J.V. Seeley, N.J. Micyus, J.D. McCurry, S.K. Seeley, Am. Lab. 38 (2006) 24.

[67] R.W. LaClair, P.A. Bueno, J.V. Seeley, J. Sep. Sci. 27 (2004) 389.

[68] J.V. Seeley, S.K. Seeley, E.M. Libby, J.D. McCurry, J.Chromatogr. Sci. 45 (2007) 650.

[69] J.V. Seeley, E.M. Libby, S.K. Seeley, J.D. McCurry, J. Sep. Sci. 31 (2008) 3337.

[70] M. Poliak, M. Kochman, A. Amirav, J. Chromatogr. A 1186 (2008) 189.

[71] M. Poliak, A.B. Fialkov, A. Amirav, J. Chromatogr. A 1210 (2008) 108.

[72] P.McA. Harvey, R.A. Shellie, P.R. Haddad, J. Chromatogr. Sci. 48 (2010) 245.

[73] B. Quimby, J. McCurry, W. Norman, LC-GC the peak April (2007) 7.

[74] P.Q. Tranchida, G. Purcaro, A. Visco, L. Conte, P. Dugo, P. Dawes, G. Dugo, L. Mondello, J. Chromatogr. A 1218 (2011) 3140.

Chapter 3

Research in the field of comprehensive two-dimensional gas chromatography coupled to various forms of mass spectrometry

3.0 Multidimensional gas chromatographic techniques applied to the analysis of lipids from wild-caught and farmed marine species

3.1. Introduction

Comprehensive two-dimensional gas chromatography-mass spectrometry was exploited for the obtainment of fatty acid fingerprints in fish and molluscs from South Italy. Scope of the lipidomic investigation was to highlight differences in the fatty acid profiles of samples from aquaculture and from the wild. Another aim was to find a correlation between the diet fed to fish and the expression of specific fatty acids in muscle composition. According to the Organization for Economic Cooperation and Development (OECD) and to the Food and Agriculture Organization (FAO), in 2022 the world aquafarming will be increased by a 35% factor, while traditional fishing only by 5% [1]. The global production of aquafarmed seafood for human consumption will increase from 49% in 2012, to 62% in 2030. In Italy, the most cultivated fish species are: Gilthead sea bream (*Sparus aurata*), brown trout (*Salmo trutta*), sea bass (*Dicentrarchus labrax*), and rainbow trout (*Oncorhynchus mykiss*). Among shellfish, a kind of mussels (*Mytilus galloprovincialis*) and a variety of clams are those with the highest rate of production. Fish represents an important source of nutrients, providing proteins and fats of animal origin. Lipids from fish, for instance, constitute a topic of primary interest in the scientific community, due to a series of diverse, health-correlated effects, exerted in humans [2]. Nonetheless, EU regulations on food safety are present, and cannot be ignored, even in this field, in order to guarantee humans' security. As a matter of fact, fish farming implies the establishment of rearing conditions that are far from those of wild species.

Animals from aquaculture are raised under controlled conditions and regularly fed a diet program. In other words, along with fish, the feed administered to fish enters the human food chain in directly as well, also in consideration of the fact that some species are becoming available only from aquafarms and are rarely wild-caught. Scope of this work consisting of the assessment of quality and safety of Mediterranean seafood and to see how the feeding regime can affect the fatty acids composition of some fish and bivalve species coming from Sicily.

As concerns fish, a group of publications focused on a differentiation between wild and aquafarmed individuals, using fatty acids composition as discriminant factor [3–6]; other studies were based on: i) determination of oxidative stress upon lipids during fish ageing [7]; comparison between fatty acid profiles of fish from freshwater and seawater, and from seawater (wild caught) and the market [8, 9]; correlation between fish diet and fatty acids profile [10, 11]; changes of fatty acid composition upon irradiation [12]; determination of branched-chain fatty acids [13].

In this study, a method based on the use of comprehensive gas chromatography (GC×GC) was developed for the achievement of bidimensional fingerprints of fatty acids extracted from edible fish and shellfish. Samples were fish (sea bass and gilthead sea bream) from aquafarms and from the wild. Mussels were from aquaculture while clams were harvested in a local salt lake. The bidimensional plots obtained highlighted, in real time, differences between samples having different origin.

3.2 Experimental

3.2.1 Samples and sample preparation

Samples of clams (V. aurea var. laeta) were harvested in the salt lake of Ganzirri (Sicily, Italy), where the bivalve species is native. Mussels (M. galloprovincialis) were kindly provided by mollusc farms, located in a minor salt lake, lake of Faro, in proximity of Ganzirri lake. Fish samples were sea bass (D. labrax) and gilthead sea bream (S. aurata), coming in great part from the Sicilian aquafarm located in the neighbourhood of Syracuse. Other fish samples of both species were wild caught in the Strait of Messina, Mediterranean Sea, by traditional fishing.

To obtain the lipid fraction, samples were extracted according to Bligh & Dyer method [14] Specifically, 10 gr of animal's flesh were homogenized with 10 mL of chloroform ($CHCl_3$) and 20mL of methanol (MeOH). The resulting mixture was added again with 10 mL of $CHCl_3$ and 10 mL of water, and stirred. Successively, the mixture was filtered through paper and the obtained solution was allowed to stand. Finally, the solution was centrifuged for 15 min at 3000 rpm. The bottom layer was then collected and transferred into a rotating evaporator. For an exhaustive extraction, the upper layer was subjected again to all the steps above described.

For transesterification of fatty acids, at 100 mg of lipidic extract were added 1 mL of sodium methoxylate and heated at 100°C for a period of 15 min. After cooling down the solution, 1 mL of boron trifluoride/methanol (14% BF_3) was added, and again temperature, was raised to 100°C for 15min. 1 ml of hexane was added to the cool solution, along with 4mL of a saturated sodium chloride solution. After agitation and centrifugation, the organic layer containing fatty acid methyl esters (FAMEs) was collected and injected in the GC systems.

3.2.2 GC-FID analysis

For quantification of FAMEs, a GC-2010 system was used, equipped with a Supelcowax-10 column (dimensions: 30 m 0.25 mm id 0.25 mm d_f). Oven temperature program was as follows: 50°C, at 3°C/ min, to 280°C (5 min). Injector and FID temperatures were both set at 280°C. Carrier gas was He, at a constant linear velocity of 30.0 cm/s and an initial head pressure of 99.5 KPa. Prior to injection, at the sample of FAMEs was added undecanoic acid as internal standard. Injection volume was 1.0 mL of FAMEs in hexane, with a split ratio 1:100. Raw FID areas were corrected by relative response factors, measured for each FAME against the C11:0 FAME, added as internal standard to each concentration level:

$$RRF = \frac{(FID\ area_{i.s})(Conc.FAME)}{(FID\ area\ FAME)(Conc._{i.s.})}$$

where *i.s*. is internal standard and Conc. is concentration (ppm). Calibration curves were built on five concentration levels, with triplicate analyses for each calibration point.

3.2.3 GC×GC–MS analysis

The GC×GC analyses were carried out on a gas chromatograph-quadrupole mass spectrometer, (GCMS-QP 2010), loop-type, dual stage ZOEX thermal modulator. The GC was equipped with an AOC-20i auto- injector, and a split/splitless injector (350°C). The first column was connected by using an SGE SilTite mini-union to an uncoated tubing (1 m 0.25 mm ID), and was finally connected to the secondary column by using a mini-union. Cryogenic modulation was applied every 5 s, with a hot jet (325°C) duration of 400ms.

The first dimension was an SLB-5 ms 30 m 0.25 mm ID 0.25 mm d_f column, while the second one was a Supelcowax-10, 1.5m 0.10mm ID 0.10 mm d_f column. The oven temperature program was from 100°C to 270°C at 2°C/min. The carrier gas (helium) was delivered at an initial pressure of 260 kPa. Injection was performed in the split mode (20:1); injection volume was 0.2 mL, at constant linear velocity (1D: 20 cm/s, 2D: 213 cm/s).

MS parameters: the sample was analyzed in the full scan mode with a scan speed of 20,000 amu/s, a mass range of 40–400m/z and a sampling frequency of 33 spectra/s; interface and ion source temperatures were 220 and 200°C, respectively. MS ionization mode: electron impact. Data were acquired by using the GCMSsolution software ver. 4.0 (Shimadzu). Bidimensional chromatograms were generated by using the ChromSquare software ver. 2.0 (Shimadzu, Kyoto, Japan). Peak assignment was carried out by exploiting three tools: (i) mass spectral matching with dedicated library [20wor]; (ii) co-injection with standards; (iii) Retention Index comparison (experimental vs. published).

3.3 Results and discussion

3.3.1 Fatty acid composition and distribution

Table 1 reports the GC-FID composition of FAMEs determined in all samples under investigation. Values are expressed as g/100g (weight%) and were obtained by applying FID peak area normalization with the use of response factors (RFs). Along with quantitative values, Retention Indices are reported from both experimental and published data, whose comparison supported the identification procedure. Quantitative data from Table 1 were also plotted in Figure 1, where the main classes of fatty acids, namely saturated (SFAs), polyunsaturated (PUFAs), and monounsaturated (MUFAs), were grouped.

The in-sample distribution of fatty acids in fish was dominated by MUFAs and PUFAs in sea bass (both farmed on dry land and in open seawater) and in farmed gilthead sea bream. The scenario appeared to be significantly different in wild gilthead individuals, where a noticeable reduction of MUFAs was demonstrated. This finding can be justified by the observation of Figure. 2 relatives to gilthead sea bream fish. It can be seen that predominant components in wild individuals are DHA, palmitic, stearic, and arachidonic acids. This composition was very different from that shown by aquafarmed individuals of the same species.

DHA was present at about 4 versus 21%, palmitic 13 versus 22%, and stearic 4 versus 13 in cultivated and wild fish, respectively. Furthermore, farmed individuals highlighted an abundant presence of oleic and linoleic acids (36 and 19%). Such dissimilarity between wild and raised fish subjects could be ascribed to animals' nutrition. For instance, fish oil and rapeseed oil are among the constituents of the fish feed administered to animals in the aquafarm (see Table 2). Rapeseed oil typically contains around 60% oleic acid, 10% linolenic acid, and 22% linoleic acid [15]. Indeed, these three fatty acids were not present, or present at reduced amounts, in wild type samples, while they were determined in farmed fish at considerable levels. Also, traces of erucic acid, a typical constituent of the raw rapeseed oil, were found in the aquafarmed individuals.

Table 1. GC × GC composition of fatty acid methyl esters expressed as weight% (wt%) in fish and shellfish under investigation

				Farmed gilthead	Wild gilthead	Farmed sea bass	Farmed sea bass (open sea)	Clams	Mussels
FAME	RI_{lib}	RI_{exp}	R.F.	Wt%	Wt%	Wt%	Wt%	Wt%	Wt%
C12:0	1523	1521	1.09	0.19	–	0.04	–	0.04	0.14
C13:0	1624	1621	1.09	0.01	–	–	–	–	–
C14:1n5	1714	1708	1.07	0.06	–	0.04	0.05	–	–
C14:0	1724	1722	1.09	1.70	0.98	2.04	2.39	1.91	0.58
C15:0 iso	1787	1783	1.08	0.08	–	0.03	0.03	0.06	1.12
C15:0 anteiso	1795	1791	1.08	0.05	–	0.05	0.06	–	–
C15:0	1825	1821	1.08	0.23	0.57	1.16	0.25	0.25	0.67
C16:4n1	1882	1879	1.08	0.22	–	0.2	0.24	–	1.03
C16:0 iso	1888	1885	1.09	0.04	–	0.03	–	0.4	–
C16:3n4	1888	1885	1.08	0.20	–	0.21	0.24	–	0.99
C16:2n6	–	1887	1.07	0.07	–	0.09	0.08	–	–
C16:3n3	1894	1890	1.08	0.11	–	0.1	0.09	–	–
C16:0 anteiso	1894	1893	1.09	0.03	2.04	0.05	0.21	–	–
C16:1n9	1897	1898	1.07	0.48	0.3	0.54	0.40	–	–
C16:2n4	1905	1898	1.07	0.12	–	0.12	0.08	0.68	0.76
C16:1n7	1903	1907	1.07	3.33	1.18	2.89	3.12	3.85	10.59
C16:1n5	1902	1909	1.07	0.07	0.26	0.07	0.09	0.58	0.23
C16:0	1925	1920	1.09	12.78	21.96	12.82	15.24	13.79	12.49
C17:1	2002	1985	1.06	0.17	0.89	0.17	0.12	–	0.11
C17:0 iso	–	1987	1.08	0.13	–	0.10	0.15	0.97	0.36
C17:0 anteiso	2026	1990	1.08	0.11	0.27	0.12	0.12	0.76	–
C17:0	2026	2020	1.08	0.07	0.17	0.06	0.07	1.34	8.62
C18:3n6	2080	2070	1.01	0.41	0.44	0.31	0.26	–	0.24
C18:4n3	2078	2075	1.01	0.47	0.26	0.48	0.61	0.55	3.38
C18:2n9	2078	2077	1.01	0.27	1.73	0.32	0.20	–	1.04
C18:1n7	2103	2080	1.02	0.09	1.5	2.66	2.32	0.96	–
C18:3n4	2089	2084	1.01	–	–	–	0.14	–	–
C18:3n3	2107	2086	1.01	3.67	–	3.78	3.59	0.33	1.27
C18:2n6	2096	2087	1.01	18.80	1.75	19.08	18.78	0.74	1.03
C18:1n11	2095	2108	1.02	2.75	–	0.11	0.10	6.55	1.56
C18:1n9	2098	2115	1.02	36.10	7.89	33.83	27.54	7.59	4.38
C18:0iso	–	2120	1.05	0.03	0.29	–	0.19	0.31	–
C18:2n3	–	2121	1.01	–	–	–	0.11	0.20	–
C18:0	2126	2122	1.05	3.61	12.78	3.55	3.47	9.72	6.44
C19:1	–	2235	1.01	0.30	–	0.25	0.20	–	–
C19:0	2227	2240	1.01	0.07	0.14	0.06	0.07	–	–
C20:4n6	2252	2248	0.99	0.25	11.32	0.18	0.18	1.85	1.86
C20:5n3	2258	2256	0.99	1.73	2.98	2.92	4.05	7.09	28.49
C20:3n6	2271	2267	0.98	0.25	0.15	0.15	0.16	0.11	–
C20:2n4	2280	2275	0.98	0.62	0.33	0.91	0.81	1.3	0.27
C20:4n3	2280	2275	0.99	0.45	–	0.38	0.43	0.24	0.72
C20:2n6	2294	2287	0.98	0.22	–	0.07	0.07	1.27	0.42
C20:1n9	2298	2291	1.00	0.16	–	0.11	0.11	1.47	1.55
C20:3n4	–	2305	0.98	0.31	–	–	0.72	0.12	–
C20:0iso	2288	2315	1.01	–	–	–	–	–	1.27
C20:0	2326	2319	1.01	0.36	0.14	0.3	0.32	0.33	–
C20:1n11	2297	2317	1.00	2.05	0.31	1.59	2.52	1.58	1.66
C20:1n7	2300	2319	1.00	–	–	–	–	–	1.15
C21:5n3	2362	2356	0.99	1.04	–	1.11	1.07	0.35	0.15
C21:0	2429	2422	0.99	0.17	–	0.12	–	–	–
C22:5n7	2439	2431	0.99	0.08	2.29	0.13	0.21	0.62	1.42

(*Continued*)

Table 1. (*Continued*)

FAME	RI_{lib}	RI_{exp}	R.F.	Farmed gilthead Wt%	Wild gilthead Wt%	Farmed sea bass Wt%	Farmed sea bass (open sea) Wt%	Clams Wt%	Mussels Wt%
C22:6n3	2444	2440	0.99	3.69	20.83	4.78	7.26	22.37	1.39
C22:4n6	2454	2446	0.99	0.11	2.22	0.16	0.20	–	–
C22:1n9	2500	2489	0.98	0.10	–	0.07	–	–	–
C22:5n3	2110	2498	0.99	1.34	2.13	0.97	1.08	2.63	–
C22:4n3	–	2507	0.99	0.13	–	–	–	–	–
C22:0	2528	2520	0.98	0.02	0.12	0.02	–	–	–
C24:1n9	2703	2698	0.97	0.25	–	0.04	0.15	–	–
C22:2n6	2294	2700	0.99	–	–	–	–	7.12	2.80
C23:1	–	2705	0.99	0.04	–	0.04	–	–	–
C23:0	2629	2710	0.99	0.08	–	0.06	–	–	–
C24:0	2729	2722	0.99	0.06	1.8	0.06	0.06	–	–
ω6/ω3				*1.61*	*0.61*	*1.37*	*1.07*	*0.33*	*0.18*
Average wet weight (g)				239.6 ± 97.77	517.5 ± 208.59	289.78 ± 150.88	571.33 ± 35.79	0.33 ± 0.07	4.5 ± 0.6
Average total length (cm)				25.28 ± 3.84	36.20 ± 5.27	30.44 ± 6.72	37.68 ± 2.58	1.7 ± 0.5	6.6 ± 0.4
Number tested				10	5	10	10	N/A	N/A

RI_{lib}, Retention Index retrieved from GC-MS library "FAMEs" [20]; RI_{exp}, Retention Index experimentally determined on SLB-5 ms column; R.F., Response factor; N/A, not available.

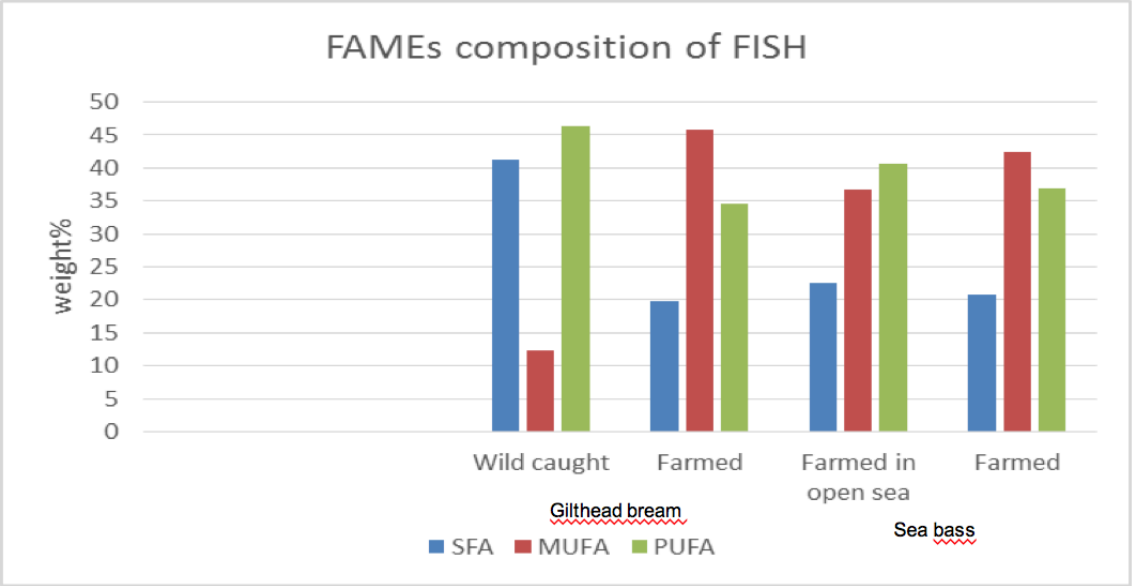

Figure 1. Fatty acid classes determined in fish samples. SFA, saturated fatty acids; MUFA, monounsaturated fatty acids; PUFA, polyunsaturated fatty acids.

The composition of fatty acid classes in molluscs was, with the exception of SFAs, significantly different from that of fish (see Figure 3). Both mussels and clams reported a lower percent of MUFAs (25 vs. 40% ca.) and a higher

percent of PUFAs (50 vs. 40% ca.). It is worth highlighting that the clam species under investigation, namely *V. aurea* var. *laeta,* is native to Ganzirri lake. Only few data are available in literature about this clam species. When observing the distribution of predominant fatty acids in the two types of molluscs (Figure 4), it is evident that DHA dominates the composition in clams, whereas EPA is the predominant fatty acid in mussels. Similar levels of palmitic acid were determined, while a short remark should be given about C17:0 fatty acid.

The latter was determined in both molluscs but in a definitely higher percentage in mussels. This is in accord with previous findings from other research studies [16,19]. As above mentioned, from the observation of literature data the clam species *Venerupis aurea* appears to be under investigated. Therefore, a comparison of the present data with those elsewhere reported for the species *Tapes decussatus* and *Tapes philippinarum* (often confused with each other), has been made. The latter species are those commonly found in the fish market. When taking in consideration the distribution of predominant fatty acids, the composition of *V. aurea* resulted to be closer, but not superimposable, to that of *T. philippinarum.* In fact, compared either to *T. decussatus* or to *T. philippinarum,* the clam species under investigation showed similar contents of DHA (22.4 vs. 14–20%, respectively) and of oleic acid (7 vs. 5–10%, respectively) [17,18].

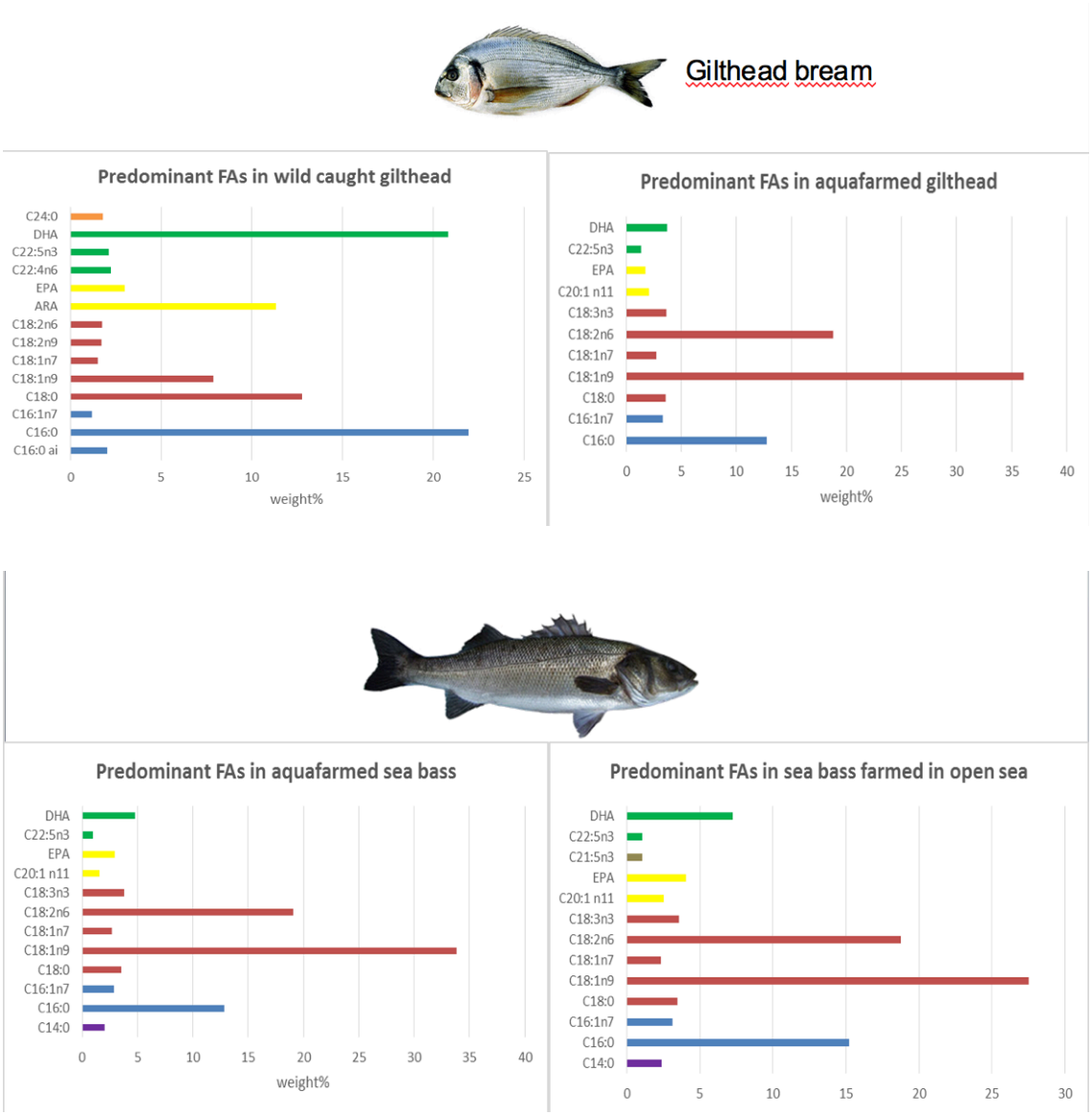

Figure 2. Predominant fatty acids determined in fish samples.

3.3.2 GC×GC distribution pattern

Figures 5 and 6 show two bidimensional chromatograms obtained from a sample of wild caught and farmed gilthead sea bream, respectively. The different spatial arrangement of fatty acid groups clearly indicates the differences between the two samples, specifically reported in Table 1

Table 2. Fish feed composition and label information

Food	Component %
Fish meal	Crude protein (43%)
Soybean meal	rude fat (21%)
Corn gluten	Crude fiber (1.9%)
Fish oil	Ash (9%)
Soybean protein conc.	Phosphorous (1.16%)
Guar germ meal	Sodium (0.23%)
Pea	Calcium (1.61%)
Rapeseed oil	
Wheat meal	

Single blobs of fatty acids distribute according to the number of carbon atoms (carbon number, CN) and the omega number (proximity of the double bonds to the end of the acyl chain) in the first dimension, and degree of unsaturation in the second dimension; the omega number decreases along the 1D axis. The group-type arrangement in the 2D space is today a well-known tool for boosting qualitative analysis in comprehensive GC.

Beyond relying on the three identification procedures listed above, the GC×GC distribution pattern represents an interesting means for confirming uncertain peaks or predicting their identity. As explained, spatial distribution follows specific rules, depending upon the set of columns used and their selectivity.

The crowded chromatogram shown in Figure 6 highlights the complexity of the lipidic samples here analyzed. Quite often, even the most accurate GC-MS systems fail in peak assignment's procedure, mainly because of impure mass spectra deriving from co-elutions.

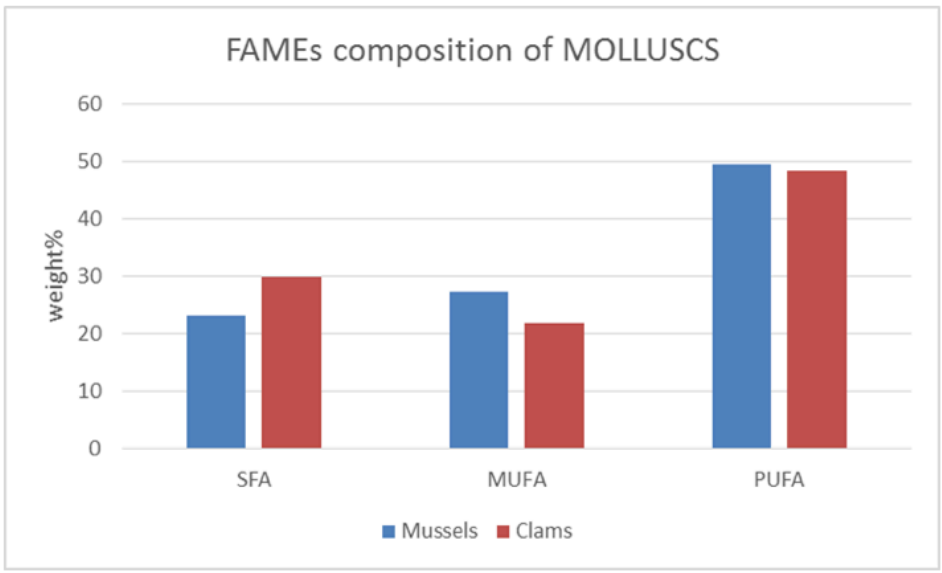

Figure 3 Fatty acid classes determined in fish and shellfish samples. SFA, saturated fatty acids; MUFA, monounsaturated fatty acids; PUFA, polyunsaturated fatty acids.

The increased separation power and higher sensitivity of comprehensive GC allow for an almost complete fingerprint to be obtained. The GC×GC method was tested for repeatability through measurement of RSD% of retention times (RSD % <0.6 and <0.4%, for the first and second dimensions, respectively) and peak areas (RSD% range: 0.9–12.7%) coming from three replicates.

Inter-day precision was assessed by considering the same variables derived from single runs in four consecutive days (RSD% <1.0%, <0.9% for 1D and 2D retention times; RSD% range: 3.8–14.5%).

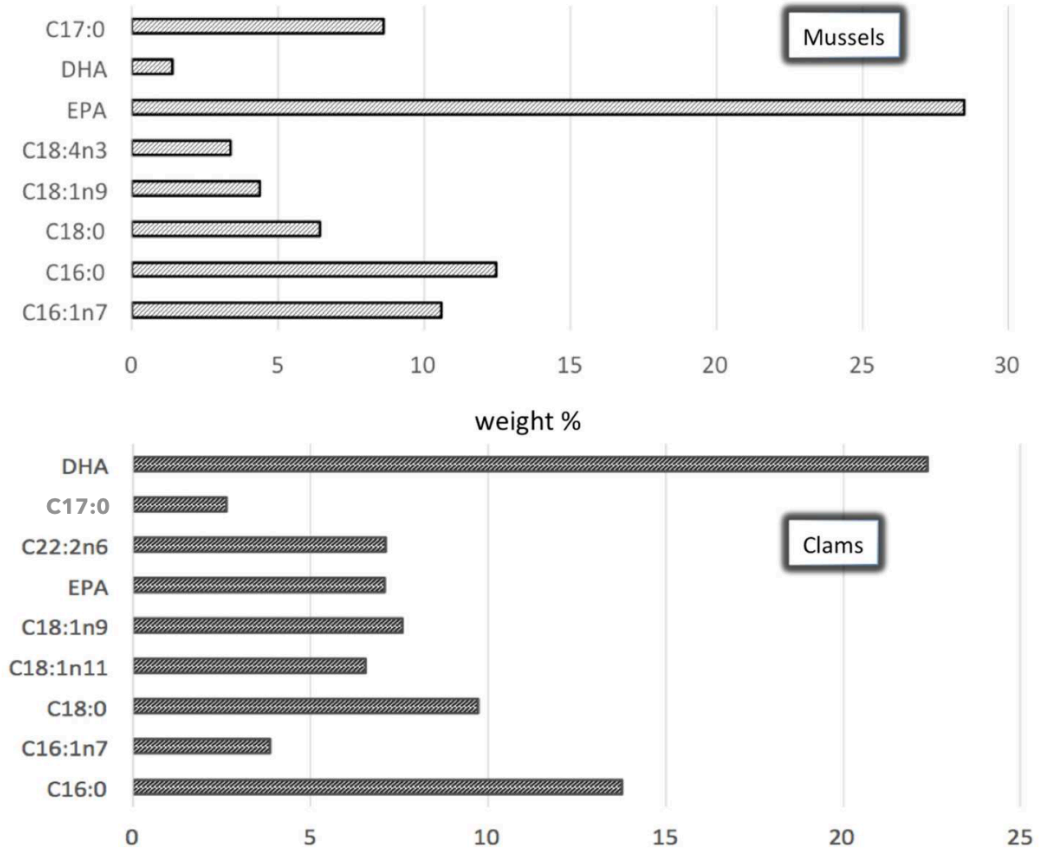

Figure 4. Predominant fatty acids determined in clams and mussels.

3.4 Conclusion

Comprehensive two-dimensional gas chromatography coupled with mass spectrometry was exploited for the obtainment of fatty acid fingerprints in fish and molluscs from aquaculture and from the wild. The lipidomic profiles of fish samples highlighted relevant differences between farmed and wild individuals. Due to the diet fed to animals in captivity, the total weight of fatty acids was found to be higher in aquafarmed fish. However, the beneficial omega-3 fatty acids were naturally more concentrated in wild fish, whereas their presence in cultivated fish was lower and in favour of omega-6 and oleic

acid, as an evident consequence of food supplementation. Some fatty acids were detected only in one type of fish (wild or farm-raised), or were

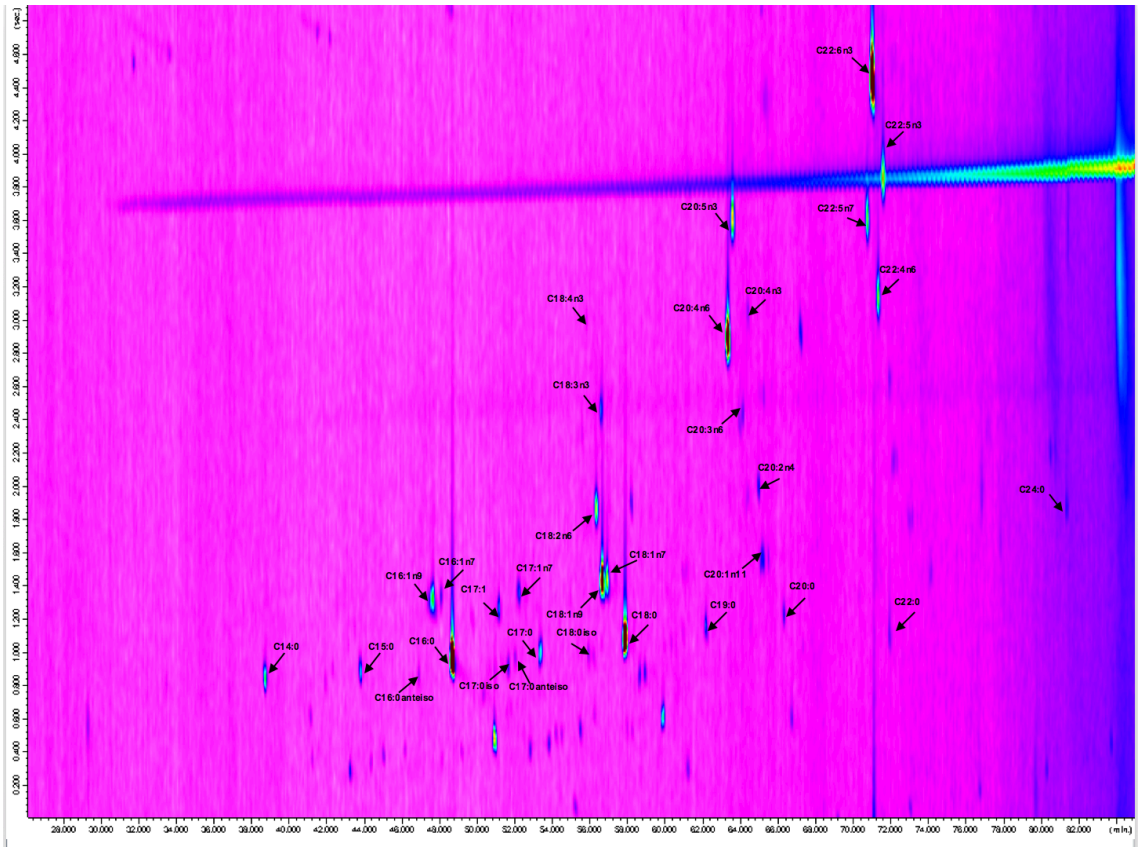

Figures 5 Bidimensional plots obtained for samples of wild caught gilthead sea bream by means of GC×GC- MS

determined at very different levels. For instance, the biological mediator arachidonic acid, was almost 50 times more concentrated in wild-caught fish. On the other hand, when considering the content of mercury, aquafarmed fish resulted to be safer compared to wild fish.

The latter reported the maximum tolerable amount of mercury, according to the EC regulation.

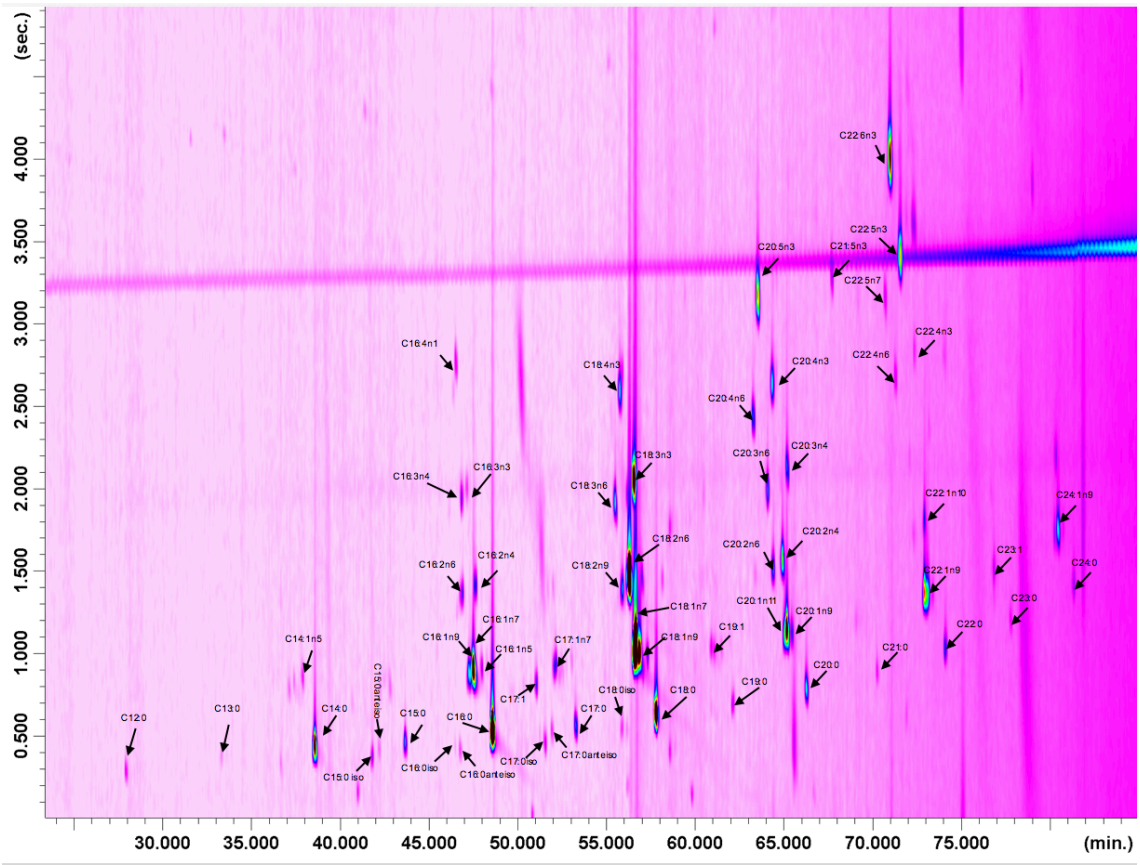

Figures 6 GC×GC-MS chromatogram of aquafarmed gilthead sea bream

This finding emphasizes the role of bioaccumulation of toxins from pollution in the Mediterranean Sea up the food chain and into the flesh of wild-caught fish versus aquafarmed fish, which were raised in the same waters but were fed a controlled diet. Both mussels and clams were characterized by an abundant presence of polyunsaturated fatty acids, and ultralow level of mercury. In particular, the clam species *V. aurea* var. *laeta,* was here investigated for the first time relatively to its lipidic profile. No relevant differences could be observed when making a comparison with the more common clams found in the fish market. The level of mercury found in the

bivalves resulted to be much lower than that previously reported for samples collected in other Italian coastal sites. In some cases, (lipidomic analysis and mercury content of clams), the information here provided resulted to be valuable and unprecedented.

References

[1] FAO, The state of world fisheries and aquaculture. Rome, 2012

[2] Schwab, U., Lauritzen, L., Tholstrup, T., Haldorsson, T. I., et al., Effect of the amount and type of dietary fat on cardiometabolic risk factors and risk of developing type 2 diabetes, cardiovascular diseases, and cancer: A systematic review. Food Nutr. Res. 2014, 58, 25145.

[3] Saglik, S., Alpaslan, M., Gezgin, T., CS etintu€rk, K., et al., Fatty acid composition of wild and cultivated gilthead seabream (Sparus aurata) and sea bass (Dicentrarchus labrax). Eur. J. Lipid Sci. Technol. 2003, 105, 104–107.

[4] Orban, E., Nevigato, T., Di Lena, G., Casini, I., Marzetti, A., Differentiation in the lipid quality of wild and farmed seabass (Dicentrarchus labrax) and gilthead sea bream (Sparus aurata). J. Food Sci. 2003, 68, 128–132.

[5] Monti, G., De Napoli, L., Mainolfi, P., Barone, R., et al., Monitoring food quality by microfluidic electrophoresis, gas chromarography, and mass spectrometry techniques: Effects of aquaculture on the sea bass (Dicentrarchus labrax). Anal. Chem. 2005, 77, 2587–2594.

[6] Fasolato, L., Novelli, E., Salmaso, L., Corain, L., et al., Application of nonparametric multivariate analyses to the authentication of wild and farmed European sea bass (Dicentrarchus labrax). Results of a survey on fish sampled in the retail trade. J. Agric. Food Chem. 2010, 58, 10979– 10988.

[7] Passi, S., Ricci, R., Cataudella, S., Ferrante, I., et al., Fatty acid pattern, oxidation product development, and antioxi- dant loss in muscle tissue of rainbow trout and Dicentrarchus labrax during growth. J. Agric. Food Chem. 2004, 52, 2587– 2592.

[8] Ozogul,Y., Ozogul, F., Alagoz S., Fatty acid profiles and fat contents of commercially important seawater and freshwater fish species of Turkey: A comparative study. Food Chem. 2007, 103, 217–223.

[9] Prato, E., Biandolino, F., Total lipid content and fatty acid composition of

commercially important fish species from the Mediterranean, Mar Grande sea. Food Chem. 2012, 131, 1233–1239.

[10] Nasopoulou, C., Smith, T., Detopoulou, M., Tsikrika, C., et al., Structural elucidation of olive pomace fed sea bass (Dicentrarchus labrax) polar lipids with cardioprotective activities. Food Chem. 2014, 145, 1097–1105.

[11] Aslan, S. S.,CS oban, B., Tekinay, A., Gezgin, T., Guven, K. C, Effects of pellet and extruded feed on fatty acid composition of European sea bass (Dicentrarchus labrax) using HRGC-MS. Fresen. Environ. Bull. 2009, 18, 112–116.

[12] Erkan, N., O€zden, O€, The changes of fatty acid and amino acid compositions in sea bream (Sparus aurata) during irradiation process. Radiat. Phys. Chem. 2007, 76, 1636–1641.

[13] Hauff, S., Vetter, W., Quantification of branched chain fatty acids in polar and neutral lipids of cheese and fish samples. J. Agric. Food Chem. 2010, 58, 707–712.

[14] Bligh, E. G., Dyer, W. J., A rapid method of total lipid extraction and purification. Can. J. Biochem. Physiol. 1959, 37, 41–53.

[15]AOCS lipid library, available at www.lipidlibrary.aocs.org/ OilsFats/content.cfmItemNumber = 39461

[16] Otles, S., Sengor, G., Effect of various technological processes on the fatty acid composition of mussel (Mytilus galloprovincialis, L.). Int. J. Food Eng. 2005, 1, art. 5.

[17] Beninger, P. G., Stephan, G., Seasonal variations in the fatty acids of the triacylglycerols and phospholipids of two populations of adult clams (Tapes decussatus L. and T. philippinarum) reared in a common habitat. Comp. Biochem. Physiol. 1985, 81B, 591–601.

[18] Teshima, S.-I., Kanazawa, A., Koshio, S., Mukai, H., et al., Fatty acid details for bivalves, Tapes philippinarum and Corbucola japonica, and marine types of algae, Nannochlor- opsis sp. and Chlorella sp. Mem. Fac. Fish.

Kagoshima Univ. 1990, 39, 137–149.

[19] Bongiorno, T., Iacumin, L., Tubaro, F., Marcuzzo, E., et al., Seasonal changes in technological and nutritional quality of Mytilus galloprovincialis from suspended culture in the Gulf of Trieste (North Adriatic Sea). Food Chem. 2015, 173, 355–362.

[20] Mondello, L, FAMEs Fatty Acid Methyl Esters: Mass Spectral Database. Wiley, Hoboken 2011.

Chapter 4

Fast gas chromatography

4.0 Introduction

Since the introduction of GC, there has been a continuous interest in increasing the speed of GC analyses. Faster GC obviously has a considerable number of advantages. Throughput in the analytical laboratory can be increased significantly, resulting in lower operational costs per sample, better utilization of high-cost equipment. The shorter "time-to-result" of fast GC is attractive for situations where the results of the analysis are needed, for *e.g.* process control, or product or feedstock clearance. Moreover, fast GC has, therefore, attracted a great deal of attention in on-line process analysis. Last but not least advantage of fast GC is that it allows several replicated analyses of a sample in the same time as a single conventional GC separation, thus obtaining improved precision and sensitivity. Since the introduction of capillary column the basic principles and theory of fast GC were already established, even then, many studies on the theoretical background of fast GC, the development of suitable instrumentation and applications of the technique have been published. Viewed the huge application area of GC and the widely differing types of questions that are resolved using GC the evaluation of the result is very difficult. As an example, using a very narrow capillary column, the fast GC separation of nine peaks in less than 0.7 s had already been demonstrated more than a decade ago [1]. Short narrow-bore columns are also successfully used to determine the main components in natural gas [2]. Unfortunately, this separation speed cannot be extrapolated to the vast majority of other separations. As an example, nine peaks in 0.7 s would mean that the 209 PCBs can be separated in approx. 16 s. At this moment, however, separation of these PCBs requires close to one hour and more than one analytical column [3]. From this, it is evident that the use of short narrow-bore columns provides a

method for very fast analysis, but that this is not a universal method. The same holds for the many other methods for faster GC that have been proposed in the literature. The wide variety of approaches for faster GC seriously complicates the situation for the analyst interested in reducing the run time of a given separation. There is no single universal method and the question of which approach to select is by no means trivial. In this article, an overview is given of the various methods available for fast GC. Some of these are more or less trivial and apply to all situations. Others are only applicable to very specific situations. Guidelines for the selection of the optimum method for increasing the speed of analysis for a given separation will be discussed, starting with the theory that describes analysis time in GC. To aid this selection process, a system for the classification of chromatograms is proposed. Successful exploitation of any method for faster GC requires careful adjustment of the settings of the GC instrument. Injection has to be fast enough to be compatible with the reduced band broadening of fast GC. Detection should be sufficiently fast and sensitive, etc. Such requirements will be addressed in some detail. In particular, we will discuss what can be done when using instrumentation that is now commercially available. Applications of successful fast GC will be discussed, but the consequences of selecting an incorrect method or neglecting the stringent instrumental requirements will also be described.

4.1. Routes towards faster separation

Various parameters influence the speed of the GC analysis, but to understand how to increase it, one should take a look at the equations that express the analysis time as a function of the various operational parameters of a GC system. Cramers and Leclercq derived pertinent equations using the Golay-Giddings plate height equation and the Hagen-Poiseuille flow relation [4,5]. The explicit relationships can be obtained only under extreme conditions of

either a high or a very low ratio of inlet to outlet pressure (*P= pi=po*) and negligible influence of the stationary phase on chromatographic band broadening. For high pressure-drop conditions, which in practice already prevail at inlet pressures of more than about 2–3 bar, the following equation holds:

$$t_R = (1+k)N_{req}^{3/2}\frac{9}{8}\sqrt{3F}(k)\left[\frac{\acute{\eta}}{p_0 D_{m,o}}\right]^{1/2} d_c \quad (\mathbf{4.1})$$

where:

$$N_{req} = 16\,{R_s}^2\left[\frac{1+k}{k}\right]^2\left[\frac{\alpha}{\alpha-1}\right]^2 \quad (\mathbf{4.2})$$

Here, *k* is the retention factor,

$$F(k) = \frac{1+6k+11k^2}{96(1+k)^2} \quad (\mathbf{4.3})$$

η the dynamic viscosity, p_o the outlet pressure, $D_{m,o}$ the diffusion coefficient of the solute in the gas phase at the outlet pressure, and *dc* the internal diameter of the capillary column; α is the relative retention ($=k_2/k_1$), Rs= Δt_R= 4σc the resolution between a critical pair of components, and σ_c the standard deviation of the chromatographic peak broadening expressed in time units. From Equations 4.1 and 4.2, which explicitly show the various parameters that affect analysis time in capillary GC, it is evident that there are basically three general routes towards a faster separation:

1. Minimise the resolution to a value just sufficient. In order to minimise N_{REQ} in Equations 4.1, and thus minimise the analysis time, R_S should

never be better than strictly necessary and only those peaks that are really important should be separated. R_S = 1.0 might already be sufficient for quantification if the degree of accuracy needed is not too high. R_S= 1.5 suffices for all analyses, even those requiring utmost accuracy.

2. Maximise the selectivity of the chromatographic system. Selectivity is the ability to distinguish between compounds. This can be done through separation or through detection (once the method for sample preparation has been selected). Select a column that gives the maximum selectivity for the critical pairs and/or apply selective detection.

3. Implement a method that reduces analysis time at constant resolution. If the analysis time in the minimum acceptable resolution situation still exceeds the desired or permitted time, options that reduce the analysis time at constant resolution can be exploited.

For each of the three general approaches, a number of distinct options for faster separations can be distinguished (Table 4.1.). Because route (i) - "Minimising the resolution" - is the fastest and lowest-risk route towards a shorter analysis time, it is recommended that it is investigated first. If this fails to give the desired result, the more elaborate routes (ii) and (iii) should be explored.

4.2 Selecting the optimal method for minimising time of operation

In Table 4.1. are reported 18 options for speeding up a given GC separation. As reported before, there are many methods that will result in a significant time reduction for all applications. Furthermore, very often, more than one

route can be adopted with the same results eventually. Capillary GC is routinely applied to an extremely wide range of analytical problems in an equally diverse range of application areas. Therefore, it is impossible to discuss how to speed up each of these single separations.

Table 4.1 Routes towards faster GC

No.	SPEEDING UP OPTIONS	GAIN IN TIME AND PRACTICAL ASPECTS
(I) Minimise resolution to value just sufficient		
1	*Shorter column length*	Time gain is proportional to length reduction in isothermal GC (IGC). In temperature-programmed GC (TPGC), gain is smaller if larger temperature range is covered, because run time is now determined by time taken for oven to reach temperature needed to elute last component. Shortening a column is irreversible. Recommend starting with option 2.
2	*Above optimum carrier gas velocity*	Time gain is proportional to velocity increase in IGC. Gain in TPGC is small, especially if larger temperatures are covered. Maximum velocity restricted by pressure regulators.
3A	*Higher isothermal temperature (isothermal GC only)*	Gain approx. two-fold for each 15 °C temperature increase (IGC). Bear in mind maximum operating temperature.
3B	*Higher initial temperature*	Gain in TPGC strongly depends on original and final programme. Typical gains only several minutes.
3C	*Higher final temperature*	
4A	*Faster temperature programming*	Gain proportional to increase in rate (TPGC). Programming rates above approx. 20–40 °C/min. require special instrumentation.
4B	*Convert isothermal GC to temperature-programmed GC*	Substantial gains possible upon going from IGC to TPGC.
5	*Pressure/flow programming*	Gain generally modest; requires electronic pressure/flow control.
6	*Lower film thickness*	Gain proportional to reduction of film thickness (thin-film columns); larger gains for thick-film columns.
(II) Maximise selectivity of chromatographic system		
7	*Use more selective stationary phase or apply coupled columns*	Significant gain in elution time is possible, but phase selection can be tedious.
8	*Use (conventional) 2D GC**	Unresolved peaks can be transferred to second column for further separation on different stationary phase. Very large gain possible, but more complex instrumentation is required.
9	Use selective detection	Significant gain possible because compounds of interest have to be separated only from each other. Separation from matrix compounds no longer necessary. Can also be used in combination with other options.
10	Apply MS detection	Significant gain possible, especially in combination with spectral deconvolution techniques. Can also be used combined with other options.
11	*Apply backflush*	Typical gain, 2–5-fold. Requires special instrumentation.
(III) Implement method that reduces analysis time at constant resolution		
12	*Reduce column inner diameter*	Gain proportional to reduction of column i.d. (high-pressure drops) or square of reduction (low-pressure drops). Ruggedness can be a problem.
13	*Use hydrogen as carrier gas*	Gain 60% *vs.* He or 100% *vs.* N_2; requires special safety precautions.
14	*Apply vacuum-outlet conditions*	Up to 6-fold gain for short, wide-bore columns. Gain for standard columns negligible. Only possible with MS detection.
15	*Apply turbulent-flow conditions*	Not a viable option for daily practice.

Fortunately, a closer look at the full range of applications shows that the various chromatograms can be categorised into a limited number of classes. Thirteen basic GC chromatogram classes (Table 4.2.) can be distinguished, based on the two most important degrees of freedom the number of peaks and the difference in boiling point between the first and the last eluting peak. The fact that, frequently in a real chromatogram, not all peaks are equally important is also considered. Now that we have discussed the various options for speeding up GC separations as well as the system for the classification of chromatograms, the applicability of each option for each type of chromatogram can be evaluated. The results for all classes are summarised in Table 4.3. Below, this process will be illustrated for two types of chromatograms. Type IV chromatograms contain a limited number of peaks, well separated under temperature-programmed conditions and eluting in a relatively narrow temperature range (about 100°C). The type IV chromatogram is clearly over- resolved. Therefore, the first step in reducing the run time starts with trading resolution for time. Good options to achieve this are shortening the column length or operating the column at a higher carrier-gas velocity. Figure 4.1. is a good example of a faster separation obtained by shortening the column. It shows the separation of Chamomile essential oil, which, under normal conditions, takes about 30 min. [6,7]. Other ways for speeding up a type IV separation are increasing the initial and/or final temperature of the temperature programme, using a higher programming rate, working with a thinner-film column or applying pressure/flow programming. The most significant reduction of analysis time is achieved by faster temperature programming, as demonstrated for an industrial glycol mixture in Figure 4.2 [8]. The analysis of this sample with a standard GC on a standard column temperature programmed at 15°C/min. took 9 min. Most of the other options in Table 4.1. would also result in a shorter analysis time for this

separation. They are, however, more difficult to implement and should therefore not be one's first option. Once the various options for speeding up this type IV separation have been fully exploited, the final chromatogram is no longer type IV, but type VI or VII, depending on the way the resolution reduction was realised and the exact effects of the route selected on the elution times of the various peaks. If a type VII (e.g. PCB analysis in Figure 4.3.) [9]) has to be made faster, options 1–6 are generally of no use.
They would all result in an unacceptable loss of resolution. This is demonstrated in Figure. 4.4., where a short normal-bore column was used to analyse Aroclor 1254 [10]. Reduction of the analysis time can now be obtained only by using one of the "constant-resolution" methods of Table 4.1. Valid options are the use of columns with a reduced inner diameter or/and using hydrogen as the carrier gas (Figure 4.5.) [9].

Applying vacuum outlet conditions is not a valid option; it is attractive only if the chromatogram requires a relatively low plate number (<20,000) so that a short, wide-bore column can be used [4]. The use of this option with a column of 10 m × 0.53 mm ID leads to a very fast separation, but, unfortunately, it also leads to a significant loss of resolution compared to normal conditions (Figure 4.6) [11]. For detailed PCB analysis, vacuum-outlet GC, although fast, is clearly not acceptable. On the other hand, it can be attractive for rapid screening. Another option that fails to produce the desired results is turbulent-flow GC.

Table 4.2. Classification system of chromatograms

Type	Chromatogram	Description
I	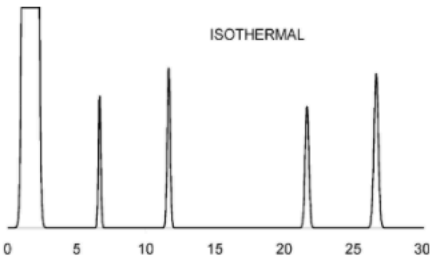	Limited number of peaks, well separated isothermally
IIA	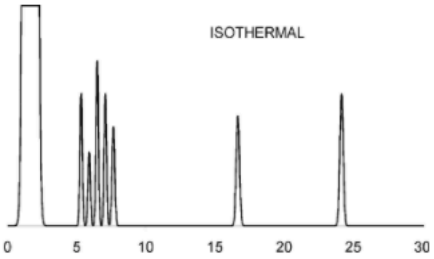	Low number of well-resolved peaks next to one or more critical pairs/groups in early part (isothermal conditions).
IIB	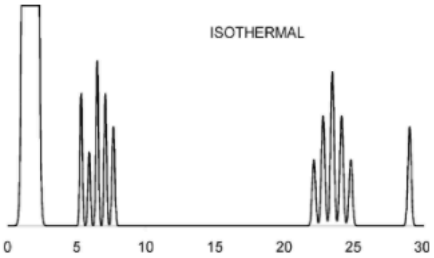	Low number of well-resolved peaks next to one or more critical pairs/groups in various positions in chromatogram (isothermal conditions).
IIC	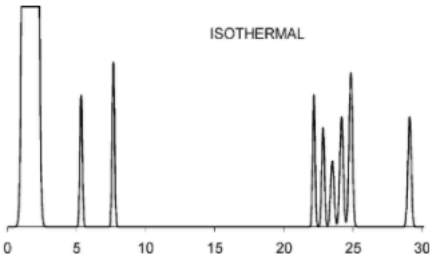	Low number of well-resolved peaks next to one or more critical pairs/groups in final part (isothermal conditions).
III	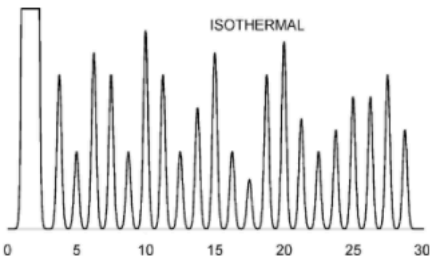	Loaded with peaks, hardly any baseline at all (isothermal conditions).

Table 4.2. continued

Type	Chromatogram	Description
IV	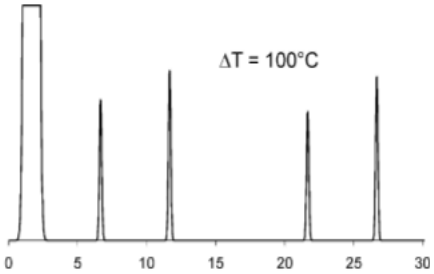	Limited number of peaks (temperature programmed). Temperature range relatively narrow (approx. 100C).
V	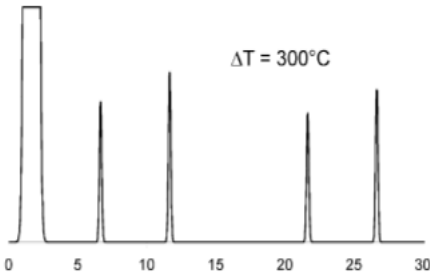	As type IV, but temperature range large (e.g. 300C).
VIA	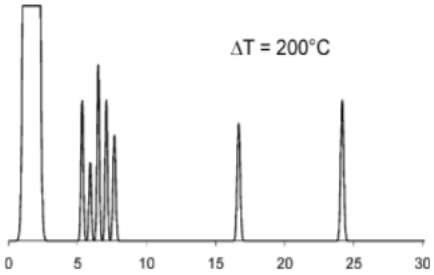	Comparable to type IIA, but now separation is temperature programmed.
VI B	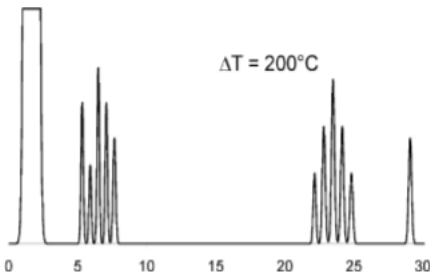	Comparable to type IIB, but now separation is temperature programmed.
VI C	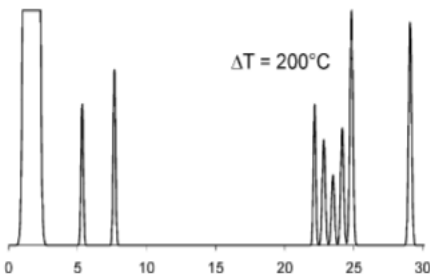	Comparable to type IIC, but now separation is temperature programmed.

Table 4.2. continued

Type	Chromatogram	Description
VII	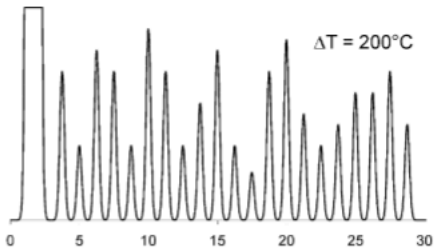	Temperature-programmed analogue of type III.
VIII	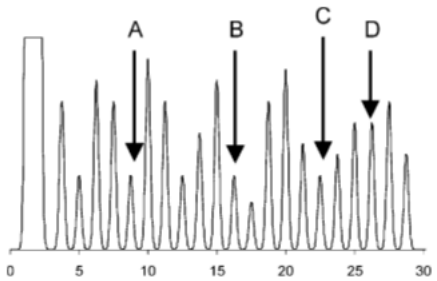	Similar to types III and VII, but now only limited number of peaks is relevant (peaks A, B, C and D)
IX	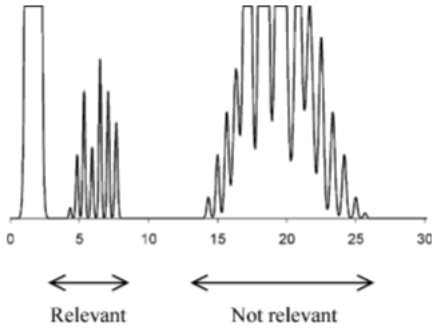	All important information in first part of chromatogram. After important peaks have eluted, long conditioning at high temperature is required to remove high boilers.

Table 4.3. Overview of preferred options to speed up a given GC separation

Chromatogram type	Increased speed option number (Table 1)																
	1	2	3A	3B	3C	4A	4B	5	6	7	8	9	10	11	12	13	14	15
I	++	++	++	NA	NA	NA	++	+	+	–	–	–	–	–	+/–	+	+	–
IIA	–	–	–	NA	NA	NA	++	+	–	+	+	–	+ if	–	+	+	+/–	–
IIB	–	–	–	NA	NA	NA	–	–	–	+	+	–	+ if	–	+	+	+/–	–
IIC	–	–	–	NA	NA	NA	–	–	–	+	+	–	+ if	–	+	+	+/–	–
III	–	–	–	NA	NA	NA	–	–	–	–	–	–	+ if	–	+	+	–	–
IV	+	+	NA	+	+	++	NA	+	+	–	–	–	–	–	+	+	+	–
V	–	–	NA	+	+	++	NA	–	–	–	–	–	–	–	+	+	+	–
VIA	–	–	NA	–	+	++	NA	–	–	+	+	–	+ if	–	+	+	+/–	–
VIB	–	–	NA	–	+–	–	NA	–	–	+	+	–	+ if	–	+	+	+/–	–
VIC	–	–	NA	+	–	–	NA	–	–	+	+	–	+ if	–	+	+	+/–	–
VII	–	–	NA	–	–	–	NA	–	–	–	–	–	+ if	–	+	+	–	–
VIII	–	–	NA	–	–	–	NA	–	–	–	–	+	+ if	–	+	+	+/–	–
IX	–	–	NA	–	+	+	NA	–	+	–	–	–	–	+	+	+	–	–

++: Significant gain or very easy to achieve and reasonable gain. +: Reasonable gain or significant gain but slightly more difficult to realise. -: No viable option. +/-: Significant option only for medium-resolution GC or combined with MS detection for selected ion monitoring. + if: Valid option only if neighbouring peaks contain unique ions. NA: Not applicable.

Turbulent flow can be applied only for chromatograms in which a limited number of peaks elute at low retention factors [12]. The use of a more selective stationary phase is probably also of little benefit for fast PCB separations. The chromatogram has almost no empty baseline and the use of another stationary phase is very likely to result in a similar number of (other) co-elutions.

2D chromatography is only suitable if the sample contains only one or just a few narrow regions with insufficient resolution, which clearly is not the case here. Backflush or selective detection are also of no use, unfortunately. However, the use of mass spectrometric detection is attractive, in principle; if all neighbouring peaks contain unique mass fragments, spectral deconvolution can compensate for a loss of chromatographic resolution. In the case of PCB analysis, this is not a viable option, because congeners with identical numbers of chlorines cannot be resolved by mass spectrometry (MS).

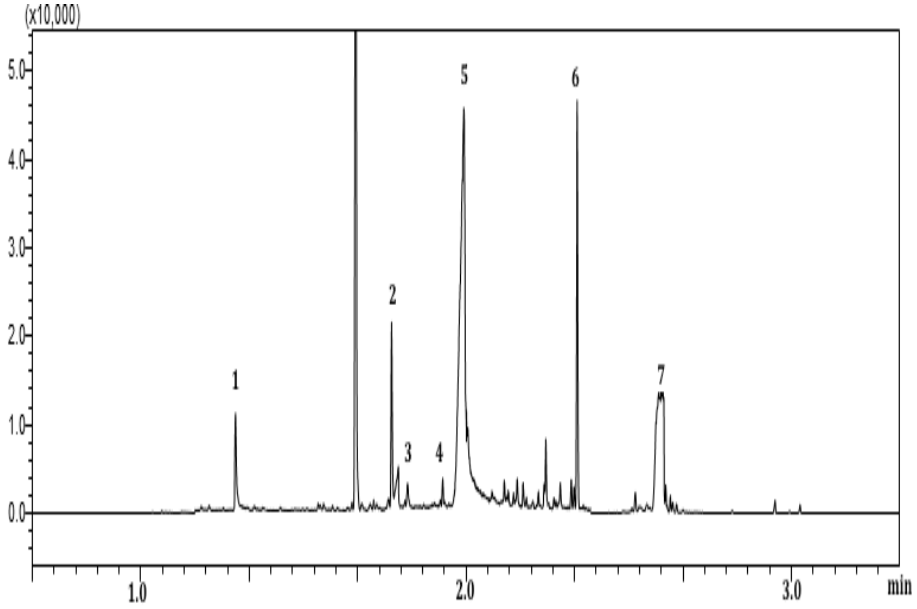

Figure 4.1. Fast GC-FID of a chamomile essential oil on a OV-1701 column (5 m × 0.25mm ID × 0.3 μm). Temperature programme: 100°C, 40°C/min. to 250°C (2 min.). Hydrogen flow through column: 1.4 ml/min. Injection: Split, 230°C; split ratio 1:20.Compounds: (1) trans-β-farnesene; (2) bisabolol oxide B; (3) α-bisabolol; (4) β-bisabolone oxide A; (5) bisabolol oxide A; (6) chamazulene; and, (7) spiroether.

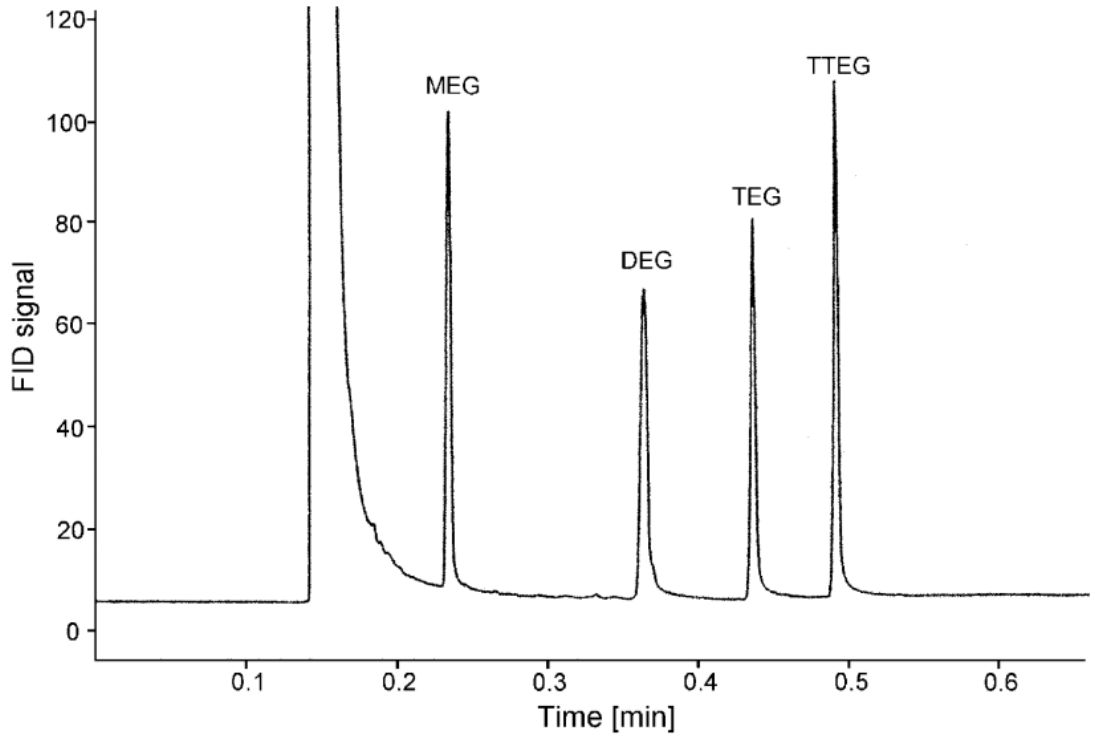

Figure 4.2. Fast GC-FID of (MEG) monoethylene glycol ($C_2H_6O_2$), (DEG) diethylene glycol ($C_4H_{10}O_3$), (TEG) triethylene glycol ($C_6H_{14}O_4$) and (TTEG) tetraethylene glycol ($C_8H_{18}O_5$) on a RTX-5 column (5 m × 0.32 mm ID × 0.25 μm). Temperature programme of EZ Flash: 40°C, 15°C/s to 300°C. Temperature programme of oven: 40°C, 120°C/min. to 100°C. He-inlet pressure: 45 kPa. Injection: Split; split flow 300 ml/min

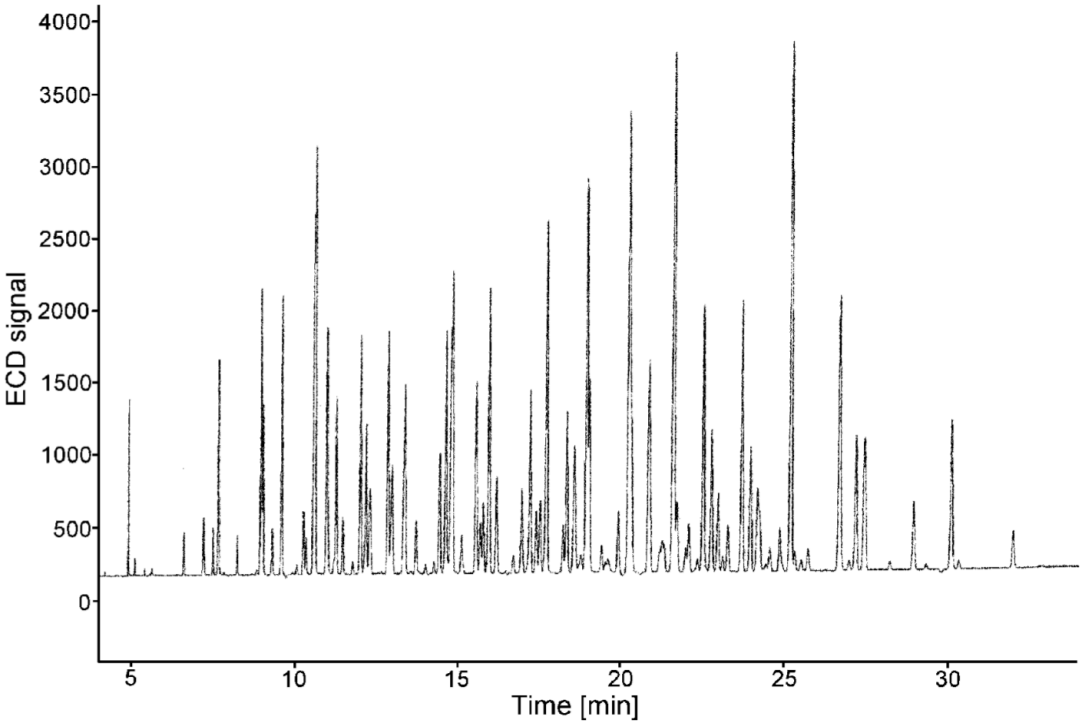

Figure 4.3. Conventional GC of PCB mixture on HP-5 column (30 m × 0.25 mm ID × 0.25 μm). Temperature programme: 50°C (1 min.), 40°C/min. to 150°C; 4°C/min. To 270°C (5 min.). Hydrogen-inlet pressure: 51 kPa. Injection: Splitless, 1 μl, 250°C, 0.75 min. splitless time. Detection: μ-ECD, 320°C.

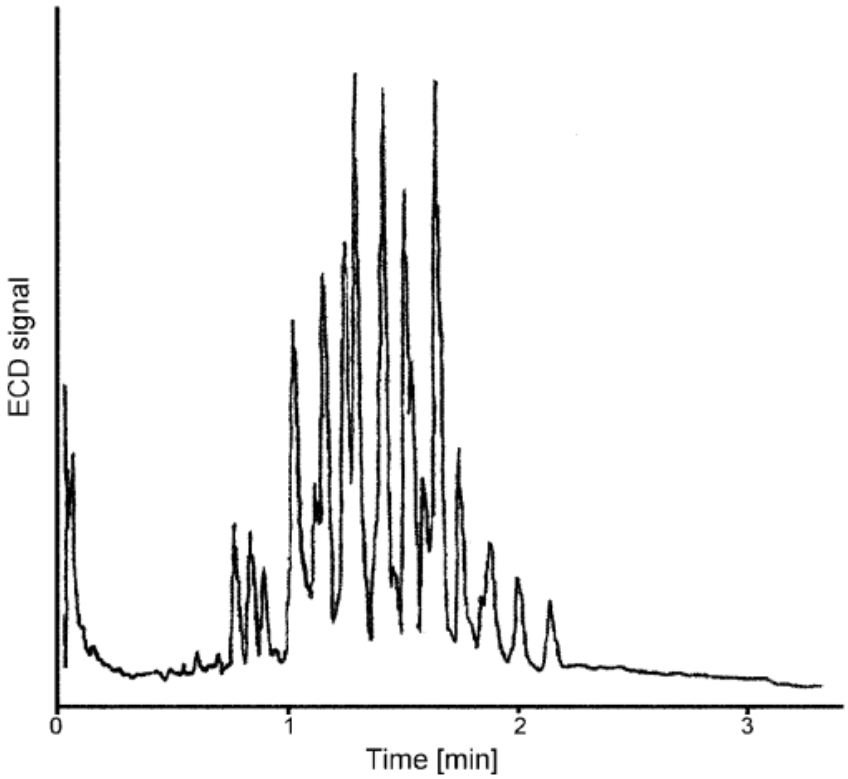

Figure 4.4. Fast GC of Aroclor 1254 on DB-1 column (3 m × 0.25 mm ID). Temperature programme: 100°C, 12.5°C/min. to 150°C. Hydrogen carrier gas: 100 cm/s. Injection: Splitless, 1 µl, 250°C, followed by cold trap cooled by continuous flow of liquid nitrogen at -90°C. Sample concentration: 0.5 mg/ml. Detection: ECD, 300°C, 40 Hz.

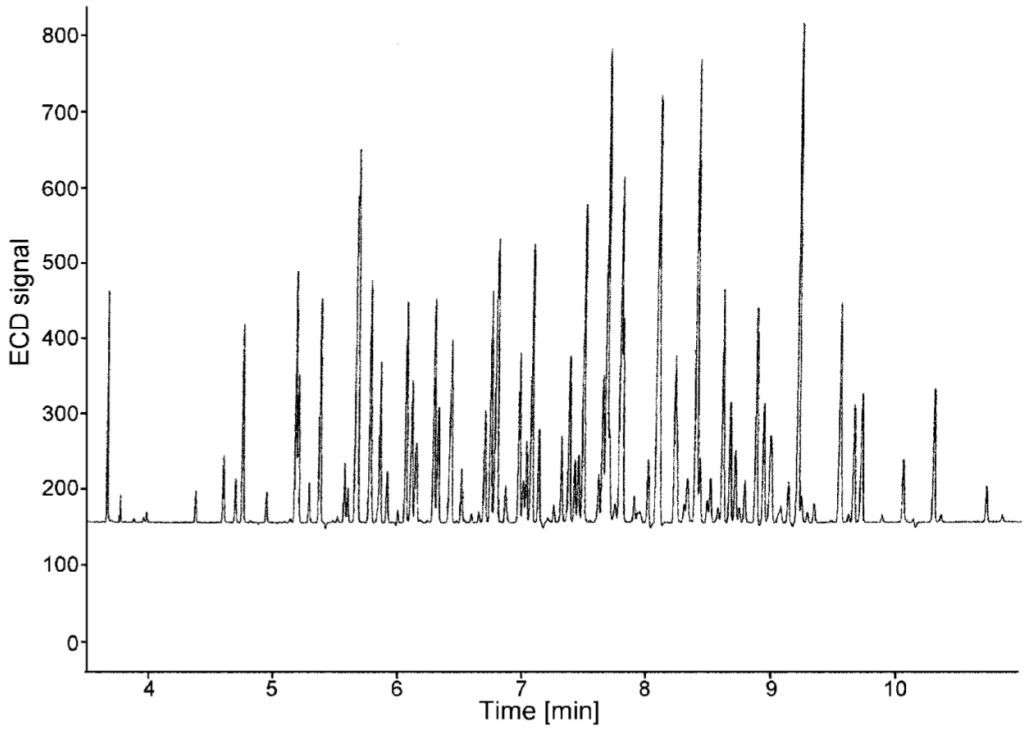

Figure 4.5. Fast GC of PCBs on HP-5 column (10 m × 0.1 mm ID × 0.1 μm). Temperature programme: 50°C (1 min.), 40°C/min. to 150°C, 14.2°C/min. to 270°C (1.06 min.). Hydrogen-inlet pressure: 177 kPa. Injection: Splitless, 1 μl, 250°C, 0.5 min. splitless time. Detection: μ-ECD, 320°C.

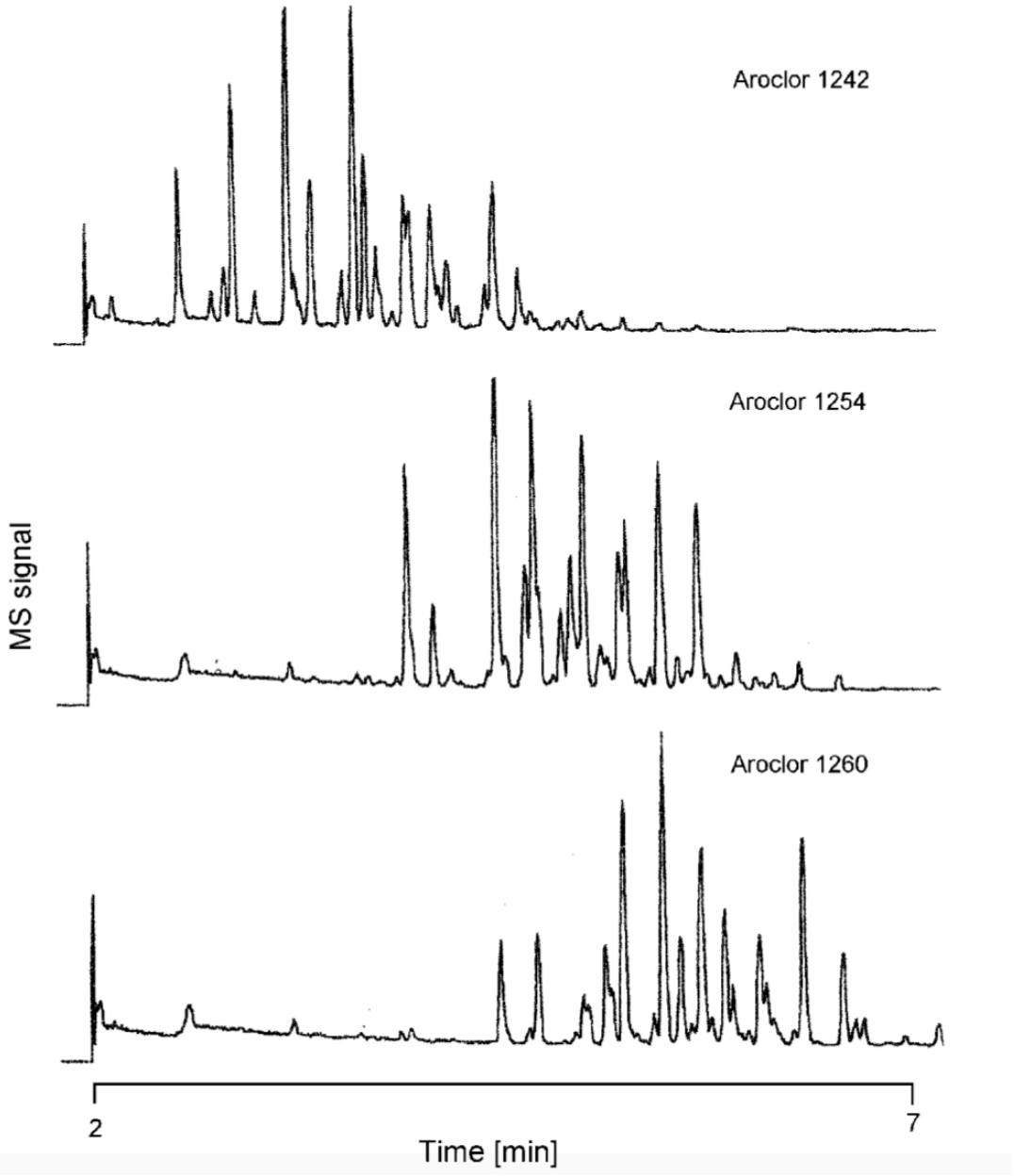

Figure 4.6. Fast GC of Aroclors 1242, 1254 and 1260 on CP-Sil 8 CB column (10 m × 0.53 mm ID × 0.25 μm), connected with restriction (50 cm × 0.1 mm ID deactivated capillary) at injection side. Temperature programme: 65°C (1 min.), 20°C/min. to 280°C. He-inlet pressure: 130 kPa. Injection: splitless, 1 μl, 250°C. Sample concentration: 50 μg/ml. Detection: Saturn 2000 ion trap MS, 250°C.

4.3 Definitions in fast GC

The definition of "fast GC" has been debated for some time. Concepts relating fast GC to run times clearly indicate the bottom-line need of getting analytical results faster. The final analysis time strongly depends on the complexity of the mixture. For very complex samples containing several dozen peaks, the minimum obtainable separation time will typically be in the range of minutes. For other samples, however, separations in the millisecond range can be achieved. Therefore, there are often discussions as to what can truly be considered "high-speed", "fast GC", "ultra-fast GC", etc. This classification is not academic, but is highly relevant with regard to the requirements of the instruments to be used. Van Deursen et al. [13] suggested a classification based on the peak widths obtained, because every reduction of analysis time results in an identical reduction of the chromatographic zone widening due to the shorter residence time of the components in the column. Faster GC can then be classified as:

1. Fast GC: separation in the range of minutes; peak width (2.354 s), 1–3 s.
2. Very fast GC: separation in the range of seconds; peak width, 30–200 ms.
3. Ultra-fast GC: separation in the sub-second range; peak width, 5–30 ms.

Such a classification is very useful because it clearly shows the major requirements for instrumentation. As an example, the final peak width determines the injection requirements, the detector time constant, the required programming rate, etc. It is obvious that, in daily practice, most interest will be in fast GC. Very fast and ultra-fast GC are suitable for only very simple

separations, although they have played an important role in the development of fast GC.

4.4 Instrumentation

The purpose of faster GC is to obtain the sample information required in a shorter time. Several options to realise this have been discussed above. In this section, the practical consequences of implementing these options will be discussed. In part, these consequences are "option specific"; and, in part, they apply to all methods for faster GC. An example of the latter is the need for fast detection in fast GC. In fast GC, the peaks elute in a shorter time frame and the registration system should be able to record and process the information generated in real time, irrespective of which method of faster GC has been used. An "option specific" requirement is, for example, implementing the vacuum-outlet option for faster GC.

4.4.1 Carrier gas

The carrier gas choice can have a substantial influence on analysis speed. This influence depends on the column pressure drop (p_d). Hydrogen is clearly the best carrier gas for the fastest analysis speed because of its large binary diffusion coefficient values, some laboratories are uncomfortable using hydrogen as a carrier gas because of safety concerns. There are means (e.g., accurate safety information, safety interlocks, H_2 generators with limited capacity, and inherently safe instrument designs) of satisfying safety requirements and concerns within most organizations. If hydrogen carrier gas use is not allowed, helium is a good second choice. It has to be emphasised that comparing the relative speeds of helium and hydrogen it follows, that at a low p_d (short wide bore columns) helium is approximately 20% slower than hydrogen, at a high p_d (narrow-bore columns) a 40% speed disadvantage of

helium over hydrogen is produced. In Quasimeme laboratory performance studies on PCBs and pesticides in marine biota in 1997, 20 out of 27 participants used hydrogen as the carrier gas [14].

4.4.2 Pressure regulators

Pressure could be a limiting factor for a number of options for faster GC. For example, the use of shorter columns is limited by the minimum inlet pressure required for stable operation of the carrier-gas system. However, with long narrow-bore columns or turbulent flow operation, the maximum pressure may become a limitation. The new generation of chromatographs is equipped with electronic pressure/flow control units (EPC) with the inlet pressure limit up to 1000–1200 *k*Pa. These pressures are compatible with most narrow bore columns. As an example, a pressure of 1100 *k*Pa is sufficient for columns of 50 μm ID up to a length of 15 m. Such a column would generate the same number of plates as a 100 m × 320 μm ID column. EPC allows continuous change in the column head pressure with the modes of constant flow (also with temperature programming) and programmed flow (important for thermo labile com pounds).

4.4.3 Injection systems

The most critical step in fast GC is the injection. To avoid peak width broadening, the injected sample plug has to be narrow compared to the total chromatographic band broadening. The simplest way to achieve the narrow initial band width is the utilisation of high split flows. When working with analytes that are not too heavy and operating the system at very high split ratios (split flows up to 2 l/min have been reported), band-widths in the millisecond range can be obtained [15]. A drawback of these high split ratios is the poor detection limits (LODs). Under temperature-programmed

conditions, operation at a much lower split flow is possible, because the input band is refocused by thermal focusing at the initial temperature. Because of the focusing effects, also splitless, PTV (programmed temperature vaporization) and even on-column injection techniques can be combined with fast GC. However, successful use of these methods requires a number of precautions. Splitless injection, e.g., requires an injector liner with a small ID to obtain acceptable splitless times at the low column flow of a narrow-bore column [16]. On-column injection onto narrow-bore columns is possible by coupling a wider-bore retention gap (250 or 320 μm ID) to the separation column [17,18]. In doing so, it is extremely important to keep the dead volumes to an absolute minimum. For very fast and ultra-fast GC, this is impossible. Hence, on-column injection is not compatible with these fastest forms of GC. The most important group of injection methods for very fast and ultra-fast GC involve miniaturised mechanical switching valves. A portable, high-speed, GC system using micro machined valves and a sample loop on a silicon chip is commercially available [19]. Its inlet system is optimised for use with short narrow-bore columns. Micro-GC instruments are used in field analysis for, e.g., screening of unknown wastes [20], pre-screening of environmental samples [21], on-site BTU (British Thermal Unit) analysis in the natural gas industry and geological screening using gas concentrations of hydrogen in near-surface soil [20]. The microinjection valves can be used for gaseous samples only. If sensitivity permits, liquid samples can be injected using split injection at a very high split flow. Non-splitting liquid-injection methods can be coupled only to very fast and ultra-fast GC if combined with anon-column or pre-column focusing device [22,23]. The broad plug of sample is accumulated and refocused by cryogenic cooling. For re-injection of the sample, the trap is rapidly heated. Peak widths can be as low as 5–10 ms [23]. Specially-designed low-thermal mass cryo-focusing devices are used

for sample collection and subsequent re-injection in the analysis of BTEX (benzene, toluene, ethylbenzene and total xylene) and natural gas samples [23] and PCBs [10], as was shown in Figure 4.4.

4.4.4 Columns

Column choice in faster GC depends on the application. From the group of "constant-resolution" options, the most logical option is the use of columns with a reduced ID for faster GC. Obviously, their use can cause some problems. Injection in narrow-bore GC is critical and dead volumes have to be kept to a minimum. Even the tiniest dead volume can result in significant peak tailing because of the very low flow in narrow-bore GC (ID <150 μm). Other limitations of narrow-bore columns are their low load ability and their unfavourable LODs. One might expect that the LODs in all forms of faster GC will improve because the analytes elute as narrower and, hence, higher peaks.

Very often however, the injection volume will have to be reduced to keep the injection band-width at an acceptable level. For narrow bore columns, the minimum detectable amount is indeed improved significantly, but the much more relevant minimum detectable concentration is generally going up [24]. Therefore, in most applications, 50–150 μm ID columns are used. Nowadays, columns of 100 μm ID are readily available and improved column technology allows the production of a wide choice of stationary phases. Columns of 100 μm ID offer a compromise with respect to analysis time and instrument compatibility. Good results with 0.1 mm ID columns were reported for the analysis of nutmeg and Californian lemon oil, bacterial fatty acid methyl esters and PCBs [9]. As an example, with an essential oil, all compounds were separated in less than 13 min. compared to 75 min. on a 0.25 mm ID column. The resolution was the same in both cases. Another application is the

separation of 40 commonly used solvents in less than 4.9 min. [25]. This would require over 45 min. with standard megabore or 0.32 mm ID columns.

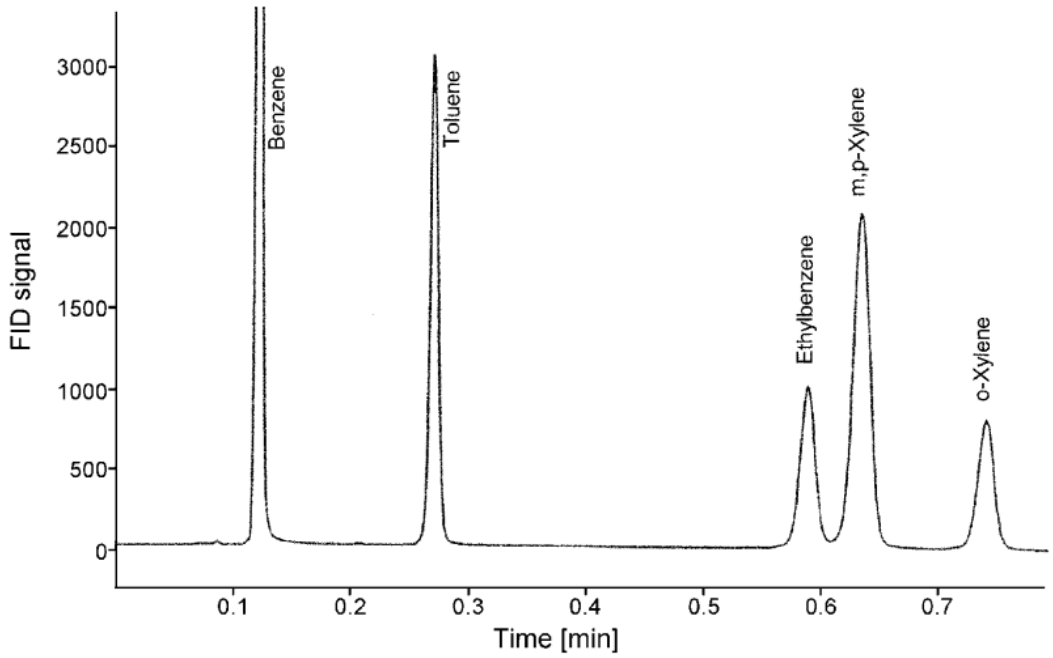

Figure 4.7. Headspace GC-FID of BTEX on multi-capillary column. Length column: 1 m; diameter of capillaries: 40 µm; number of capillaries: approx. 900. Inlet pressure: 375 kPa. Injection: 20 µl vapour. Temperature programme: 40°C (0.5 min.), 25°C/min. to 200°C. Injection: Split, split-flow 800 ml/min., column outlet-flow 200 ml/min.

To overcome the limitation of narrow-bore columns with regard to sample capacity, the multi-capillary column was introduced. This column is made by combining some 900 capillaries of 40 µm ID into a bundle. A BTEX analysis performed on a multi-capillary column within 60 s is shown in Figure 4.7.
This chromatogram is a good example of a type VI C chromatogram, where a low number of well resolved peaks occurs next to one or more critical

pairs/groups positioned in the final part. The experimental plate number was about 12,500 at a theoretical maximum of 25,000.

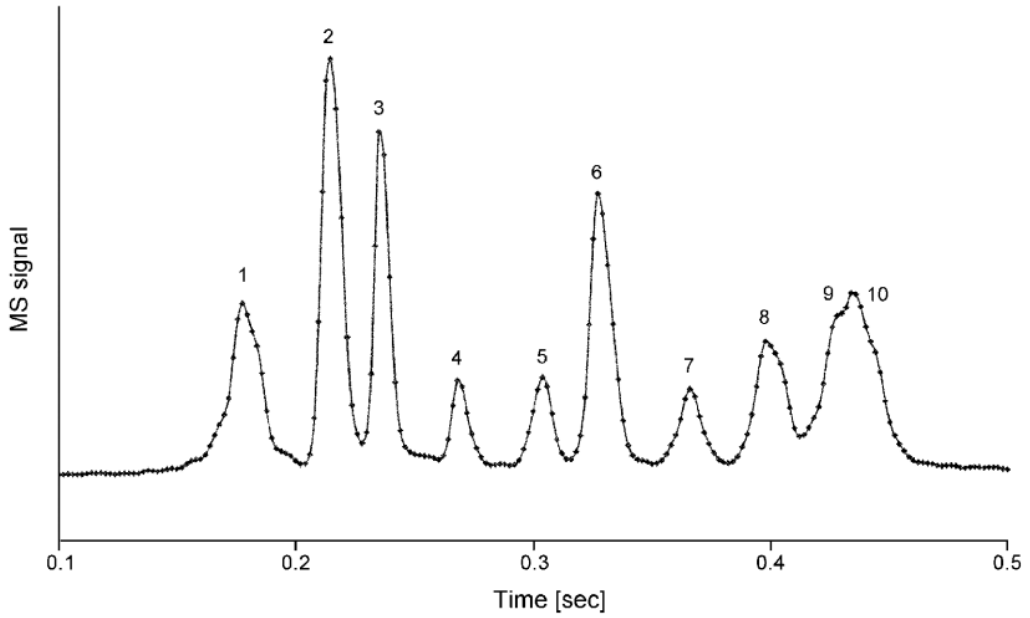

Figure 4.8 Ultra-fast GC-TOF-MS of 10 compounds on OV-1 column (0.3 m × 50 µm ID × 0.17 µm). Oven temperature: 75°C. He-inlet pressure: 450 kPa. Injection: split, 1 ml, headspace (≈1 ng/compound), 250°C, split flow 400 ml/ min., followed by a cryogenic focussing system. T transferline = 275°C; T source = 200°C. Scan rate= 500 spectra/s (m/z 40–200). Compounds: (1) pentane; (2) 2,3-dimethylbutane; (3) hexane; (4) benzene; (5) heptane; (6) methylcyclohexane; (7) toluene; (8) trans-1,4-dimethylcyclohexane; (9) octane; (10) cis-1,4-dimethylcyclohexane.

To obtain the maximum performance, all capillaries should have exactly the same diameter. Differences of diameter will cause serious band broadening and a loss of efficiency. The multi capillary column is currently available with a length of 1 m only and is therefore suitable only for relatively simple mixtures requiring low plate numbers only [26]. To speed up ‘‘over-resolved’’ separations, reduction of the column length or the use of a higher carrier-gas

velocity is beneficial, particularly for type I and IV chromatograms. Dagan and Amirav [27] demonstrated the separation of a mixture of thermolabile compounds, including steroids, carbamate pesticides and antibiotic drugs, on a 0.25 mm ID column of only 4 m length with MS detection. The sample contained seven compounds and could be separated in about 80 s. Short columns are also frequently applied for rapid profiling of complex mixtures, such as PCBs (Figure 4.4; ECD detection), fats and oils or pesticide extracts from water samples [7,10,28].

4.4.5 GC ovens

An optimal temperature-program rate for fast GC is that which renders the best separation in the least time. For speeding up separations of type IV, V and VI faster temperature programming is an attractive option. A chromatograms- samples that contain a limited number of peaks covering a wide range of boiling points. Therefore, the maximum allowable heating rate, and evidently also the cooling time, of the oven are important parameters. Additionally, if other methods for faster GC are implemented, the heating rate has to be adapted. For constant resolution situations (solutions 12–15 of Table 1.1), the typical guideline is that the ratio (programming rate/column void time) should be kept constant. In general, the optimal ratio is about 10°C/void time [29]. As an example, if the column diameter is adjusted, the temperature-programming rate should be increased proportionally to the reduction of the column ID The latest generation of GC ovens allows maximum programming rates of 50-100°C/min. Higher rates are difficult to obtain because of the higher thermal mass of standard ovens. For faster heating, systems based on resistive heating were recently developed. In the commercial EZ Flash system, an upgrade to existing GC instruments, the capillary column is placed inside

a resistively heated metal tube. It provides fast and reproducible heating rates up to 1200°C/min. and can cool from 300°C to 50°C in less than 30 s [8,30]. The system is compatible with standard split/splitless injectors. The potential of the EZ Flash system was demonstrated by separating a mixture containing some 20 n-alkanes, PAHs, triazines or organophosphorus pesticides on a 5 m × 0.25 mm ID × 0.2 μm capillary operated at a programming rate of 100°C/min. [30]. The

analyses took 30 s to 3 min.; the total analysis times (analysis and cooling) were 1–3.5 min. There were significant resolution losses compared with a standard-length column operated at heating rates of 10–15°C/min. But, because the original separations were far better than needed, the peaks of interest could still be separated. That is a good example of trading resolution for time. The narrow peaks obtained in the fast separation resulted in very low LODs (FID detection) of around 5 ρg for n-alkanes and PAHs and 10–30 ρg for the pesticides. This demonstrates that rapid temperature programming has distinct potential for the rapid screening for micro-contaminants. Unfortunately, it is not suitable for detailed analysis of complex samples (e.g. types III or VII). A disadvantage of fast programming can be the substantially higher elution temperature of the peaks of interest, especially if the linear velocity is not adjusted [30].

4.5 Conclusions

The first step to increase the speed analysis should always be to minimise the resolution to a value that is just sufficient. As reported above, it can be achieved by applying a shorter column length, higher isothermal/initial/final temperature, an above optimum carrier-gas velocity, pressure/flow programming, faster temperature programming or a lower film thickness. The successive step is to try to maximise the selectivity of the chromatographic

system by using a more selective stationary phase or coupled columns, applying selective or MS detection, using (conventional) 2D GC or using backflush techniques. This will lead to over-resolved separations in the same time and, thus, allows the repeated use of the options from the first step. Finally, if a further reduction is necessary, methods can be implemented that reduce analysis time at constant resolution (smaller column ID, hydrogen as the carrier gas, vacuum-outlet conditions or turbulent-flow conditions). The selected option strongly depends on the application of interest. Here, a classification system containing 13 basic classes of chromatogram, with various options for speeding up, can be used to advantage. The use of faster GC has long been hindered by a lack of instrumentation. Today, commercial instrumentation is available and fast GC can be implemented for routine analysis. The latest generation of commercial chromatographs can be equipped with electronic pressure control units operating up to about 12 bar, sufficiently high for columns of 50 μm ID. They can perform an automated safety shut-off of carrier gas if there is a sudden pressure drop, allowing safe use of hydrogen as the carrier gas. All common injection systems can be used for injection in fast GC. For narrower injection bands, cryogenic focusing is available. Columns of 100 μm ID are available and there is a wide choice of stationary phases. For higher sample capacity, the multi-capillary set-up can be used. The latest generation of GC ovens allows programming rates up to 50–100°C/min, while resistive heating enables rates up to 1200°C/min. and cooling from 300°C to 50°C in less than 30 s. Finally, most commercial detection systems are compatible with fast GC requirements, while TOF-MS is specifically useful for fast GC-MS and provides up to 500 scans/s without distortion of the spectra.

References

[1] A. van Es, J. Janssen, C.A. Cramers, J. Rijks, J. High Resolut. Chromatogr. Chromatogr. Commun. 11 (1988) 852.

[2] M. Klemp, A. Peters, R. Sacks, Environ. Sci. Technol. 28 (1994) 369A.

[3] J. de Boer, Environmental Analysis, Handbook of Analytical Separations 3 (2001) 237.

[4] C.A. Cramers, P.A. Leclercq, CRC Crit. Rev. Anal. Chem. 20 (1988) 117.

[5] P.A. Leclercq, C.A. Cramers, J. High Resolut. Chromatogr. Chromatogr. Commun. 8 (1985) 764.

[6] J.B. Phillips, J. Beens, J. Chromatogr. A 856 (1999) 331.

[7] C. Bichi, C. Brunelli, M. Galli, A. Sironi, J. Chromatogr. A 931 (2001) 129.

[8] M.M. van Deursen, J. Beens, C.A. Cramers, H.-G. Janssen, J. High Resolut. Chromatogr. 22 (1999) 509.

[9] F. David, D.R. Gere, F. Scanlan, P. Sandra, J. Chromatogr. A 842 (1999) 309.

[10] J.S. Alvarado, J. Silzer, F. Lemley, M.D. Erickson, Anal. Commun. 34 (1997) 381.

[11] J. de Zeeuw, J. Peene, H.-G. Janssen, X. Lou, J. High Resolut. Chromatogr. 23 (2000) 677.

[12] A.J. van Es, J.A. Rijks, C.A. Cramers, M.J.E. Golay, J. Chromatogr. A 517 (1990) 143.

[13] M.M. van Deursen, J. Beens, H.-G. Janssen, P.A. Leclercq, C.A. Cramers, J. Chromatogr. A 878 (2000) 205.

[14] Quasimeme laboratory performance studies, Round 10, BT-2 Exercise 330, Chlorobiphenyls & organochlorine pesticides in marine biota, June–October 1997.

[15] A.J. van Es, H.-G. Janssen, R. Bally, C.A. Cramers, J.A. Rijks, J. High Resolut. Chromatogr. Chromatogr. Commun. 10 (1987) 273.

[16] P.G. van Ysacker, H.M. Snijders, H.-G. Janssen, C.A. Cramers, J. High Resolut. Chromatogr. 21 (1998) 491.

[17] F.I. Onuska, J. Chromatogr. 289 (1984) 207.

[18] P. Korytar, E. Matisovà, H. Lefflerovà, J. Slobodnık, J. High Resolut. Chromatogr. 23 (2000) 149.

[19] J.B. Angell, S.C. Terry, P.W. Barth, Sci. Amer. 248 (1983) 44.

[20] E.B. Overton, K.R. Carney, Trends Anal. Chem. 13 (1994) 252.

[21] R. Rodgers, Amer. Lab. 25 (1993) 20K.

[22] Z. Liu, J.B. Phillips, J. Microcol. Sep. 1 (1989) 249.

[23] M.A. Klemp, M.L. Akard, R.D. Sacks, Anal. Chem. 65 (1993) 2516.

[24] A. van Es, High Speed Narrow Bore Capillary Gas Chromatography, Huthig, Heidelberg, Germany, 1992.

[25] T.K. Chen, J.G. Phillips, W. Durr, J. Chromatogr. A 811 (1998) 145.

[26] M.M. van Deursen, M. van Lieshout, R. Derks, H.- G. Janssen, C. Cramers, J. High Resolut. Chromatogr. 22 (1999) 119.

[27] S. Dagan, A. Amirav, J. Amer. Soc. Mass Spectrom. 7 (1996) 737.

[28] G.P. Jackson, A.R.J. Andrews, Analyst 123 (1998) 1085.

[29] L.M. Blumberg, M.S. Klee, Anal. Chem. 70 (1998) 3828.

[30] J. Dalluge, R. Ou-Aissa, J.J. Vreuls, U.A.Th. Brinkman, J. High Resolut. Chromatogr. 22 (1999) 459.

Chapter 5
Cryogenic modulation fast comprehensive gas chromatography-mass spectrometry by using a 10m micro-bore column combination: concept, method optimization and application

5.0 Introduction

The present research is based on the concept of using a 10 m × 0.1 mm id column for cryogenic modulation fast comprehensive two-dimensional gas chromatography-quadrupole mass spectrometry separations. Specifically, an 8.9 m × 0.1 mm id low-polarity column was used as first dimension, while a 1.1 m × 0.1 mm id medium-polarity one was used as second dimension. The main scope of the investigation was to develop a high peak-capacity method, with an analysis time of approx. 10 min. Various aspects related to method optimization are discussed, as well as separation parameters such as peak capacity (in each dimension, and as a total value), peak widths, modulation ratio, sensitivity enhancement, and number of spectra per peak. The fast approach was evaluated in applications involving a mixture of cosmetic allergens, and a sample of perfume. The approach proposed enables high-resolution separations in a short time (across the C_8 to C_{23} alkane range), as well as a considerable reduction of the consumption of gases for modulation cooling and heating.

Comprehensive two-dimensional gas chromatography (GC×GC) was first reported in 1991, by Liu and Phillips [1]. This now well-known multidimensional technology is commonly performed by using a conventional column (i.e., 30 m × 0.25 mm id × 0.25 μm d_f) as first dimension (1D), and a short micro-bore column segment (i.e., 1-2 m × 0.1 mm id × 0.1 μm d_f) as second dimension (2D) [2]. The analysis timeframes are about the same as those observed in one-dimensional GC applications (1-2 h), even though variations do exist. For example, the first published GC×GC experiment was carried out in a rapid manner (analysis times did not exceed 5 min), by using an accelerated temperature program (43°C min^{-1}) [1]. Furthermore, Bruckner et al. described the first flow-modulation experiment in 1998, it being performed by using a switching valve located between a 4.9m × 0.53 mm id ×

3 μm d_f ^{1}D capillary, and a 0.85m × 0.18 mm id × 0.15 μm d_f ^{2}D one [3]. A GC×GC experiment was performed on a sample of white gas in 75 s. It is noteworthy that the investigations described by Liu & Phillips and Bruckner et al. were both achieved by using consumable-free forms of modulation [1,3]. Cryogenic modulation (CM) is currently the most efficient form of modulation, if both GC×GC peak capacity and sensitivity are considered [4]. However, the most popular versions of such modulators (loop-type and quad-jet) require cryogenic fluids, as well as high volumes of gas for the heating and cooling steps. Cryogenic modulators with no cooling fluid requirements have been developed, even though the necessity of cooling and heating gases still remains. As a consequence, one must bear in mind the effectiveness of cryogenic modulation, as well as the convenience of reducing the consumption of cryogenic fluids and/or that of cooling/heating gases. A simple manner to reach such an objective is to perform faster GC×GC applications.

Fast CM GC×GC applications, even though scarce, have been reported in the literature; for example, Adahchour et al. used a 4 m × 0.1 mm id × 3.5 μm d_f ^{1}D non-polar column, and a 0.5 m × 0.05 mm id × 0.05 μm d_f ^{2}D medium-polarity one, for the separation of diesel oil [5]. The temperature program was: 40°C (2 min) to 250°C (2 min) at 10°C min^{-1}, for a total analysis time of 25 min. A short modulation time of 3 s guaranteed 4-5 modulations per peak. Junge et al. carried out fast CM GC×GC by combining a 5m × 0.1 mm id × 0.1 μm d_f ^{1}D column, with a 0.3m×0.05 mm id × 0.05 μm d_f ^{2}D one [6]. A mixture of 29 compounds was separated through the application of the following temperature gradient: 80°C to 250°C (0.14 min) at 35°C min-^{1}, for a total analysis time of 5 min. Modulation time was very short, namely 1 s; under such conditions, ^{1}D peaks were sampled once or twice. Finally, Purcaro et al used a low-polarity 11.4 m × 0.1 mm id × 0.1 μm d_f ^{1}D capillary, linked to a 1 m × 0.05 mm id × 0.05 μm d_f ^{2}D one, for the analysis of bacterial fatty

acid methyl esters [7]. It was reported that the last compound of interest eluted within 25 min.

The scope of the present research is obviously not to perform, for the first time, a rapid GC×GC analysis; rather, the investigation is focused on the development of a fast CM GC×GC method, combined with single quadrupole mass spectrometry (QMS), by using a low-polarity 8.9 m × 0.1 mm id × 0.1 μm d_f ^{1}D column, connected to a medium-polarity 1.1 m × 0.1 mm id × 0.1 μm d_f ^{2}D Thus, the analytical columns together, were equivalent to a 10 m micro-bore column. The latter are well-established tools to perform fast and very fast GC separations [8], and the concept is in part here moved to GC×GC.

5.1 Experimental

5.1.1 Standard compounds and sample

The cosmetic allergens listed in Table 5.1 were supplied by MilliporeSigma. A solution at the 1 mg L^{-1} level was prepared in n-hexane. A sample of commercial perfume was diluted 1:10 (*v/v*) in n-hexane

5.1.2 Instrumentation

All CM GC×GC-QMS applications were performed on a system formed of two Shimadzu GC-2010 gas chromatographs, and a QP2020 quadrupole mass spectrometer (Kyoto, Japan). Data were acquired by using the GCMS solution software (Shimadzu). The MS database used was the FFNSC v. 3.0 (Shimadzu). Bidimensional chromatograms were generated by using the ChromSquare software v. 2.3 (Shimadzu).

The first gas chromatograph (GC1) was equipped with an AOC-20i auto-injector, and a split–splitless injector (310°C). The ^{1}D column was an SLB-

5ms [(silphenylene polymer which can be considered equivalent in polarity to poly (5%diphenyl/95% dimethylsiloxane)] with dimensions 8.9 m × 0.10 mm id × 0.10 μm d_f. A 1.5m × 0.10 mm id uncoated column was used to create the modulator loop. The ^{2}D column was an SLB-35ms [(polymer which can be considered equivalent in polarity to poly (35%diphenyl/65% dimethylsiloxane)] with dimensions 1.1 m × 0.10 mm id × 0.10 μm d_f. All the columns used were provided by Sigma-Aldrich/Supelco (Bellefonte, PA, USA). The connections between the ^{1}D and ^{2}D columns, and the modulator loop, were made by using two SilTite mini unions (Trajan/SGE, Ringwood, Victoria, Australia). Helium was supplied at the GC1 inlet at a pressure of 480.5 kPa; volume and mode of injection: 2 μL in the split mode (10:1), for the solution of allergens, and 2 μL in the split mode (100:1), for the perfume sample.

Gas chromatograph conditions: GC1 temperature program: 50-250°C at 17.5°C min^{-1}; GC2 temperature program: 65-265°C at 17.5°C min^{-1}. Modulation was performed by using a cryogenic fluid-free modulator; modulation period was 2.5 s (the heating step was performed at 350°C, for 0.3 s).

Mass spectrometry conditions: the temperature of the interface was 250°C; the ion source temperature was 220°C, with analyte fragmentation induced by electron ionization (70 eV). A spectral generation frequency of 50 Hz was applied.

Peak/Compound	w_b (ms)	ΔLRI	*s/n* increase
1. Benzaldehyde	93	12	4
2. β-Pinene	93	5	
3. Benzyl alcohol	107	1	6
4. Linalool	93	0	
5. Camphor	107	2	4
6. Menthol	107	-8	
7. Methyl Salicylate	107	0	
8. Citronellol	107	-5	3
9. Neral (Citral isomer I)	93	0	
10. Carvone	107	-2	
11. (*E*)-Cinnamaldehyde	120	4	4
12. (*E*)-Anethol	93	0	
13. (*E*)-Cinnamyl alcohol	107	0	
14. α,α-Dimethylphenethylacetate	107	1	
15. Eugenol	133	1	9
16. Majantol	120	5	
17. Caryophyllene	120	-1	
18. Isoeugenol	93	1	
19. α-Isomethyl ionone	107	1	7
20. Lilial	107	-8	
21. 3-Propylidenephthalide	133	0	
22. α-Amyl cinnammaldehyde	120	6	
23. Lyral isomer 2	160	1	
24. α-Amyl cinnamyl alcohol	147	6	

25. β-Santalol	106	7	
26. α-Hexyl cinnamaldehyde	147	4	5
27. Benzyl benzoate	147	6	5
28. Galaxolide	120	7	
29. Benzyl salicylate	160	11	
30. 16-Hexadecanolide	160	1	3
Means	117	4 (absol.)	5

Table 5.1. Identification, peak widths, linear retention index deviations (ΔLRI) with respect to MS database values, and S/N increase (compared to an unmodulated experiment), for compounds numbered in Figure 1. The last line reports average values. The average ΔLRI value is an absolute one.

5.2. Results and Discussion

The ^{1}D capillary was of low polarity, and of dimensions 8.9 m × 0.1 mm id× 0.1 μm d_f; the ^{2}D column was of medium polarity, and of dimensions 1.1 m × 0.1 mm id × 0.1 μm d_f. An uncoated 1.5 m × 0.1mm id capillary was used as delay loop. The initial objective was to develop a fast GC×GC method with a duration of approx. 10 min. Method development was rather complex because it involved a series of variables, namely the temperature program (in the two GC ovens - GC1 and GC2), constant gas velocities in the two dimensions and in the delay loop (automatically calculated by a software supplied with the instrumentation), modulation period (cooling and heating times), average number of modulations per peak, and MS spectral generation frequency. Optimization was carried by using a C7-30 alkane series and a mixture of cosmetic allergens, with a great number of applications involved. A 50- 250°C temperature range was applied in GC1 (and GC2), with a gradient of 17.5°C min-1 (analysis time: 11.4 min); the applied inlet pressure

generated a gas velocity in the first dimension of 50 cm s^{1}. The alkane series was subjected to an unmodulated experiment: the elution range observed extended from alkanes C8 to C23. Peaks widths (wb - 4σ) for alkanes C10, C16, and C23 were 1.3, 1.6, 1.6 s, respectively. With an average peak width of 1.5 s (for the 3 alkanes), it would be necessary to have a modulation period of 0.5 s to attain 3-4 modulations per peak.

A series of modulation periods were tested and it was found that a cooling period of at least 2 s was necessary to efficiently trap the more volatile alkanes (≤ C10). The cryogenic fluid-free CM system used was capable of reaching operational temperatures of approx. -90°C. A modulation period,

composed of a 2 s cooling step and a 0.3 s heating (350°C) one, was found to perform efficient entrapment/re-injection processes across the entire elution range.

A mixture of cosmetic allergens (1 mg L^{-1} solution), characterized by a variety of molecular weights and chemistries, was subjected to fast GC×GC-QMS analysis. The allergens subjected to analysis have all been highlighted by the Scientific Committee on Consumer Safety (SCCS) as skin sensitizers [9]. When using equivalent temperature programs in both ovens, it was observed that rapid elution from the ^{1}D column was the cause of rather low ^{2}D analysis temperatures. Slight excessive stationary-phase retention lead to wrap-around of several polar compounds, them eluting in the low-polarity part of the chromatogram (^{2}D t_R < 0.75 s). It was found that the use of a positive offset of 15°C, applied in the GC2 oven, along with an extension of the modulation period (2.2 s cooling step), enabled a more appropriate occupation of the two-dimensional space. Thirty representative compounds, distributed across the entire separation space, are numbered in Figure 5.1 (for identification refer to

Table 5.1). Non-polar compounds, such as hydrocarbons (e.g., β-pinene peak 2; caryophyllene- peak 17), were situated in the lower part of the chromatogram, while the contrary was observed for the more polar compounds [e.g., benzyl alcohol - peak 3; (*E*)- cinnamaldehyde - peak 11; benzyl salicylate - peak 29]. The applied inlet pressure generated gas velocities in the loop and in the second dimension of approx. 95 and 185 cm s^{-1}, respectively. Considering previous research, such an intra-loop velocity condition enables efficient re-injection conditions [10]. It is noteworthy that the use of columns with the same internal diameter enabled the generation of satisfactory He linear velocities (for the scopes of the research) in the first and second dimension, as well as in the delay loop.

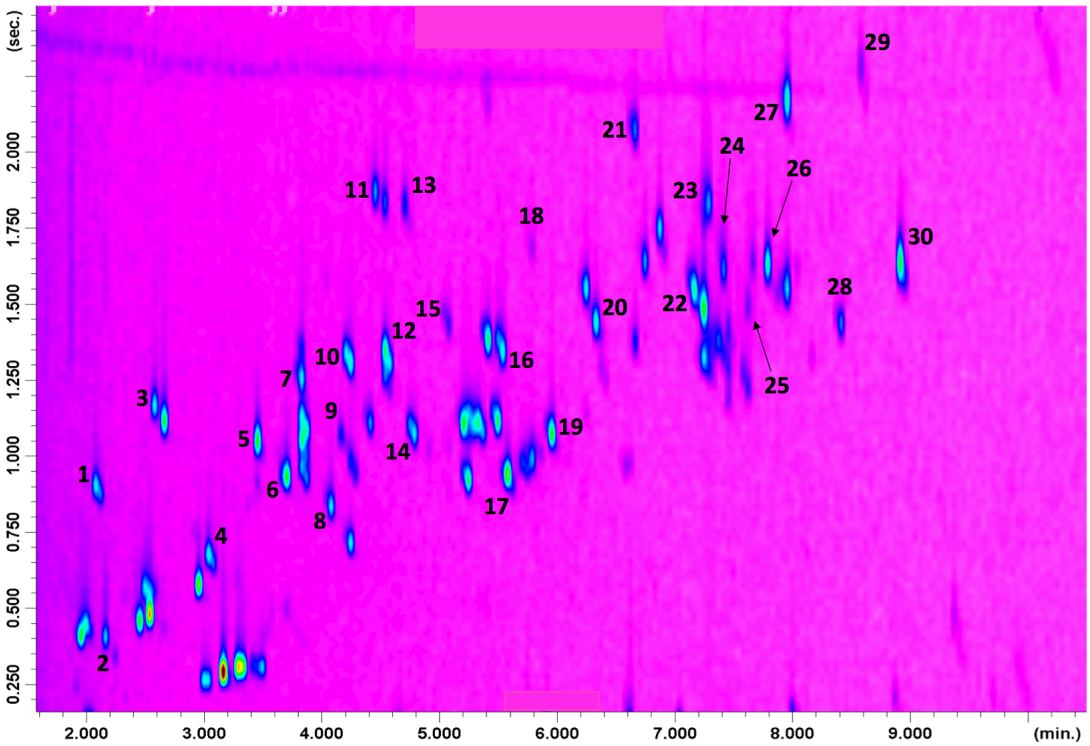

Figure 5.1. Fast GC×GC-QMS chromatogram of a mixture of cosmetic allergens; the identity of the 30 numbered peaks is reported in Table 5.1.

Even though the analyte positions in the two-dimensional were those expected, on the basis of polarity, the occurrence of wrap-around was investigated. Considering the ^{2}D gas velocity, a dead time of circa 0.6 s would be expected; consequently, a compound such as β-pinene, with an apparent ^{2}D retention time of about 0.4 s, is certainly characterized by wrap-around. Furthermore, as the peak widths for the thirty compounds are rather similar (Table 5.1), it can be deduced that all such analytes undergo the same number of "wrap-arounds". The general degree of wrap-around was evaluated by first doubling the modulation period to 5 s: β-pinene was still characterized by a retention time of approx. 0.4 s. After, a modulation period of 7.5s was applied: β-pinene presented a retention time of approx. 5.4 s. Such data indicated the occurrence of two "wrap-arounds". The retention time of β-pinene was confirmed through the application of other extended modulation periods (e.g., 12.5 s, 15 s). So, it was concluded that it was necessary to add 5 s to the apparent ^{2}D retention times of the analytes listed in Table 1 to attain their real retention times.

The method peak capacity was calculated by following a straightforward approach [11]: first-dimension peak capacity was roughly evaluated to be 420, it being calculated by dividing the elution time window (630 s) by the average width of the previously-mentioned non-modulated alkanes (1.5 s). Second-dimension peak capacity was roughly evaluated by calculating the average peak width value for the 30 allergens listed in Table 5.1. Initially, 6σ peak width values were derived by counting the number of spectra contained in each peak, from the peak uprise to its return to the baseline. It was not possible to manually measure such a parameter on printed chromatograms, because the peaks were so narrow that the x-axis time intervals (expressed in

minutes) did not accurately define peak widths. The QMS spectral production frequency was 50 Hz, with peaks reconstructed with 8, 9, 10, 11, 12 or 13 spectra, leading to a 6σ peak width range of 140-240 ms. The number of spectra generated per peak should be sufficient for the scopes of reliable quantification, if desired [12]. Four-sigma peak widths were derived from the 6σ values, and were calculated to be in the range of 93-160 ms, with an average approx. value of 117 ms.

Considering the entire modulation period, the void time was also considered because such space was occupied by wrap-around peaks - approx. 21 peaks could potentially elute one after another during each ^{2}D analysis. The product of the ^{1}D and ^{2}D peak capacities reaches a value of 8820. However, such a value must be corrected for undersampling: a "low" modulation ratio (MR) of 0.6 was calculated [13], considering the 1.5-s average peak width of the alkanes. Under the modulation conditions applied, ^{1}D peaks were sampled maximum once or twice, with such an event having a detrimental effect on ^{1}D resolution, and on the overall peak capacity. The reduction in peak capacity (β-correction) was calculated by exploiting theoretical considerations introduced by Davis et al. [14]. Specifically, a β value of 3.1 was calculated, leading to a corrected value of approx. 2850.

Apart from the negative impact on peak capacity, modulation undersampling should have a positive effective on sensitivity enhancement; very simply, ^{1}D peaks are distributed in a lower number of ^{2}D peaks (in this case one or two). The increase in sensitivity for 10 analytes, crossing the entire elution range, was evaluated by comparing S/N values in modulated and unmodulated experiments (n = 3). In the modulated experiment, and in the case of two modulations for a single compound, the most intense modulated peak was

considered. In the unmodulated application, the spectral generation frequency was adjusted (5 Hz) to attain approximately 10 spectra per peak. Peak areas in the modulated and unmodulated experiments were also controlled to assure that similar sample amounts reached the ^{1}D column inlet. It is noteworthy that the general increase in signal intensities attained through the CM process was accompanied by a rather intense background noise, due to the 50-Hz spectral generation frequency; on the other hand, the background noise was much less in the unmodulated experiments. Moreover, it is obvious that the use of a short micro-bore ^{1}D column limited the extent of band broadening (compared to a conventional GC column). For such reasons, the S/N values were always higher in the GC×GC experiments, even though the enhancement was less than initially expected: S/N values were increased on average by a factor of approx. 5 for the 10 compounds, with minimum and maximum increases by factors of 3 and 9, respectively (Table 5.1). A final factor subjected to evaluation was the difference between experimental linear retention index (LRI) values and those present in the MS database used the latter being constructed by using a conventional GC column with the same stationary phase as that used in the first GC×GC dimension. As can be seen from the information listed in Table 5.1, the maximum LRI difference observed was that of 12 units for benzaldehyde; moreover, an absolute average LRI difference of 4 units was calculated. As expected, a majority of positive LRI differences (19 compounds) were observed, due to the additional ^{2}D column retention. Such results indicate that the application of a tolerance range of ± 15 LRI units can be applied during the MS database search, to delete incorrect matches from the MS "hit" list.

Finally, a commercial perfume was subjected to fast GC×GC-QMS analysis (Figure 5.2); peak assignment was performed by using two filters, based on:

i) a minimum spectral similarity of 90% ii) an LRI tolerance range of ± 15 units. The results of the MS database search are reported in Table 5.2: overall 36 peaks were assigned, with spectral similarities in the range 90-96%. Moreover, an absolute average LRI difference of 3 units was calculated, in good agreement with the data reported in Table 5.1. Eighteen compounds (reported in bold in Table 5.2), among the thirty-six, have been highlighted by the SCCS as skin sensitizers [9].

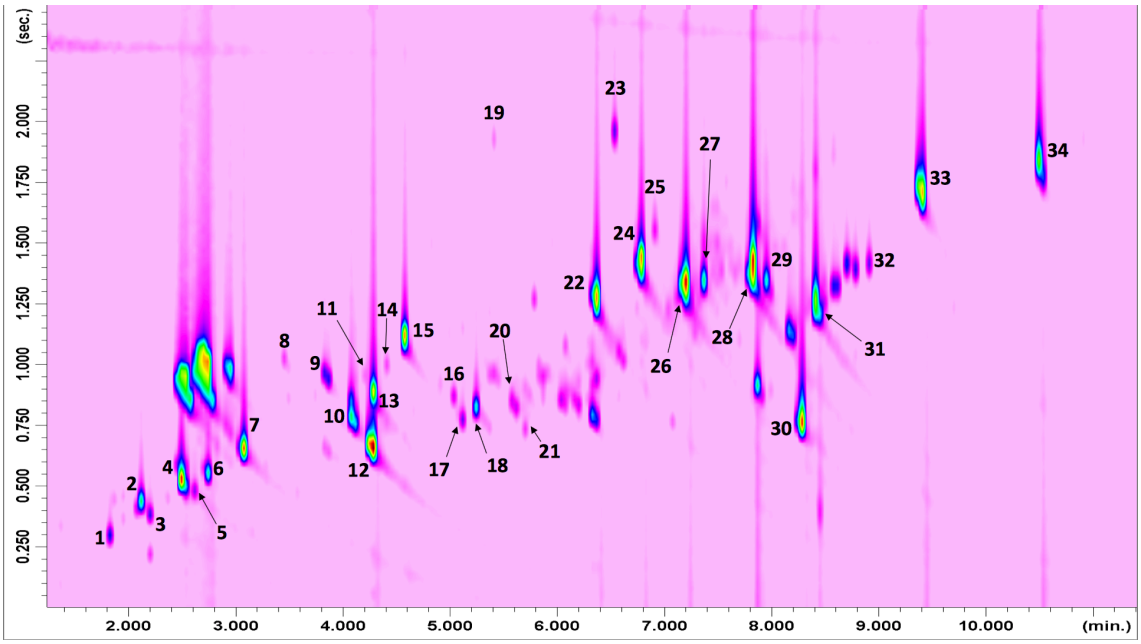

Figure 5.2. Fast GC×GC-QMS chromatogram of a sample of commercial perfume; for peak assignment refer to Table 5.2.

Table 5.2. Identification, linear retention index deviations with respect to MS database values, and spectral similarity values, for compounds numbered in Figure 2. Cosmetic allergens are reported in bold.

Peak/Compound	ΔLRI	Similarity %
1. α-pinene	2	96
2. **β-Pinene**	-1	96
3. Myrcene	3	95
4. **Limonene**	-2	96
5. (*E*)-β-Ocimene	1	90
6. γ-Terpinene	4	95
7. **Linalool**	5	96
8. **Camphor**	1	93
9. **α-Terpineol**	1	94
10. **Citronellol**	0	94
11. **Neral (Citral isomer I)**	5	91
12. **Linalyl acetate**	3	96
13. **Geraniol**	1	94
14. **Geranial (Citral isomer II)**	2	90
15. **Hydroxycitronellal**	0	95
16. α-Terpinyl acetate	2	93
17. cis-Geranyl acetate	1	94
18. trans-Geranyl acetate	1	95
19. **Vanillin**	7	90
20. **Caryophyllene**	-1	95
21. α-Guaiene	1	90
22. Lilial	2	92
23. Raspberry ketone	10	94
24. Phthalate diethyl	4	93
25. Isobutyl quinoline	7	92
26. cis-Methyl dihydrojasmonate	2	93
27. trans-Methyl dihydrojasmonate	5	94
28. **α-Hexyl cinnamaldehyde**	3	94
29. (*2Z*)-Hexyl cinnamaldehyde	2	95
30. Isopropyl myristate	3	95
31. **Galaxolide**	7	94
32. Ambrettolide	9	96
33. Ethylene brassylate	9	94
34. **Sclareol**	3	92
	3	

5.3 Conclusion

The scope of the present research was not to propose a fast GC×GC-QMS method, of general application, but to emphasize its concept, method optimization aspects, and potential. In fact, the approach herein developed can be applied to samples characterized by a C8-23 alkane boiling point range. The results described for the mixture of allergens and for the sample of perfume were certainly satisfactory. However, for other sample-types, one or more modifications of the many parameters which characterize a CM-GC×GC-QMS method would be necessary.

In the case of fast GC-QMS experiments, using a 10 m × 0.1 mm id column, the main advantage over conventional GC-QMS applications, is the shorter analysis time. On the other hand, the benefits in the development of a fast CM GC×GC-QMS method are several, compared to a conventional approach. Apart from the obvious reduction in analysis time, there is also a decrease (in this investigation) of the consumption of heating and cooling gases. For CM systems using cryogenic fluids, there would be an additional economical advantage: the number of high-resolution GC separations, per unit volume of cryogenic fluid, would be much higher. Finally, the use of the same internal diameter in the first and second dimension, and in the delay loop, enables the generation of satisfactory gas velocities in all such zones.

References

[1] Liu Z., Phillips J.B., Comprehensive two-dimensional gas chromatography using an on-column thermal modulator interface, J. Chromatogr. Sci. 1991, 29, 227-231.

[2] Cortes H.J., Winniford B., Luong J., Pursch M., Comprehensive two dimensional gas chromatography review, J. Sep. Sci. 2009, 32, 883-904.

[3] Bruckner C.A, Prazen B.J., Synovec R.E., Comprehensive two-dimensional high-speed gas chromatography with chemometric analysis, Anal. Chem. 1998, 70, 2796-2804.

[4] Edwards M., Mostafa A., Górecki T., Modulation in comprehensive two-dimensional gas chromatography: 20 years of innovation, Anal. Bioanal. Chem. 2011, 401, 2335-2349.

[5] Adahchour M., Taşöz A., Beens J., Vreuls R.J.J., Batenburg A.M., Brinkman U.A.T., Fast comprehensive two-dimensional gas chromatography (GC×GC) using 50-μm ID second-dimension columns, J. Sep. Sci. 2003, 26, 753-760.

[6] Junge M., Bieri S., Huegel H., Marriott P.J., Fast comprehensive two-dimensional gas chromatography with cryogenic modulation, Anal. Chem. 2007, 79, 4448-4454.

[7] Purcaro G., Tranchida P.Q., Dugo P., La Camera E., Bisignano G., Conte L., Mondello L., Characterization of bacterial lipid profiles by using rapid sample preparation and fast comprehensive two-dimensional gas chromatography in combination with mass spectrometry, J. Sep. Sci. 2010, 33, 2334-2340.

[8] Donato P., Tranchida P.Q., Dugo P., Dugo G., Mondello L., Rapid analysis of food products by means of high speed gas chromatography, J. Sep. Sci. 2007, 33, 508-526.

[9] Opinion on fragrance allergens in cosmetic products, SCCS/1459/11, June 2012.

[10] Tranchida P.Q., Zoccali M., Franchina F.A., Cotroneo A., Dugo P., Mondello L., Gas velocity at the point of re-injection: An additional parameter in comprehensive two-dimensional gas chromatography optimization, J. Chromatogr. A 2013, 1314, 216-223.

[11] Fitz B.D., Wilson R.B., Parsons B.A., Hoggard J.C., Synovec R.E., Fast, high peak capacity separations in comprehensive two-dimensional gas chromatography with time-of-flight mass spectrometry, J. Chromatogr. A 2012, 1266, 116-123.

[12] Adahchour M., Brandt M., Baier H-U.,Vreuls R.J.J., Batenburg A.M., Brinkman U.A.Th., Comprehensive two-dimensional gas chromatography coupled to a rapid-scanning quadrupole mass spectrometer: principles and applications, J. Chromatogr. A 2005, 1067, 245-254.

[13] Khummueng W., Harynuk J., Marriott P.J., Modulation ratio in comprehensive two- dimensional gas chromatography, Anal. Chem. 2006, 78, 4578-4587.

[14] Davis J.M., Stoll D.R., Carr P.W., Effect of first-dimension undersampling on effective peak capacity in comprehensive two-dimensional separations, Anal. Chem. 2008, 80, 461-473.

Chapter 6

Ultra-High Pressure Liquid Chromatography Coupled with Ion Mobility Mass Spectrometer

6.0 Introduction to ultra-high pressure liquid chromatography

Over recent decades, different advances in the development of comprehensive solutions to increase the separation efficiency and reduce the analysis time have been made. Different approaches have been reported to provide improved chromatographic separation. Among these, silica-based monolith columns, which consist of a single piece of porous material with several unique features in terms of high permeability and efficiency, plus low resistance to mass transfer, could be interesting [1,2]. However, the limited number of available columns dimensions and surface chemistries has restricted the progress of this technology. Another possible way to increase the efficiency on standard LC instrumentation consists in the use of long columns by coupling standard LC columns with totally porous particles and operation at high temperatures, allowed by the reduced mobile phase viscosity and hence lower pressure drop along the analytical column [3,4,5]. Unfortunately, the technical constraints as the longer analysis time, the limited number of available stationary phases capable of withstanding elevated temperatures, and the question of stability of the analytes, make this approach difficult to practice. Analogously, the use of partially porous stationary phases, also known as fused core or core-shell particles, allows to serially couple columns and boost the separation efficiency [6,7,8]. The stationary phase particle consists of a thin layer of porous shell fused to a solid particle (Figure 6.1). This technology drastically reduces the pressure drop when compared to fully porous (sub-2 μm) stationary phases, mainly when high temperatures are applied, making it possible to operate such phases on a conventional LC instrument [9].

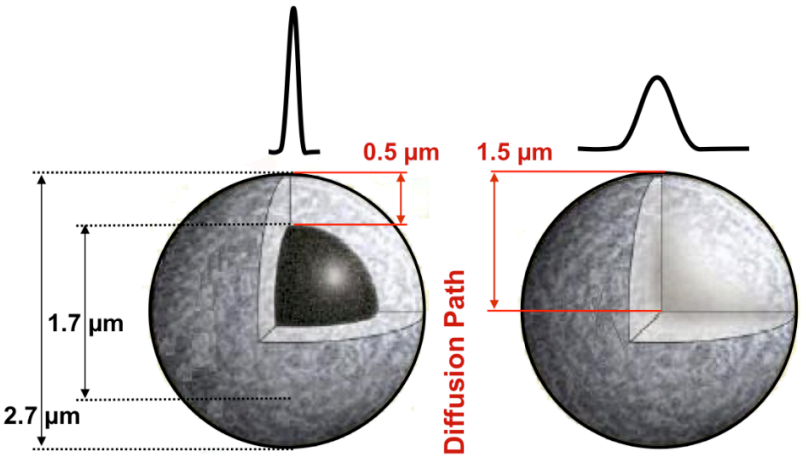

Figure 6.1. Partially porous technology (Fused core, on the left) and totally porous particles (on the right).

Since the introduction of the first commercially available HPLC columns packed with 10 µm particles in the early 1970s, the use of ever smaller particles has become the most popular way to improve chromatographic separations [10-13].

As reported by Giddings in 1991, there is a linear correlation between the pressure drop (ΔP) and the linear velocity (u) in the column [14] (Equation 6.1):

$$\Delta P = \frac{\varphi \eta u L}{d^2{}_p} \quad (\mathbf{6.1})$$

where φ, η, L, and d are the flow resistance, viscosity of the mobile phase, length of the column, and particles diameter, respectively. It has been demonstrated that using a column 25 cm long packed with 5 µm particles an

inlet pressure <25 bar is required for the chromatographic analysis, whereas reducing at 1 μm the particles diameter needs an inlet pressure of 2000 bar [15,16]. Consequently, dedicated instrumentation and columns are necessary [17-20]. Recent HPLC developments have been focusing, on the one hand, on the design of pumping devices, injection system and flow paths, capable of operating at very high pressures (600 to 1000 bar) and detectors capable of high acquisition rate; on the other hand, on the manufacturing of stationary phase particles that are stable enough to tolerate such elevated pressures. The term "ultra-high pressure liquid chromatography" (UHPLC) to describe the higher performance achieved by the novel instrumentation, in combination with small particles, was coined by Jorgensen in 1997 [21]. Nowadays this technique is also known with the name of "ultra-high performance liquid chromatography" (UPLC). The first commercially available UHPLC system was introduced in 2004. The real success of any UHPLC system is correlated to the use of columns packed with sub-2 μm particles. The Van Deemter plot (Figure 6.2) shows that smaller particles have the advantage of much flatter H values at higher flow velocities. This result means that speed can not only be doubled by halving particle diameter, but can also be doubled and doubled again by operating at higher flow velocities, without any efficiency loss. The numerous applications on UHPLC suggest a considerable enthusiasm towards this technique [22-26]. Compared to conventional HPLC, it offers a series of advantages such as improved resolution, higher peak efficiency, shorter retention times, and reduced solvent consumption. Furthermore, the narrower peaks (sharper peaks) and the lower detection limits (LODs), due to the higher peak efficiency, provide for a greater sensitivity than HPLC. On the other hand, the technique is easily prone to several deficits. One of the major problems associated to the application of elevated pressures is the heating of

the mobile phase due to viscous friction losses [20,27,28]. This could produce radial or axial temperature gradients inside the column related to the thermal conditions under which the analysis is performed (isothermal or adiabatic operation, respectively). Both temperature gradients may compromise the separation efficiency.

6.1 UHPLC system requirements

The development of UHPLC systems represents an engineering challenge, since these instruments have to be designed to take advantage of the greater speed, higher resolution and superior sensitivity offered by small particles. Various instrumental characteristics need to be considered for satisfactory operation of UHPLC:

1. Instrument performance. It must be able to withstand the increased higher pressures than HPLC system, by improving the pressure capabilities of the pumping device.

2. Extra-column volume. The tubing volume, the mixer volume, the detector cell volume must be reduced as much as possible. A system plumbed with 0.005'' I.D. stainless steel tubing and zero dead volume fittings is preferred for UHPLC experiments.

3. Dwell volume. It represents the volume of liquid contained in the system between the point where the gradient is formed and the point where the mobile phase enters the column. This volume includes the mixer, transfer lines, and any swept volume (including the sample loop) in the injection system. After the gradient has started, a delay is observed until the selected proportion of solvent reaches the column

inlet, on account of this the sample is subjected to an unwanted additional isocratic migration. The dwell volume may differ from one instrument to another, but it can be easily measured

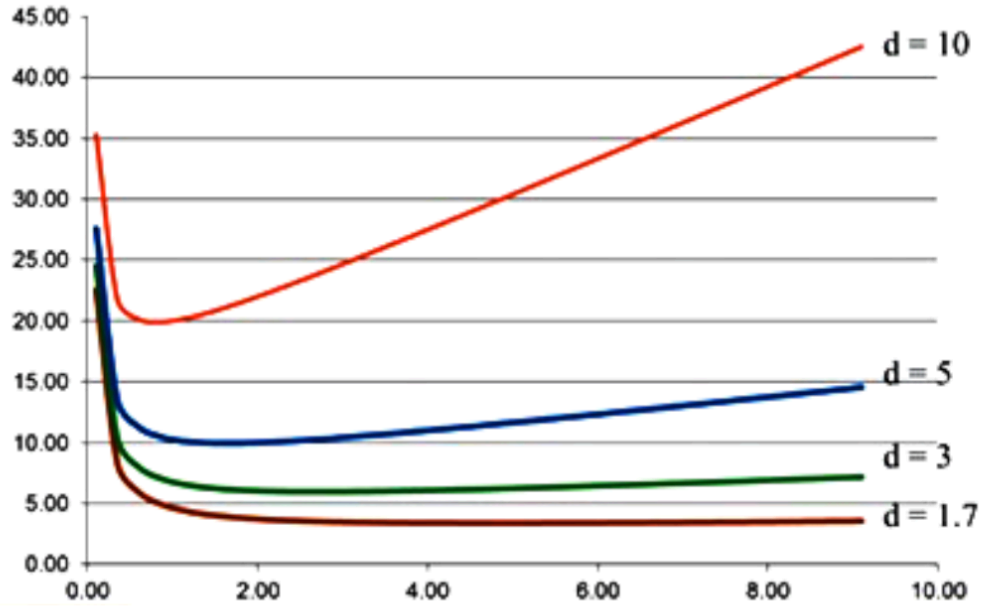

Figure 6.2. *Van Deemter plot at different d_p.*

4. Mobile phases. It is recommended the use of high-grade organic solvents (recognized UPLC or LC-MS grade), Milli-Q water or similar, being careful to microbiological growth, and store the column with pure organic solvent, because of the size of the frits and particles that are much smaller than HPLC (0.2 µm versus 2 µm).

5. Column dimension. The separation is made faster by using shorter columns, but the same should still offer sufficient column efficiency to

allow at least a baseline separation of analytes. If the primary goal is speed, it is recommended the use of a column with a length of 50 mm, otherwise it is preferable a column of 100 mm, if the main purpose is resolution. Reducing the column diameter does not shorten the analysis time, but decreases mobile phase consumption and sample volume. It is possible to find UHPLC columns with 1.0, 2.1, 4.6 mm I.D. The 2.1 mm I.D. column should be considered as optimal, while 4.6 mm I.D. can generate significant frictional heating. Concerning the 1.0 mm I.D., the compatibility between the column geometry and any UHPLC instrument is critical, and it is only used for specific reasons (e.g. severely sample limited or direct flow to MS).

6. Detector acquisition rate. The narrow peaks generated in UHPLC have to be monitored by detectors that offer acquisition rates high enough to record a reasonable data points (20 points per peak are recommended) across the chromatographic peak. Only the latest generation of instruments meets these requirements.

6.2 Moving from a HPLC method to an UHPLC

When transferring methods from HPLC to UHPLC, it is usually sufficient to maintain the resolution of the original method. A widespread approach consists in the employment of shorter columns packed with smaller particles; this strategy maintains resolution and allows faster separations. Several calculations are required to adapt some parameters, such as injection volume, flow rate, in both isocratic and gradient modes, to the new column characteristics.

In isocratic mode it is important to consider and thus adjust the flow rate and

the injection volume. The linear velocity of the mobile phase has to be increased while decreasing the particle size to work within the Van Deemter optimum. In addition, the new flow rate is scaled to the change of column cross section if the column inner diameter changes. Specifically, it must be decreased as column internal diameter decreases. The UHPLC flow rate (F_2) can be calculated with the following equation 6.2:

$$F_2 = F_1 \left(\frac{{d^2}_{c2}}{{d^2}_{c1}} \frac{d_{p1}}{d_{p2}} \right) \quad (\mathbf{6.2})$$

where d_P is the particle size. Also the injection volume should be adapted to the new column dimension, since it is proportional to the column volume. Indeed, decreasing the column internal diameter and length decreases the overall column volume and sample capacity. The new injection volume (V_{I2}) can be calculated with the equation 6.3:

$$V_{I2} = V_{I1} \frac{{d^2}_{c2}}{{d^2}_{c1}} \frac{L_2}{L_1} \quad (\mathbf{6.3})$$

where d_c and L represent the diameter and the length of the column, respectively. Practically it is important to maintain the ratio of column dead volume and injection volume constant.

In gradient mode, instead, transferring an optimized gradient elution method between instruments, columns, and MS. is more difficult than transferring isocratic elution method. Gradient methods can introduce variables that may not be easy to control. First of all, should be made the same considerations about the flow rate and volume injection previously discussed in isocratic mode. Either linear gradient or step gradient can be dissected into a combination of isocratic or gradient walks [29]. For the isocratic step (t_{iso2})

can be applied the equation 6.4:

$$t_{iso2} = t_{iso1}\left(\frac{F_1}{F_2}\frac{d^2{}_{c2}}{d^2{}_{c1}}\frac{L_2}{L_1}\right) \quad (\mathbf{6.4})$$

this is useful also for the re-equilibration time. For the gradient step, the guidelines proposed by Schellinger and Carr should be followed [30]. In order to maintain a constant selectivity, the start and the final composition of the mobile phase in the gradient should be the same than the original method:

$$t_{grad2} = \frac{\left(\%B_{final1} - \%B_{start1}\right)}{slope_2} \quad (\mathbf{6.5})$$

where $slope_2$is the slop of the new gradient and it is can be calculated with this equation:

$$slope_2 = slope_1\left(\frac{F_1}{F_2}\frac{d^2{}_{c2}}{d^2{}_{c1}}\frac{L_2}{L_1}\right) \quad (\mathbf{6.6})$$

even if these ploys is employed, the selectivity could be different because of different dwell volume [31]. In view of this, one must adjust the "effective" dwell volume, which is the total volume of starting eluent delivered to the column inlet after injecting the solutes. The "intrinsic" dwell volume is the gradient delay volume delivered to the column before the front of the gradient arrives at the column inlet. The latter is obviously an instrument constant, while the former is a modifiable parameter by delaying the injection or using an initial isocratic step [30].

6.3 Introduction to ion mobility spectrometry

The term ion mobility spectrometry (IMS) refers to the principles, methods, and instrumentation for characterizing substances in an electric field and

through a supporting gas atmosphere. [32,33] This simple definition encompasses all combinations of pressure, flow, and composition of the gases, strength and control of electric fields, and methods of forming ions from samples [34-38]. Proliferation in mobility methods during the past decade was accompanied by variations in styles, geometries, and dimensions of mobility analyzers. An attempt to summarize these advances from this period of high activity, based on principles of mobility by pressure and electric field, is shown in Figure 6.3.

For ion mobility measurement an ion cluster is injected into a drift region, using an ion shutter, which establishes the time base for the measurement (Figures 6.4a and 6.4b). In the drift region, the ion cluster moves through purified air at ambient pressure in a voltage gradient or electric field (*E* in V/cm) as shown in Figure 6.4b, with drift velocities v_d determined from the time (ms) needed for the ions to traverse the distance (*d*, cm) between the ion shutter and detector (i.e., the drift time t_d):

$$v_d = {}^{d}/_{t_d} \quad (\mathbf{6.7})$$

The length of drift regions for modern in-field IMS analyzers is typically 4 to 20 cm an ion cluster moving 6 cm with a drift time of 15 ms in an electric field of 200 V/cm has a drift velocity of 4 m/s. The normalization of drift velocity to *E* produces the mobility coefficient *K*, which is cluster velocity per unit field (cm^2 /Vs):

$$K = {}^{v_d}/_{E} \quad (\mathbf{6.8})$$

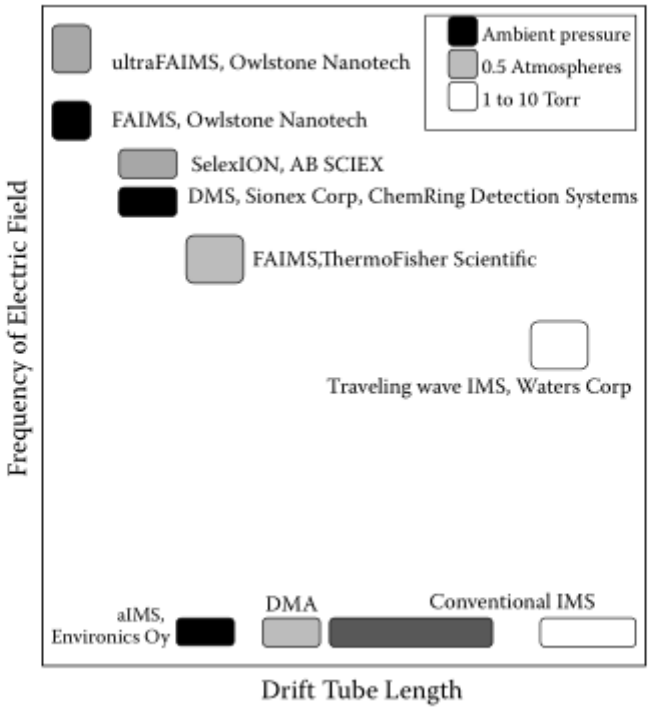

Figure 6.3. A proliferation of mobility methods occurred during the past decade, ranging over dimensions, pressures, and arrangements of electric field (constant or time dependent). Pressure of measurements is given in the fill pattern of boxes for individual methods.

and these same ions have a mobility coefficient of 2.4 cm^2 /Vs at a pressure of 660 torr and temperature of 25°C. Drift velocity is affected by temperature (T) and pressure (P) inside the drift tube, and *K* is commonly normalized to 273 K and 760 torr, producing a reduced mobility coefficient K_0:

$$K_0 = K\left({}^{273}/_{T}\right)\left({}^{P}/_{760}\right) \quad (\mathbf{6.9})$$

which here is 2.0 cm^2/Vs. The relationship between drift velocity and electric field (Equation 6.8) is valid for an ion cluster at thermal energies measured in a constant composition of gas atmosphere, pressure, and temperature. Ions are thermalized when the energy gained by ions between collisions with the supporting gas atmosphere is low compared to thermal energy.

6.4 A measurement by ion mobility spectrometry

A measurement in all experimental configurations of mobility begins when gas ions are formed from components in a sample. This is commonly accomplished using gas phase reactions between analyte molecules and a reservoir of charge called reagent ions. Ions from these reactions are called product ions, characterized for mobility in common mobility spectrometers when injected into the drift region (Figure 6.4), where drift time is determined as ions reach the end of the drift tube and collide with a detector, typically a Faraday plate.

Ions colliding on the plate are neutralized, drawing current that is transduced into voltage in an amplifier. A distinction of IMS, in contrast to mass spectrometry (MS), is that ions are formed and characterized in a supporting gas atmosphere, also called a buffer gas or the drift gas. A plot of the detector response versus drift time is called a mobility spectrum (Figure 6.4c), which contains all the information available in a mobility measurement. This includes drift time, peak shape, which is a measure of drift tube performance; and secondary spectral details, such as baseline distortion, that provide information on ion–molecule reactions in the drift region. Although mobility spectra may also contain fragment ions that are chemical class specific, [39-41].

6.5 The mobility of ions in an electric field through gases

The main question in a mobility measurement is the relationship between ion cluster velocity and the chemical identity of the ions in the cluster, associated largely with the reduced mobility coefficient. Early efforts to relate ion structure or identity to mobility coefficients arose mainly from studies of ions

in pure gases at sub-ambient pressure [42] and led to models for *K* (as in Equation 6.10) [43].

$$K = \frac{3e(2\pi)^{1/2}(1+\alpha)}{16N\left(\mu k T_{eff}\right)^{1/2}\Omega_D\left(T_{eff}\right)} \quad (\mathbf{6.10})$$

where *e* is the electron charge; *N* is the number density of neutral gas molecules at the measurement; α is a correction factor; μ is the reduced mass of ion and gas of the supporting atmosphere; T_{eff} is the effective temperature of the ion determined by thermal energy and the energy acquired in the electric field; and Ω_D (T_{eff}) is the effective collision cross section of the ion at the temperature of the supporting atmosphere.

The mass and shape of an ion strongly affect the mobility coefficient through the cross section for collision as shown in Figure 6.5.

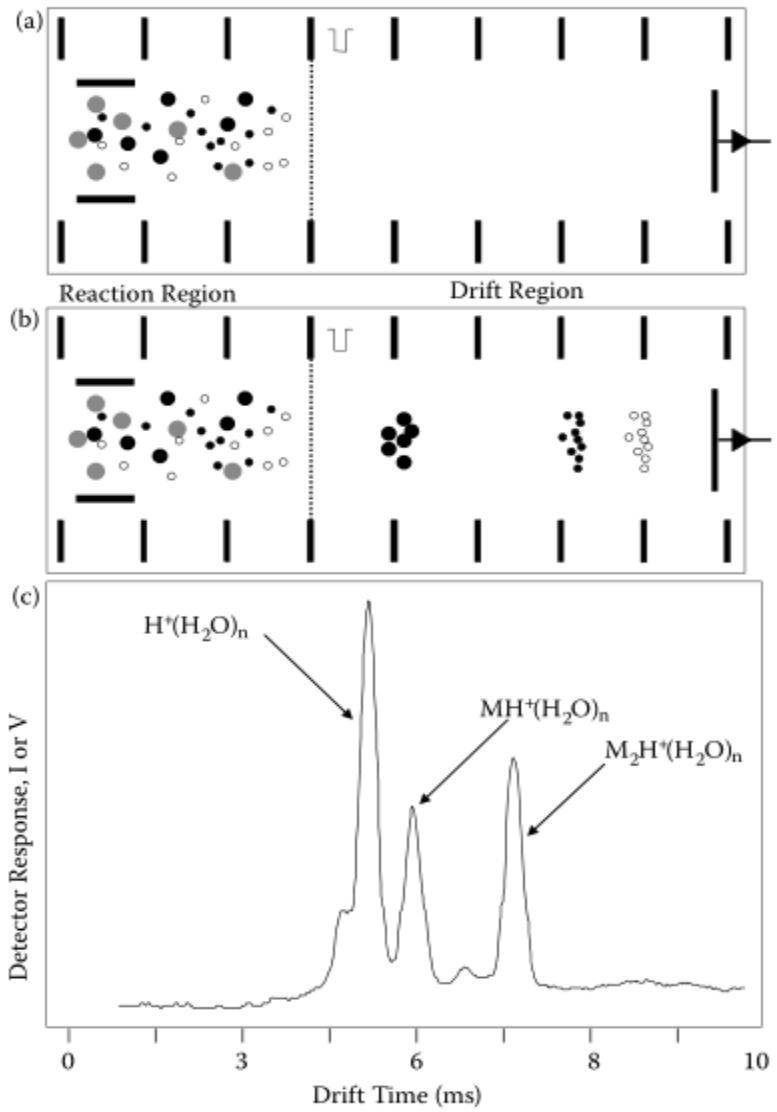

Figure 6.4. Schematic of drift tube for ion mobility spectrometry. (a) The drift tube is comprised of a reaction region and drift region, both under an electric field gradient. Two types of neutral sample molecules (small and large grey symbols) are introduced into the ion source region. (b) Sample molecules are ionized (small and large black symbols). Ions are injected using an ion shutter into the drift region and are separated according to differences in ion mobility. (c) A positive polarity mobility spectrum for 2-pentanone in air. The reactant ion peak is apparent at 4.45 ms. The protonated monomer and the proton-bound dimer appear at 5.075 and 6.225 ms, respectively.

Drift velocities are sensitive to the exact identity of ions in a cluster, which is affected by the composition of the gas atmosphere and by changes in

temperature. Thus, the relationship between K and Ω_D is inaccurately described or incomplete for large organic ions where Ω_D is influenced by polar neutrals or moisture in the drift region.

This discussion is for introduce briefly elementary aspects of IMS and to emphasize that IMS should be understood best as two sequential processes:

i) formation of ions that are representative of a sample and

ii) ii) the determination of these ions for mobilities in an electric field.

6.6 Instrumentation

The need to couple IMS and MS can either be driven by the desire to identify IMS features by mass analysis or by the wish to shape-analyze mass-selected ions. Although the two motivations approach the problem from opposite directions, they lead to instrument designs with basically identical capabilities as far as shape-mass analysis is concerned. The first perspective, upgrading an ion mobility spectrometer by adding an MS detector, logically leads to an IMS-MS configuration. The second approach may lead to a modified tandem mass spectrometer with the collision cell replaced by a drift cell.

The most general setup is schematically shown in Figure 6.6. One or several of the components shown in the figure may be omitted in individual designs. Nevertheless, in all cases ions are produced in a source, analyzed by IMS and MS, and finally detected.

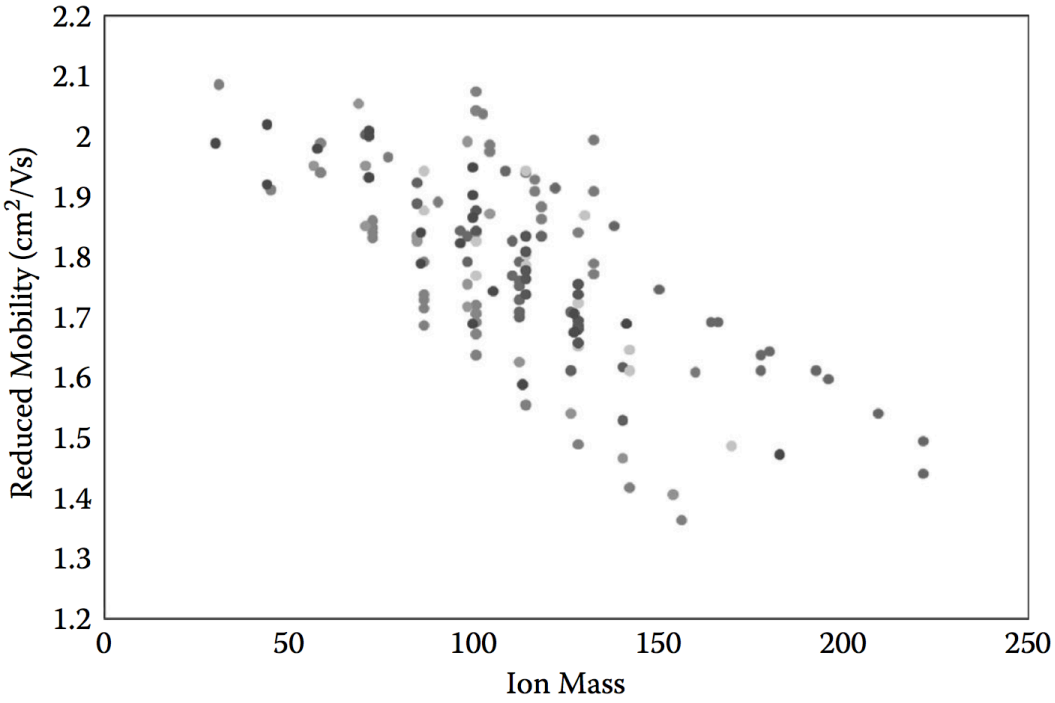

Figure 6.5. Plots of reduced mobility versus mass for volatile organic compounds. When all parameters of instrument and chemistry are controlled, the mobility coefficient is governed by size-to-charge and reduced mass of the ion in the supporting atmosphere and is an exquisitely sensitive measure of the structure and behaviour of ions in a supporting gas atmosphere. One of the key facets of IMS is the influence of structure shape and size on mobility.Mobility coefficients are influenced by ion mass and a linear relationship exists within a homologous series; however, ions of the same mass but different functional groups, or even different geometrical arrangement of the same functional groups (isomers), often exhibit different K o values, reflecting the influence of shape and size on mobility.

In addition, the IMS unit typically requires an entrance section to condition the ions prior to IMS analysis and an exit section to collect the ions afterwards. In the following paragraphs each of the individual components of a typical IMS-MS instrument are discussed.

6.6.1 Ion source

Electrospray ionization (ESI) has emerged as a powerful technique to create ions in many IMS-MS applications, although other ionization methods including matrix- assisted laser desorption/ionization (MALDI) are also common for certain applications. In fact, any ionization method used in IMS or MS will work for the IMS-MS combination as well. A review of ion sources is beyond the scope of this chapter and can be found elsewhere [44] and in any book on MS. [45]

6.6.2 IMS entrance section

IMS analysis requires a narrow pulse of ions entering the drift region. Whereas certain ion sources prepare ion pulses naturally (e.g., MALDI employing a pulsed laser), many other sources produce a continuous ion beam (e.g., ESI). In this case the continuous ion beam has to be converted into a pulsed beam. To increase the duty cycle, this is done most efficiently in an ion trap where ions are accumulated for a period of time and periodically pulsed out. Whereas any type of ion trap works in theory, [46] in practice most designs are based on ion funnels [47]. Ion funnels [48] are a natural choice because they are most often part of the front end of an MS or IMS device anyway, taking care of efficient ion transmission from the source into the analyzer, often through a number of differential pumping stages. Smart ion funnel designs allow storage of a large number of ions [49] and include mechanisms to empty the storage volume efficiently. Whereas ion pulsing may occur anywhere between the source and the IMS section, ion injection into the drift region is handled directly at the IMS entrance interface.

Depending on source design and instrument configuration a vacuum may be

required prior to IMS analysis. In this case ions have to be transferred from vacuum into the buffer gas, a process that becomes increasingly more difficult with increasing buffer gas pressure and ion cross section.

IMS units operating at pressures significantly higher than 1 Torr make ion injection from a vacuum impractical and are generally not compatible with mass selection prior to IMS analysis. In these cases, ions are either generated inside the drift chamber or are transferred from the ion source via ion guides and ion funnels. For an ESI source operating under ambient conditions coupled to an IMS unit operating with helium, the IMS interface requires a section with helium counter flow to prevent air from entering the drift region [50,51]. Keeping air out of the drift cell even in trace amounts is very important, since cross sections of ions in air are much larger than in helium.

A final function of the IMS entrance section is to restrict the flow of buffer gas out of the drift cell. This is accomplished by using a small entrance aperture. If ions enter the drift cell from vacuum, then electrostatic lenses can be used to steer the ions and focus them onto the aperture. Otherwise, ion funnels are used to guide and focus them.

In summary, the IMS entrance section is used to convert a continuous ion beam into ion pulses (if necessary), admit ion pulses into the drift region, keep unwanted neutrals out, and restrict the flow of buffer gas out of the drift region.

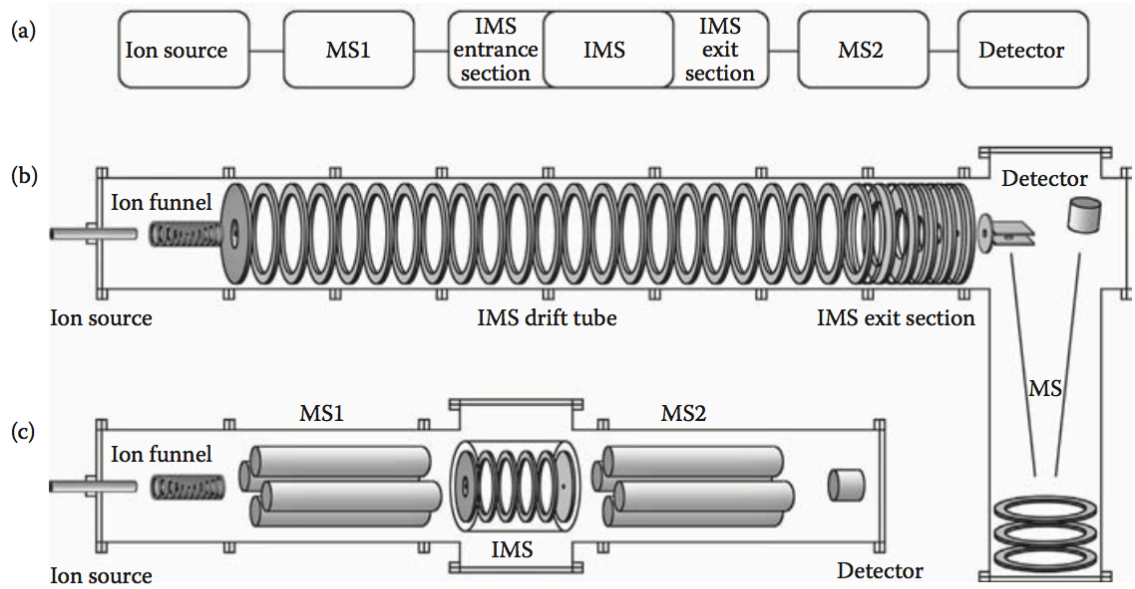

Figure 6.6 (a) Schematic setup of an IMS-MS device. The MS1 mass selection step before IMS analysis is omitted in many designs, in particular in combination with high-pressure (≥10 Torr) IMS devices and/or atmospheric pressure ion sources such as ESI. In alternative designs MS2 may be omitted. (b) Schematic drawing of a high-resolution IMS device coupled to a TOF mass spectrometer. (c) Schematic drawing of a mass spectrometer equipped with an IMS drift cell in a quad-EMS-quad arrangement.

6.6.3 IMS drift tube

Drift tubes come in all shapes and sizes. The drift length may be as short as a few centimetres or as long as several meters. Small drift cells may be fabricated of a cubic piece of copper and inserted into the vacuum chamber of a mass spectrometer. Large drift tubes may be fabricated of cylindrical sections of pipe with a mass spectrometer bolted to the last IMS section. Independent of size, the interior usually looks the same; stacks of equally spaced guard rings connected by a resistor chain provide a uniform electric field. To prevent ion loss, the inside diameter (i.d.) of the guard rings has to be larger than the spread of ions due to diffusion [Equation (6.11)]. The drift

voltage supplied to the first and last guard ring is proportional to the drift length for equal pressure and field strength.

$$x = \sqrt{\frac{4k_bTL}{\pi Ee}} = \sqrt{\frac{4k_bTL^2}{\pi Ve}} \quad (\mathbf{6.11})$$

The IMS resolution does not directly depend on the drift length. Rather, it depends on the square root of the drift voltage. However, longer drift tubes allow larger voltages to be applied across the cell (at constant field), thereby increasing the resolution. On the other hand, increasing the pressure at constant drift length will have the same effect.

IMS resolution can also be influenced by temperature, although drift tubes with adjustable buffer gas temperature are relatively difficult to design. Adjusting the temperature in larger drift tubes creates additional challenges including thermal equilibration, thermal insulation, and water condensation on cold metal parts exposed to air and carrying high voltage. Measurement of an absolute ion mobility requires knowledge of the drift time *t*, drift length *L*, drift voltage *V*, buffer gas pressure *p*, and temperature *T*. All of these parameters can easily be measured with good precision. However, any uncertainty in the parameters *t*, *L*, *E* = *V*/*L*, *N*, and the square root of T translates directly into an uncertainty in the mobility measurement.

6.6.4 IMS exit section

In an IMS-MS setup a small aperture at the end of the drift region allows a small fraction of ions to exit the buffer gas chamber and enter a mass spectrometer. In this setup most ions are lost even for short drift lengths with

a small spread of the ion cloud and relatively large apertures. As an example, for a 1-cm ion cloud only ~15% of the ions make it through a 1-mm diameter orifice.

In a design that does not address these issues the actual drift length may be considerably shorter than the drift cell length. Hence, from this point of view exit (and entrance) apertures have to be kept as small as possible, typically ≤0.5-mm diameter. If sensitivity is not an issue, the setup with a simple small exit aperture is the most straightforward approach both with respect to design and data analysis. Arrival time and spread of the ion cloud are determined entirely by the drift velocity and diffusion, respectively, in the IMS cell without perturbation by subsequent refocusing devices. On the contrary, if sensitivity is an issue, refocusing at the end of the drift region is of paramount importance as it improves the signal for large drift lengths by orders of magnitude. Whereas electro- static focusing was attempted in early designs [52] today the ion funnel is the focusing device of choice [49,50]. Hence the IMS exit interface consists of a high-transmission metal screen defining the end of the drift field, an ion funnel focusing the ion cloud down to a small diameter, and an exit aperture into the vacuum of the mass spectrometer at the exit of the funnel. The drawback of a focusing device is that the IMS resolution may suffer due to a spread in time of the different ion trajectories inside the ion funnel. Nevertheless, for most IMS designs inclusion of an exit ion funnel is not just an option, it is required to make it work.

6.7 Methods of ion mobility spectrometry

6.7.1 Field asymmetric IMS, differential mobility spectrometry, ion drift spectrometry

A new method for measurements of ion mobility was developed in 1993 in which ions do not move under thermalized conditions at ambient pressure [51]. This method is based on ions undergoing changes in mobility coefficients under strong field conditions (at constant *N*), so that mobility should be understood for most ions as

$$K(\mathrm{E/N}) = K_0\left[1 + \alpha\left(E/N\right)\right] \quad (\mathbf{6.12})$$

where α is a function describing the dependence of mobility on the ratio of electric field strength to neutral density. In this new method, called field asymmetric IMS (FAIMS) ions are carried by gas flow through a gap with conducting surfaces. An electric field is applied to this gap, using an asymmetric waveform and ion clusters move with the electric fields according to Equations 6,7 to 6.9 and 6.12. The waveform is designed so that the integrals of these two regions are equal and ions with mobility coefficients that are independent of *E*, even at high fields, will pass line of sight through the gap of the analyzer (see Figure 6.7a) and reach the detector. In contrast, ions with a dependence of K_o on *E* undergo a net displacement toward a surface with repeated exposure of the ion clusters to the periodic changes in direction and strength of the electric field. The magnitude of displacement depends on the differences in mobility at field extremes. Ions restored to the center of the gap will be passed to the detector, and a sweep of this voltage, often 10 to 40 V or fields of 100 to 500 V/cm, provides a measure of all ions in the analyzer for a given waveform. The complex mixture of ions produced

with electrospray ion sources, particularly with biological samples, sometimes require use of ion filters to reduce “chemical noise” in MS determinations [53,54,55] An ESI-FAIMS instrument was commercialized in 2005 by Thermo Scientific as an inlet to their single-quadrupole mass spectrometer. [56] In 2010 to 2011, AB SCIEX, introduced a small planar DMS attachment to their mass spectrometers under the name SelexION Technology. [57] In both the FAIMS device measurements are comparable although the DMS technology is different and getting smaller. Even smaller is the μFAIMS analyzer of Owlstone Nanotech with silicon-etched channels in place of the gaps of other analyzers [58] (Figure 6.8). The dimension is scaled in micrometers and ions pass a distance of 300μm through a gap 30-μm wide experiencing 50-MHz waveforms, where electric fields can reach 80 townsends. These magnitudes are so strong that ions are electrically heated to dissociation and fragmentation, [59] providing chemical information in detail richer than commonly possible.

6.7.2 Travelling wave methods of IMS

Perhaps one of the most important developments in IMS during the past decade with a large impact on the acceptance and use of IMS was the introduction of traveling wave methods in combination with time-of-flight mass spectrometry (TOF-MS) for investigations of biological molecules [60-63]. In travelling wave methods, a set of rings is placed at low pressure and when sample ions are introduced into the drift tube, the potential is raised on a ring, establishing an electric field and initiating swarm movement by mobility. The potential is then lowered as potential on a neighbouring ring is raised; the process of raising and dropping of potential, sequentially with some time delay, establishes a “wave” as an electric field in the drift tube and moves

ions, down the tube, in the direction of the wave. Ion clusters are propagated through the drift tube with a velocity associated with characteristics of the wave and mobility of ions.

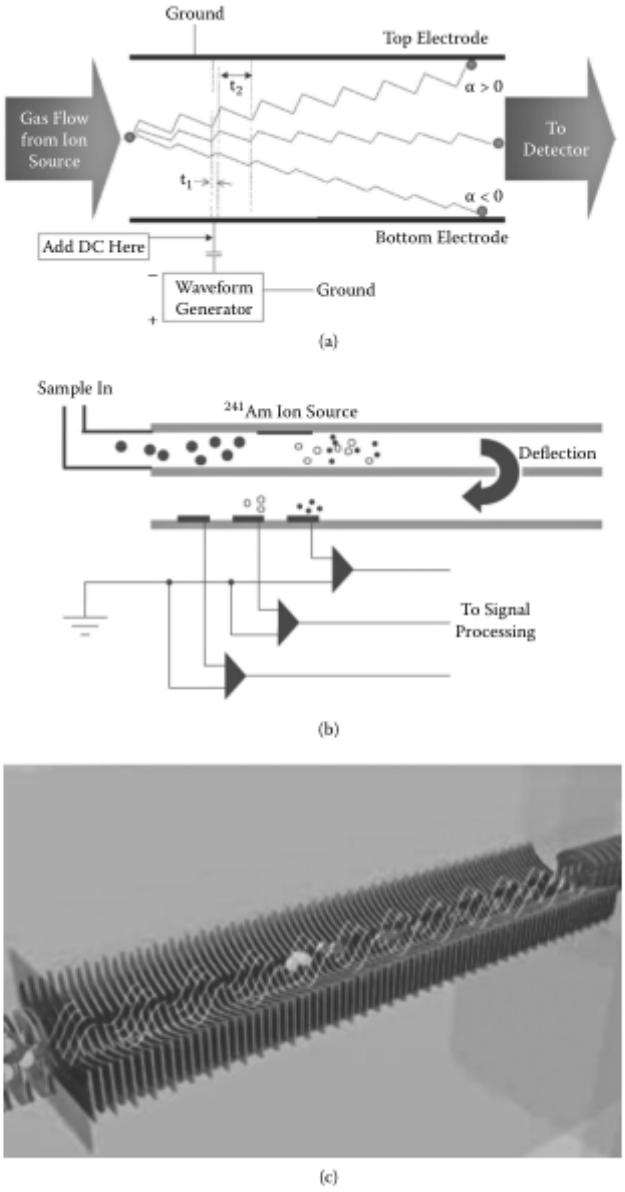

Figure 6.7 Schematics of methods for (a) differential mobility (or FAIMS), (b) aspirator, and (c) traveling wave methods of mobility measurements.

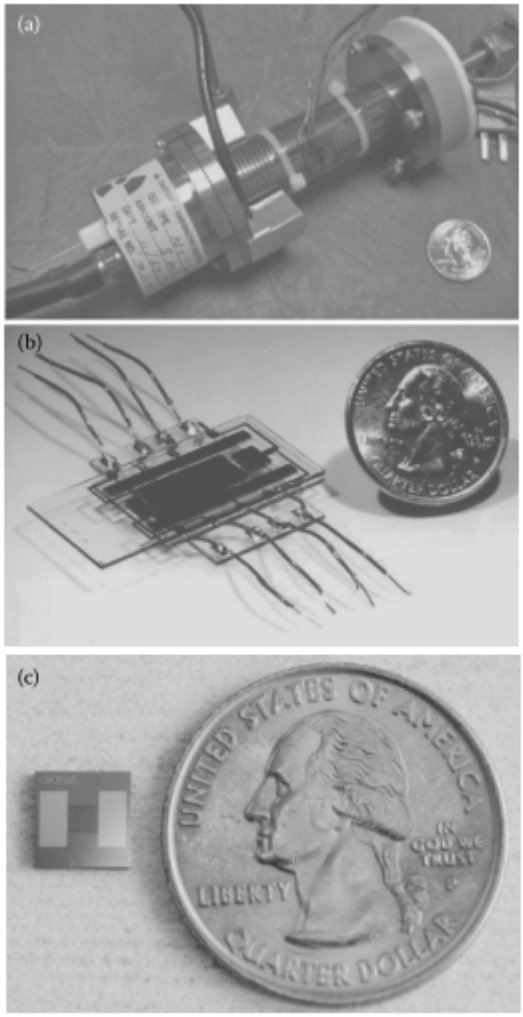

Figure 6.8 A trend in the past decade has been miniaturization of drift tube. Original drift tubes for FAIMS (a) were reduced first to 5 × 13 mm (b) and then to etched silicon with 10 mm (c).

All ions eventually reach the end of the drift tube, and ion separation is based on time or the number of waves experienced by the clusters. Ions injection is through an ion trap before the drift tube to accumulate and enter ions into the traveling wave drift region. (see Figure 6.7c)

6.7.3 Atmospheric pressure drift tube ion mobility–mass spectrometry

Mobilities at atmospheric pressure were first reported by A. J. Dempster [64]. This atmospheric pressure, or more precisely ambient pressure, ion mobility drift tube has been the backbone of the analytical applications of IMS. Since its development as an analytical tool in the 1970s, ambient pressure IMS has been interfaced to a variety of MSs for mobility–mass information. The first MS to which an ambient pressure tube was interfaced was a QMS by Franklin GNO Corporation and applied by Karasek [65]. This instrument was developed before the invention of ESI and used for the ion-mobility detection of volatile compounds from gas chromatography experiments. Later, an electrospray version of IMS was interfaced to a QMS for the evaluation of samples from liquid chromatography experiments [66]. Because quadrupole mass spectra must be obtained by scanning through the quadrupole voltages at a relatively slow rate, 2D data from IMS–QMS are not readily available. Nevertheless, when monitoring isomer and enantiomer separations by ion mobility or targeting a single compound of a complex mixture, IMS–QMS provides a sensitive and mass-selective method of detection.

An updated version of IMS is the coupling with Q-ToF-MS. Figure 6.9 is a schematic representation of an ambient pressure ESI ambient pressure IMS interfaced to a Q-TOF-MS. Sample compounds are introduced into the desolvation region of the IMS, where the electrified spray is propelled down the electric field into a counterflow of a heated buffer gas. The purpose of the desolvation chamber is to evaporate the electrospray solvent and sweep neutral vapors away from the ion mobility drift region of the spectrometer. Once the electrospray solvent has been evaporated from electrosprayed droplets, molecular ions free of solvent continue to migrate in the electric field

toward trapping ion gate. Periodically, this ion gate pushes a packet of ions into the drift region of the IMS tube where ions are separated according to their mobility which are determined by their size and charge. Ions with higher charge states experience a higher electric force resulting in higher drift velocity. In addition, ions with larger collision cross sections undergo higher number of interactions with drift gas molecules and migrate through the drift tube more slowly than smaller ones. The combination of both factors determines the overall velocity of the molecule and hence results in arrival time separations at the end of the drift tube. As the mobility coefficient is dependent on shape and charge distribution and not only on mass, structural and geometric isomers that are isobaric (and unresolved in most MSs) may be separated by IMS.

Ambient pressure IMS tubes are almost always interfaced to MSs through an interface funnel to minimize band broadening and loss of resolving power at the pressure interface; this interface also refocusing of ions and ensure high efficiency transfer in collision cell. Interface funnels are not without problems, clustering and declustering reactions can occur on the vacuum side of the interface, depending on pressure and voltage applied to that region [67]. Control of the pressure and voltage in this region of the MS enable the application of collision-induced dissociation (CID) of the analyte ions. Thus, either IMS-MS or IMS-MS^2 data can be obtained with this instrument. All the ions are further accelerated through a middle focusing lens to reach the pulser in the extraction region of the TOF-MS.

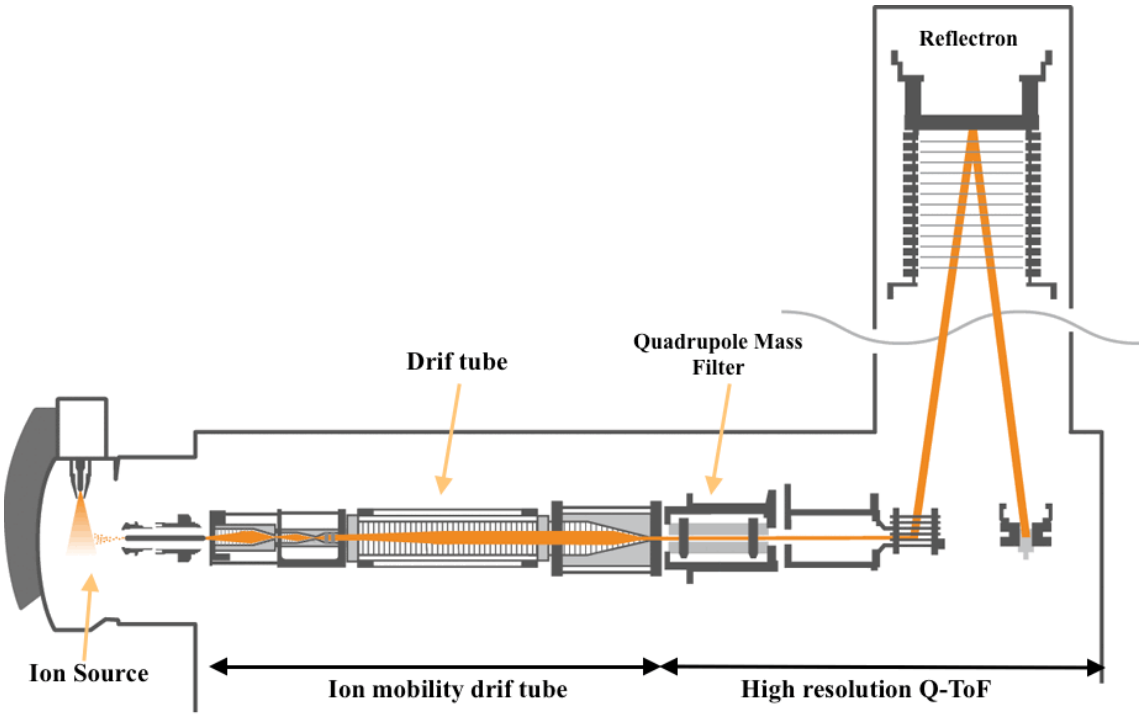

Figure 6.9. Schematic diagram of ion mobility spectrometer coupled to a Q-ToF mass spectrometer

Figure 6.10 shows an example of a lipidomics sample separated by DTIMS coupled with Q-TOF-MS. Random noise is distributed throughout the 2D space, increasing the signal/noise ratio of the metabolite response over that which would be observed in one dimension. Over 1000 metabolite peaks are observed in this spectrum with 42 isobaric pairs identified. The spectrum on the top margin is the mass spectrum integrated across the mobility space and that on the right margin is the ion mobility spectrum integrated across the mass space.

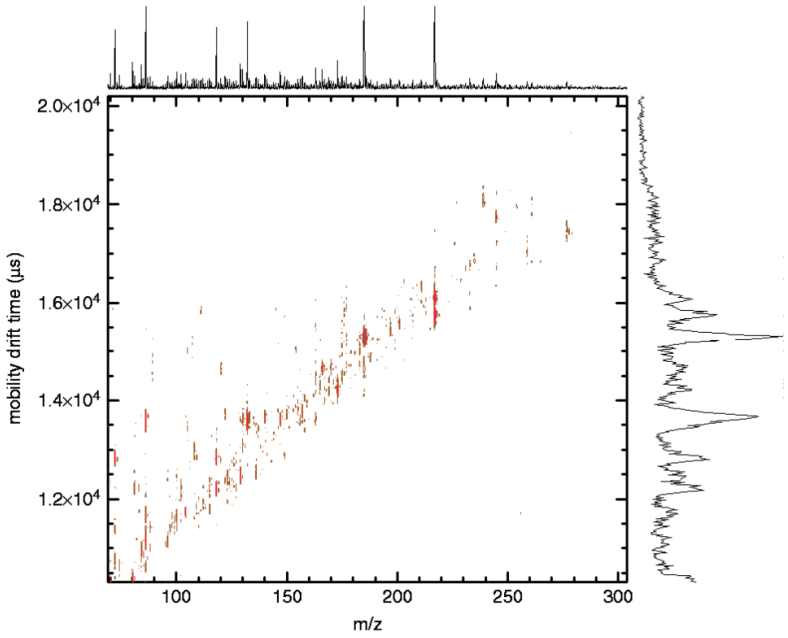

Figure 6.10. Two-dimensional ion mobility MS spectrum producing over 1,000 metabolite peaks.

References

[1] Luo Q.Z., Shen Y.F., Hixson K.K., Zhao R., Yang F., Moore R.J., Mottaz H. M., Smith R.D., Anal. Chem. 2005, 77, 5028-5035.

[2] Miyamoto K., Hara T., Kobayashi H., Morisaka H., Tokuda D., Horie K., Koduki K., Makino S., Nunez O., Yang C., Kawabe T., Ikegami T., Takubo H., Ishihama Y., Tanaka N., Anal. Chem. 2008, 80, 8741-8750.

[3] de Villiers A., Lestremau F., Szucs R., Gelebart S., David F., Sandra P., J. Chromatogr. A 2006, 1127, 60-69.

[4] Plumb R.S., Mazzeo J.R., Grumbach E.S., Rainville P., Jones M., Wheat T., Neue U.D., Smith B., Johnson K.A., J. Sep. Sci. 2007,30, 1158-1166.

[5] Sandra P., Vanhoenacker G., J. Sep. Sci. 2007, 30, 241-244.

[6] Wang X., Barber W.E., Carr P.W., J. Chromatogr. A 2006, 1107, 139-151.

[7] Cunliffe J.M., Maloney T.D., J. Sep. Sci. 2007, 30, 3104-3109.

[8] Cabooter D., Lestremau F., Lynen F., Sandra P., Desmet G., J. Chromatogr. A 2008, 1212, 23-34.

[9] Fekete S., Guillarme D., Dong M.W., LC GC N. Am. 2014, 32, 2-12.

[10] Snyder L.R., Anal. Chem. 2000, 72, 412-420.

[11] Gritti F., Guiochon G., J. Chromatogr. A 2012, 1228, 2-19.

[12] Unger K.K., Kumar D., Grun M., Buchel G., Ludtke S., Adam T., Schumacher K., Renker S.J., Chromatogr. A 2000, 892, 47-55.

[13] Eeltink S., Decrop W.M.C., Rozing G.P., Schoenmakers P.J., Kok W.Th., J. Sep. Sci. 2004, 27, 1431-1440.

[14] Giddings J.C., Unified separation Science, Wiley, New York, 1991.

[15] Colon L.A., Cintron J.M., Anspach J.A., Fermier A.M., Swinney K.A., Analyst 2004, 129, 503-504

[16] Anspach J.A., Maloney T.D., Colon L.A., J. Sep. Sci. 2007, 30, 1207-1213.

[17] MacNair J.E., Patel K.D., Jorgenson J.W., Anal. Chem. 1999,71, 700-708.

[18] Shen Y., Zhang R., Moore R.J., Kim J., Metz T.O., Hixon K.K., Zhao R., Livesay E.A., Udseth H.R., Smith R.D., Anal. Chem. 2005, 77, 3090-3100.

[19] Plumb R.S., Rainville P., Smith B.W., Johnson K. A., Castro-Perez J., Wilson I.D., Nicholson J.K., Anal. Chem. 2006, 78, 7278-7283

[20] de Villiers A., Lauer H., Szucs R., Goodall S., Sandra P., J. Chromatogr. A 2006, 1113, 84-91.

[21] MacNair J.E., Lewis K.C., Jorgenson J.W., Anal. Chem. 1997, 69, 983-989.

[22] Aguilera-Luiz M.M., J.L.M. Vidal, R. Romero-González, A. Garrido Frenich, J. Chromatogr. A 2008, 1205, 10-16.

[23] Motilva M.J., Serra A., Macià A., J. Chromatogr. A 2013, 1292, 66-82.

[24] Beltrán E., Ibáñez M., Sancho J.V., Hernández F., Rapid Commun. Mass Spectrom. 2009, 23, 1801-1809.

[25] Wilson I.D., Nicholson J.K., Castro-Perez J., Granger J.H., Johnson K.A., Smith B.W., Plumb R.S., J. Proteom Res. 2005, 4, 591-598.

[26] Cai S.S., Syage J.A., Hanold K.A., Balogh M.P., Anal. Chem. 2009, 81, 2123- 2128.

[27] Martin M., Guiochon G., J. Chromatogr. A 2005, 1090,16-38.

[28] Neue U., Kele M., J. Chromatogr. A 2007, 1149, 236-244.

[29] Stoll D.R., Paek C., Carr P.W., J. Chromatogr. A 2006, 1137, 153-162.

[30] Schellinger A.P., Carr, P.W., J. Chromatogr. A 2005, 1077, 110-119.

[31] Guillarme D., Veuthey J.L., Smith R.M., Royal Society of Chemistry 2012.

[32] Eiceman, G.A.; Karpas, Z.; Ion Mobility Spectrometry, CRC Press, Boca Raton, FL, 1994.

[33] Eiceman, G.A.; Karpas, Z., Ion Mobility Spectrometry, 2nd edition, CRC Press, Boca Raton, FL, 2005.

[34] Borsdorf, H.; Eiceman, G.A., Ion mobility spectrometry: principles and

applications, Appl. Spectrosc. Rev. 2006, 41, 323–375.

[35] Borsdorf, H.; Mayer,T.; Zarejousheghani, M.; Eiceman, G.A., Recent developments in ion mobility spectrometry, Appl. Spectrosc. Rev. 2011, 46(6), 472–521.

[36] Kanu, A.B.; Dwivedi, P.; Tam, M.; Matz, L.; Hill, H.H., Jr., Ion mobility–mass spectrometry, J. Mass Spectrom. 2008, 43, 1–22.

[37] Kolakowski, B.M.; Mester Z., Review of applications of high- eld asymmetric wave-form ion mobility spectrometry (FAIMS) and differential mobility spectrometry (DMS), Analyst 2007, 132(9), 842–864.

[38] Shvartsburg, A.A., Differential Ion Mobility Spectrometry: Non-linear Ion Transport and Fundamentals of FAIMS, CRC Press, Taylor and Francis Group, Boca Raton, FL, 2009.

[39] Bell, S.E.; Nazarov, E.G.; Wang, Y.F.; Eiceman, G.A., Classi cation of ion mobility spectra by chemical moiety using neural networks with whole spectra at various concentrations, Anal. Chim. Acta 1999, 394, 121–133.

[40] Bell, S.E.; Nazarov, E.G.; Wang, Y.F.; Rodriguez, J.E.; Eiceman, G.A., Neural network recognition of chemical class information in mobility spectra obtained at high tempera- tures, Anal. Chem. 2000, 72, 1192–1198.

[41] Eiceman, G.A.; Nazarov, E.G.; Rodriguez, J.E., Chemical class information in ion mobility spectra at low and elevated temperatures, Anal.

Chim. Acta, 2001, 433, 53–70.

[42] McDaniel, E.W.; Mason, E.A., The Mobility and Diffusion of Ions in Gases, Wiley- Interscience, New York, 1973.

[43] Revercomb, H.E.; Mason, E.A., Theory of plasma chromatography/gaseous electro- phoresis: a review, Anal. Chem. 1975, 47, 970–983.

[44] Guharay, S. K.; Dwivedi, P.; Hill, H. H., "Ion mobility spectrometry: Ion source devel- opment and applications in physical and biological sciences", IEEE T Plasma Sci 2008, 36, 1458–1470.

[45] Dass, C. Fundamentals of contemporary mass spectrometry; Wiley: Hoboken, 2007.

[46] Hoaglund, C. S.; Valentine, S. J.; Clemmer, D. E., "An ion trap interface for ESI-ion mobility experiments", Anal Chem 1997, 69, 4156–4161.

[47] Wyttenbach, T.; Kemper, P. R.; Bowers, M. T., "Design of a new electrospray ion mobil- ity mass spectrometer", Int J Mass Spectrom 2001, 212, 13–23.

[48] Shaffer, S. A.; Tang, K. Q.; Anderson, G. A.; Prior, D. C.; Udseth, H. R.; Smith, R. D., "A novel ion funnel for focusing ions at elevated pressure using electrospray ionization mass spectrometry", Rapid Commun Mass Spectrom 1997, 11, 1813–1817.

[49] Tang, K.; Shvartsburg, A. A.; Lee, H. N.; Prior, D. C.; Buschbach, M. A.; Li, F. M.; Tolmachev, A. V.; Anderson, G. A.; Smith, R. D., "High-sensitivity ion mobility spec- trometry/mass spectrometry using electrodynamic ion funnel interfaces", Anal Chem 2005, 77, 3330–3339.

[50] Kemper, P. R.; Dupuis, N. F.; Bowers, M. T., "A new, higher resolution, ion mobility mass spectrometer", Int J Mass Spectrom 2009, 287, 46–57.

[51] Dugourd, P.; Hudgins, R. R.; Clemmer, D. E.; Jarrold, M. F., "High-resolution ion mobility measurements", Rev Sci Instrum 1997, 68, 1122–

1129.

[52] Shvartsburg, A. A.; Smith, R. D., “Fundamentals of traveling wave ion mobility spectrometry”, Anal Chem 2008, 80, 9689–9699.

[53] Guevremont, R.; Purves, R.W., High eld asymmetric waveform ion mobility spectrometry-mass spectrometry: an investigation of leucine enkephalin ions produced by electrospray ionization, J. Am. Soc. Mass Spectrom. 1999, 10, 492–501.

[54] Kapron, J.T.; Jemal, M.; Duncan, G.; Kolakowski, B.; Purves, R., Removal of metabolite interference during liquid chromatography/tandem mass spectrometry using high-field asymmetric waveform ion mobility spectrometry, Rapid Commun. Mass Spectrom. 2005, 19(14), 1979–1983.

[55] Levin, D.S.; Miller, R.A.; Nazarov, E.G., Vouros, P., Rapid separation and quantitative analysis of peptides using a new nano electrospray-differential mobility spectrometer−mass spectrometer system, Anal. Chem. 2006, 78(15), 5443–5452.

[56] Thermo Electron Corporation, Press Release: Thermo Electron Acquires Provider of Novel Mass Spectrometry Ion Filtering Device, Thermo Electron Corporation, Waltham, MA, August 11, 2005.

[57] AB SCIEX SelexIONTM Technology. A new dimension in selectivity, brochure no. 2530311, 2011.

[58] Brown, L.J.; Toutoungi, D.E.; Devenport, N.A.; Reynolds,J.C.; Kaur-Atwal,G.; Boyle, P., Creaser C.S.; Miniaturized ultra-high field asymmetric waveform ion mobility spectrometry combined with mass spectrometry for peptide analysis, Anal. Chem. 2010, 82(23), 9827–9834.

[59] Wilks, A., A Consideration of Ion Chemistry Encountered on the Microsecond Separation Timescales of Ultra-High Field Ion Mobility Spectrometry, 20th annual conference, International Society for Ion Mobility Spectrometry, Edinburgh, Scotland, July 23–28, 2011.

[60] Pringle, S.D.; Giles, K.; Wildgoose, J.L.; Williams, J.P.; Slade, S.E.; Thalassinos, K.; Bateman, R.H.; Bowers, M.T.; Scrivens, J.H., An investigation of the mobility separation of some peptide and protein ions using a new hybrid quadrupole/travelling wave IMS/oa-TOF instrument, Int. J. Mass Spectrom. 2007, 261, 1–12.

[61] Williams, J.P.; Bugarcic, T.; Habtemariam, A.; Giles, K.; Campuzano, I.; Rodger, P.M.; Sadler, P.J., Isomer separation and gas-phase configurations of organoruthenium anti-cancer complexes: ion mobility mass spectrometry and modeling, J. Am. Soc. Mass Spectrom. 2009, 20, 1119–1122.

[62] Scarff, C.A.; Patel, V.J.; Thalassinos, K.; Scrivens, J.H., Probing hemoglobin structure by means of traveling-wave ion mobility mass spectrometry, J. Am. Soc. Mass Spectrom. 2009, 20, 625–631.

[63] Shvartsburg, A.A.; Smith, R.D., Fundamentals of traveling wave ion mobility spectrometry, Anal. Chem. 2008, 80, 9689–9699.

[64] Dempster, A.J., On the mobility of ions in air at high pressures, Phys. Rev. 1912, 84 (1), 53–57.

[65] Karasek, F.W.; Kim, S.H.; Hill, H.H., Mass identi ed mobility spectra of p-nitrophenol and reactant ions in plasma chromatography, Anal. Chem. 1976, 48(8), 1133–1137.

[66] Wu, C.; Siems, W.F.; Asbury, G.R.; Hill, H.H., Electrospray ionization high-resolution ion mobility spectrometry-mass spectrometry, Anal. Chem. 1998, 70(23), 4929–4938.

[67] Spangler, G., The pinhole interface for IMS/MS, NASA Conf. Pub. 1995, 3301(3), 115–133

.

Chapter 7

Discovering biological metabolite isomers from different mammalian species with liquid chromatography drift tube-ion mobility mass spectrometry

7.0. Introduction

Understanding the metabolome and its roles in biological systems is a big challenge due to the enormous diversity of metabolite structures. Metabolites are the biological end products of cellular regulatory processes, and their levels can be regarded as the ultimate response of biological systems to genetic or environmental changes [1]. The term of metabolome includes major classes of small biomolecules: lipids, amino acids/peptides, sugars, and nucleic acids. Separation and identification of metabolites remain the most challenging steps in a metabolomics workflow because of chemical complexity. Most metabolomics studies currently leverage the sensitivity and specificity of GC-MS and LC-MS. Coupling a chromatographic system to mass spectrometry provides several advantages such as separation and detection of isobars and isomers, reduce ion-suppression effects, and give possibility to separate compounds according to their chemical nature. The importance of isomers isolation because they could have different biological activities in biological systems. An appealing technology for the separation and identification of isomers from complex biological extracts is coupling ion mobility (IM) to mass spectrometry (IM-MS) to obtain a third analytical dimension [2-6]. Gas-phase IM separates ions not only by mass and charge but also by size and shape. Therefore, adding IM to routine LC-MS add new structural information to the measurement. Ions are generated by ESI or MALDI and then directed into IM drift cell, a chamber pressurized with a buffer gas, like nitrogen, with an electrical field is applied. The time required for given ions to migrate through the drift tube, called drift time, is related to its collision cross section (CCS) [3,7,8]; each packet of ions is resolved in the drift tube based on the mobility of ions, which are determined, by their size and charge. Ions with higher charge state experience a higher electric force resulting in a higher drift

velocity. In addition, ions with larger collisional cross sections undergo higher numbers of interactions with the drift gas molecules and cross the drift tube more slowly than smaller ions. The combination of both factors determines the overall velocity of the molecule and hence in arrival time separation at the end of the drift tube.

The advantages of IM-MS for complex sample analysis are several folds: (i) simultaneous characterization of all biomolecular species in a sample, (ii) minimizing sample losses and sample preparation artifacts coming from extensive purification procedure, (iii) achieve very fast two-dimensional separation of ions. (more: extra dimension of separation, no additional time for data acquisition, larger peak capacity, isobaric/isomeric species' separation). Milk is a complex matrix that consists of over 10,000 molecules, in which 32% are lipids [9]. The triacylglycerols (TGs) in human milk are beneficial for the absorption and lipid metabolism in infants [9]. Moreover, many ruminant milk lipids contain trans fatty acids produced from bio-hydrogenation by microbes in rumen. Whereas all trans fats in human milk is derived from diet [10,11]. The presence of *cis/trans*- fatty acid isomers in addition to various combination of fatty acid composition contributes to the complexity of the milk lipid profiles. Here we developed a LC-IM-MS workflow for in-depth analysis of milk lipids.

7.1 Experimental

7.1.1. Sample and sample preparation

Human breast milk samples were provided by Foods for Health Institute in UC Davis. Bovine milk samples were obtained from the Dairy Barn in University of California, Davis. Goat milk was commercially purchased from

local supermarket. Lipids were extracted with methanol and methyl tert-butyl ether and then water was added for phase separation. Specifically, 20 µL of milk were treated with 225 µL ice-cold methanol, vortexing for one minute, and then was added 750 µL of ice-cold methyl tert-butyl ether. The content was shaking for at least 5 min and finally was added water to improve the phases separation and again agitated for 2 minute into centrifuge. The upper phase was trasfered into a tubes and was dryed. To reconstitute was added a mixture of methanol and toluene (9:1) and finally injected in the LC system.

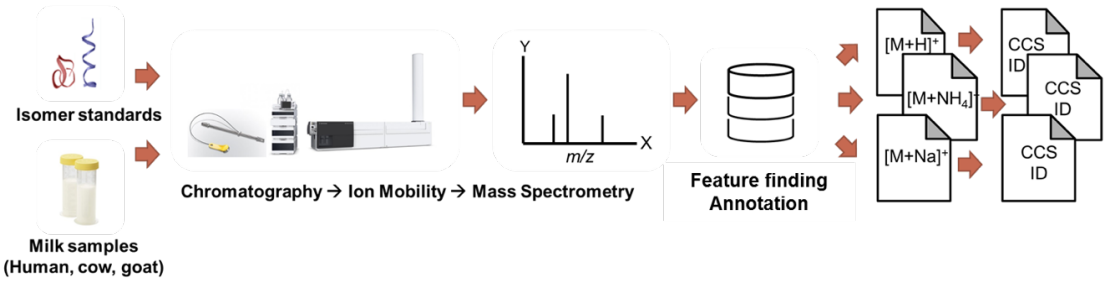

Figure 1. UHPLC-ion mobility-QTOF MS workflow for metabolomics analysis

7.1.2 UHPLC-IM-Q-ToF analysis

All measurements were carried out on an Agilent 6560 drift tube-ion mobility-Q-ToF coupled with an Agilent 1290 Infinity II LC system. 1 µL of diluted samples were separated on an Waters Acquity UPLC CSH C18 column (100 Å × 2.1 mm; 1.7 µm) coupled to an Acquity UPLC CSH C18 VanGuard pre-column (5 Å × 2.1 mm; 1.7 µm). The column was maintained at 65 °C at a

flow rate of 0.6 mL/min. The mobile phases consisted of (A) acetonitrile:water (60:40, v/v) with ammonium formate (10 mM) and formic acid (0.1%) and (B) 2-propanol:acetonitrile (90:10, v/v) with ammonium formate (10 mM) and formic acid (0.1%).

MS parameters: QTOF MS instrument was operated in electrospray ionization (ESI) in positive mode with the following parameters: mass range, 120−1700 m/z; capillary voltage, 3.5 kV; nozzle voltage, 1 kV; gas temperature, 275 °C; drying gas (nitrogen), 8 L/min; nebulizer gas (nitrogen), 35 psi; sheath gas temperature, 325 °C; sheath gas flow (nitrogen), 11 L/min; fragmentor, 400 V; acquisition rate, 1 frame/s, total cycle time, 0.5 s. Ion trap fill time was 30 ms and its ion gate release time was 300 μs. The drift tube and ion funnels were operated as follows: high pressure funnel RF, 100 V, trap funnel RF, 100 V; IM-drift tube entrance voltage, 1574 V; IM-drift tube exit voltage, 224 V; rear funnel entrance voltage, 217.5 V; rear funnel RF, 100 V; rear funnel exit voltage, 45 V. The IM drift gas pressure was maintained at ca. 4 Torr.

7.2 Results and discussions

We optimized the control over ion trapping in the drift cell, and adopted an acquisition method that is suitable for detecting small molecules under IM mode [4,5]. We examined the sensitivity and separation by using over 50 synthetic standards, which includes isomeric species of typical lipid classes, natural products. Flavonoid separations were examined for 3-hydroxyflavone and 7-hydroxyflavone that separated well in the drift tube (Figure 3b-b). For O-pentamethoxylated flavone isomers, the drift time (DT) separation attributes to the distribution of the five O-methyl groups at A and B rings: 3,3',4',5,7-pentamethoxyflavone differed at drift times from 3,4',5,6,7-

pentamethoxyflavone (Figure 3b-c). Paraxathine (1,7-dimethylxanthine) and theophylline (1,3-dimethylxanthine) were distinguished by ΔDT of 2 msec (Figure 3a).

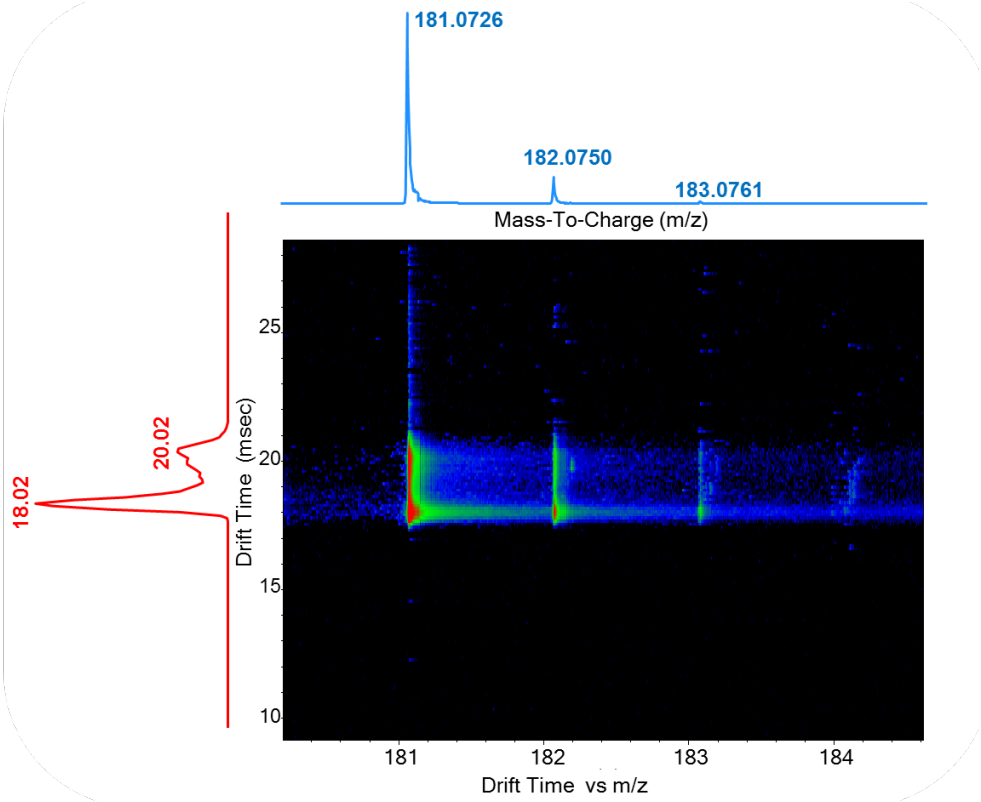

Figure 3a. Ion mobility MS ion map illustrating isomer separation. Examples of caffeine metabolites paraxathine and theophylline

Reproducibility Drift time and CCS values were of high experimental precision with inter-day drift time RSD=0.4%, CCS RSD=0.6%; intre-day variation<=0.2%. (Table 1).

Table 1: Drift time (DT) and collisional cross section measurements (Ω) are highly reproducible.

	DT (ms)			Ω (Å²)		
Inter-day	MaxΔ	Dif%	RSD	MaxΔ	Dif%	RSD
DG24:0	0.34	0.8%	0.4%	3.0	1.4%	0.6%
DG20:1	0.37	1.0%	0.4%	2.7	1.3%	0.6%
LPE17:0	0.34	0.8%	0.3%	3.7	1.7%	0.7%
Intra-day						
DG24:0	0.03	0.1%	0.0%	0.2	0.1%	0.0%
DG20:1	0.05	0.1%	0.1%	0.2	0.1%	0.0%
LPE17:0	0.17	0.4%	0.2%	0.9	0.4%	0.2%

We next analyzed lipid extract from three types of milk samples with untargeted LC-IM-MS. IM mode provided 2-3 times more molecular features compared to regular LC-MS analysis without ion mobility. Next, we used utilized Agilent Mass Profiler to report IM peak features and developed as specific command line tool in R to characterize co-eluting isobaric species, followed by downstream identification by MS-DIAL. In details, our R command screened the IM features that exhibited distinct IM drift time (e.g. ΔDT >0.4 msec) and very close m/z ratio and LC retention time. (Figure 1,2,5)

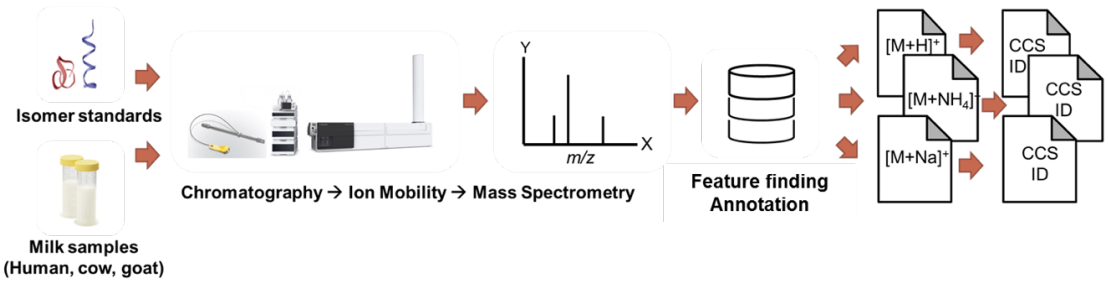

Figure 1. UHPLC-ion mobility-QTOF MS workflow for metabolomics analysis

Our LC-IM-MS untargeted analysis of milk lipids revealed that in human breast milk, >400 lipids with different CCS values were detected from both positive and negative ionization mode. Lipid classes clustered with trend lines of CCS versus *m/z*. Trendlines were also observed within each class (e.g. triacylglycerol, TG). It is noteworthy that since adduct form contributes to measured DT, ions were processed separately for each adduct type ($[M+H]^+$, $[M+NH_4]^+$, and $[M+Na]^+$). Combining m/z, retention time and CCS separation, regression models will enable assigning unidentified compounds and isomers with lipid subclass and elemental compositions (Figure 2,4)

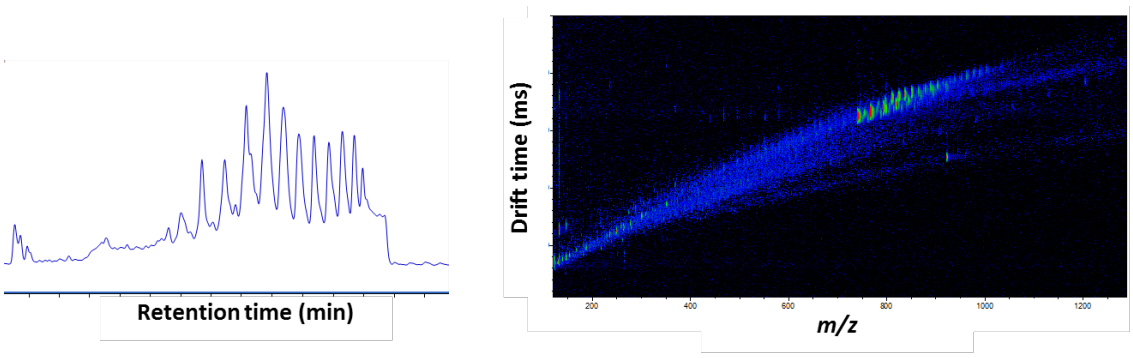

Figure 2. Reversed phase liquid chromatogram and IM-MS ion map of milk lipidome

Human, cow and goat milk lipid compositions differed mainly on triglycerides and their isomers (tentatively annotated with A, B, and C). Human breast milk TGs contained higher amount of long-chain PUFA, while cow and goat milk lipids showed shorter chain and more saturated fatty acids. (Figure 6)

Ion mobility implemented to LC-MS lipidomics workflow, advancing at: new dimension of separation, no additional time for data acquisition, 3-fold more molecular features, separates isomeric metabolites with subtle structural differences.

CCS measurements by drift tube-IMS are highly reproducible to be used in compound annotation schemes.

Prediction modeling of CCS values, the intrinsic molecular property, would significantly improve lipid identification.

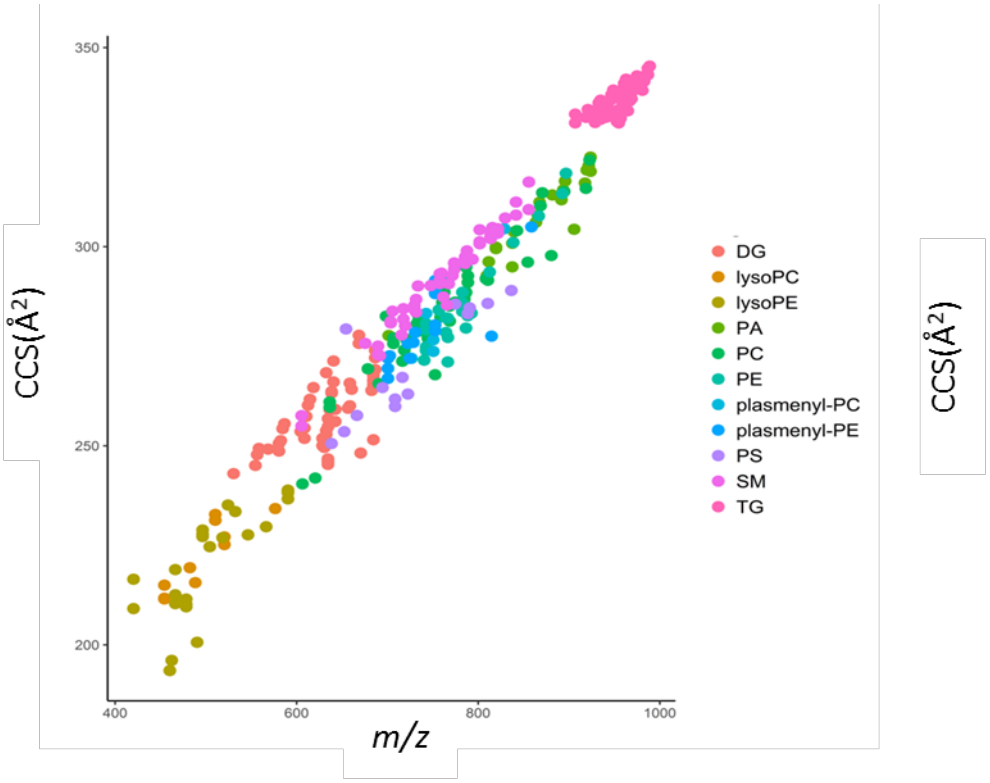

Figure 4a. Lipid classes are grouped by collisional cross section and mass (m/z)

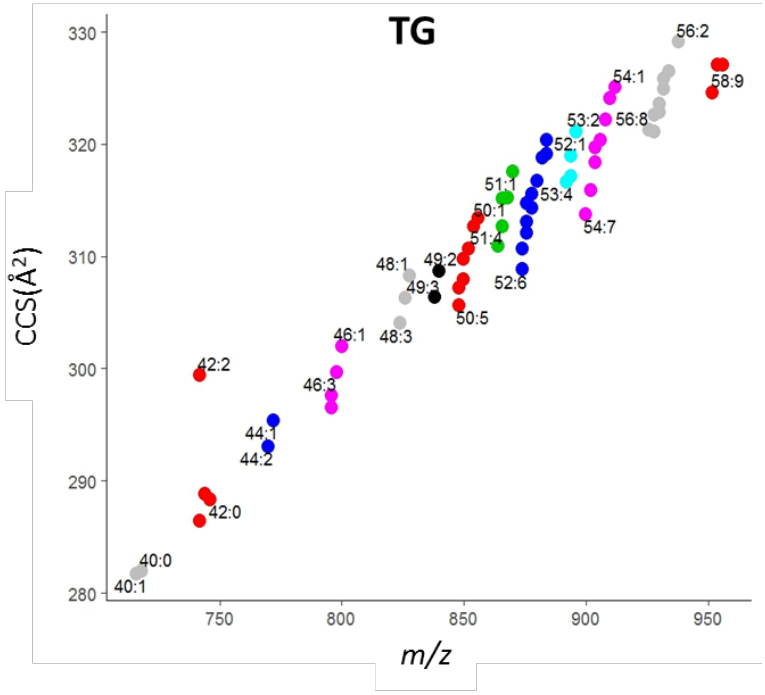

Figure 4b. Trendlines within TG (by collisional cross section and mass (m/z))

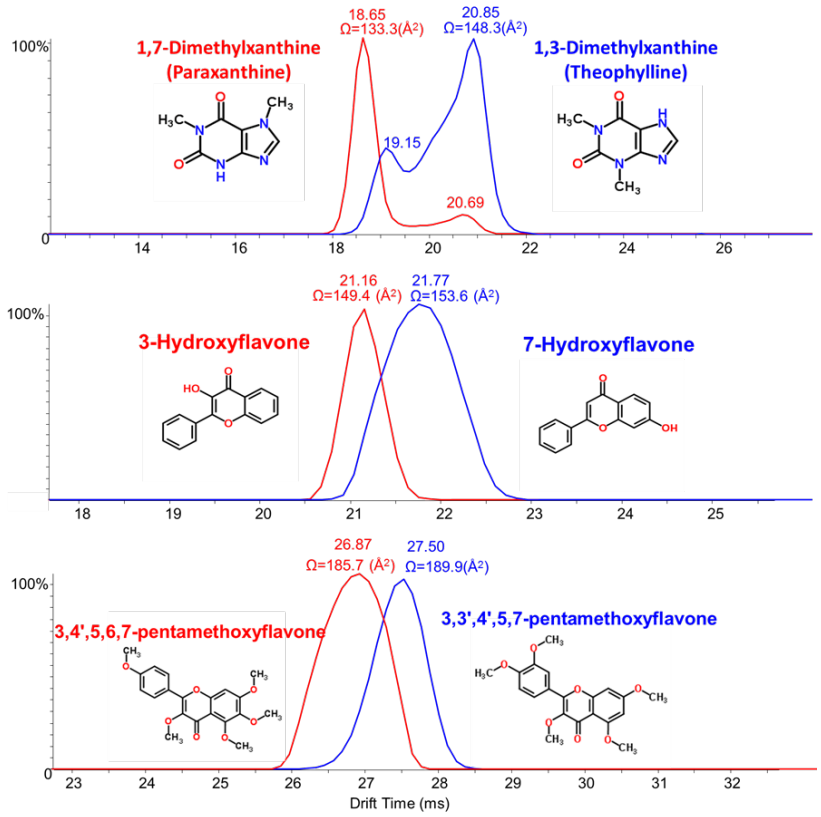

Figure 3b. Separation of isomeric species by ion mobility MS
(a) paraxathine vs. theophylline (b) hydroxyflavones (c) O-pentamethoxylated flavones

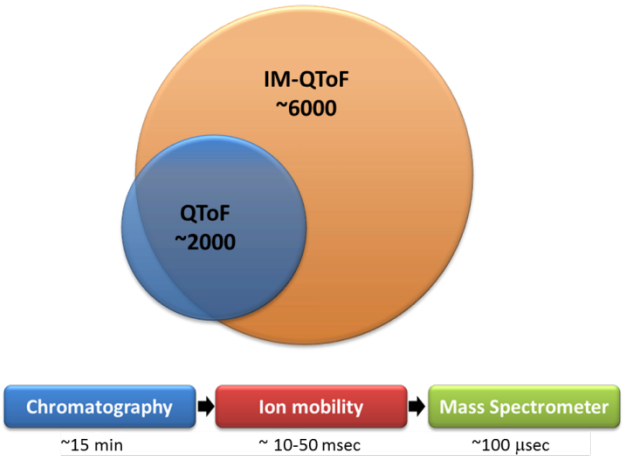

Figure 5. With ion mobility, about 3x more milk lipids are detected compared to conventional UHPLC-QTOF mass spectrometry

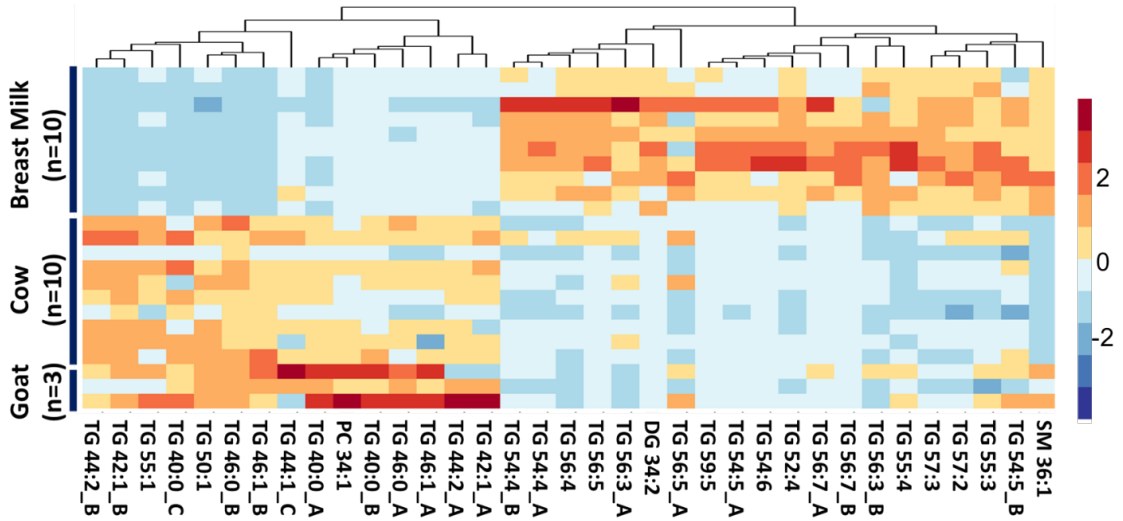

Figure 6. The composition of complex lipids in human, cow and goat milk are highly different as revealed by untargeted UHPLC-ion mobility-QTOF MS.

References

[1] Fiehn O: Metabolomics--the link between genotypes and phenotypes. Plant Mol Biol 2002, 48(1-2):155-171.

[2] Kanu AB, Dwivedi P, Tam M, Matz L, Hill HH: Ion mobility-mass spectrometry. J Mass Spectrom 2008, 43(1):1-22.

[3] Fenn LS, McLean JA: Biomolecular structural separations by ion mobility-mass spectrometry. Anal Bioanal Chem 2008, 391(3):905-909.

[4] May JC, Goodwin CR, Lareau NM, Leaptrot KL, Morris CB, Kurulugama RT, Mordehai A, Klein C, Barry W, Darland E, Overney G, Imatani K, Stafford GC, Fjeldsted JC, McLean JA: Conformational ordering of biomolecules in the gas phase: nitrogen collision cross sections measured on a prototype high resolution drift tube ion mobility-mass spectrometer. Anal Chem 2014, 86(4):2107-2116.

[5] Kyle JE, Zhang X, Weitz KK, Monroe ME, Ibrahim YM, Moore RJ, Cha J, Sun X, Lovelace ES, Wagoner J, Polyak SJ, Metz TO, Dey SK, Smith RD, Burnum-Johnson KE, Baker ES: Uncovering biologically significant lipid isomers with liquid chromatography, ion mobility spectrometry and mass spectrometry. Analyst 2016, 141(5):1649-1659.

[6] May JC, McLean JA: Ion mobility-mass spectrometry: time-dispersive instrumentation. Anal Chem 2015, 87(3):1422-1436.

[7] Paglia G, Angel P, Williams JP, Richardson K, Olivos HJ, Thompson JW, Menikarachchi L, Lai S, Walsh C, Moseley A, Plumb RS, Grant DF, Palsson BO, Langridge J, Geromanos S, Astarita G: Ion mobility-derived collision cross section as an additional measure for lipid fingerprinting and identification. Anal Chem 2015, 87(2):1137-1144.

[8] Stow SM, Causon TJ, Zheng X, Kurulugama RT, Mairinger T, May JC, Rennie EE, Baker ES, Smith RD, McLean JA, Hann S, Fjeldsted JC: An Interlaboratory Evaluation of Drift Tube Ion Mobility-Mass Spectrometry

Collision Cross Section Measurements. Anal Chem 2017, 89(17):9048-9055.

[9] Zou X, Huang J, Jin Q, Guo Z, Liu Y, Cheong L, Xu X, Wang X: Lipid composition analysis of milk fats from different mammalian species: potential for use as human milk fat substitutes. J Agric Food Chem 2013, 61(29):7070-7080.

[10] Jensen RG: The lipids in human milk. Prog Lipid Res 1996, 35(1):53-92.

[11] Saliu F, Modugno F, Orlandi M, Colombini MP: HPLC-APCI-MS analysis of triacylglycerols (TAGs) in historical pharmaceutical ointments from the eighteenth century. Anal Bioanal Chem 2011, 401(6):1785-1800.

[12] Cajka T, Fiehn O: LC-MS-Based Lipidomics and Automated Identification of Lipids Using the LipidBlast In-Silico MS/MS Library. Methods Mol Biol 2017, 1609:149-170.

[13] Kind T, Liu KH, Lee DY, DeFelice B, Meissen JK, Fiehn O: LipidBlast in silico tandem mass spectrometry database for lipid identification. Nat Methods 2013, 10(8):755-758.